1989

Searching for heavy fermion materials in Ce intermetallic compounds

Jinke Tang
Iowa State University

INFORMATION TO USERS

The most advanced technology has been used to photograph and reproduce this manuscript from the microfilm master. UMI films the text directly from the original or copy submitted. Thus, some thesis and dissertation copies are in typewriter face, while others may be from any type of computer printer.

The quality of this reproduction is dependent upon the quality of the copy submitted. Broken or indistinct print, colored or poor quality illustrations and photographs, print bleedthrough, substandard margins, and improper alignment can adversely affect reproduction.

In the unlikely event that the author did not send UMI a complete manuscript and there are missing pages, these will be noted. Also, if unauthorized copyright material had to be removed, a note will indicate the deletion.

Oversize materials (e.g., maps, drawings, charts) are reproduced by sectioning the original, beginning at the upper left-hand corner and continuing from left to right in equal sections with small overlaps. Each original is also photographed in one exposure and is included in reduced form at the back of the book. These are also available as one exposure on a standard 35mm slide or as a 17" x 23" black and white photographic print for an additional charge.

Photographs included in the original manuscript have been reproduced xerographically in this copy. Higher quality 6" x 9" black and white photographic prints are available for any photographs or illustrations appearing in this copy for an additional charge. Contact UMI directly to order.

U·M·I

University Microfilms International
A Bell & Howell Information Company
300 North Zeeb Road, Ann Arbor, MI 48106-1346 USA
313/761-4700 800/521-0600

Order Number 8920192

Searching for heavy fermion materials in Ce intermetallic compounds

Tang, Jinke, Ph.D.

Iowa State University, 1989

U·M·I
300 N. Zeeb Rd.
Ann Arbor, MI 48106

Searching for heavy fermion materials in Ce intermetallic compounds

by

Jinke Tang

A Dissertation Submitted to the
Graduate Faculty in Partial Fulfillment of the
Requirements for the Degree of
DOCTOR OF PHILOSOPHY

Department: Physics
Major: Solid State Physics

Approved:

Signature was redacted for privacy.

Signature was redacted for privacy.

In Charge of Major Work

Signature was redacted for privacy.

For the Major Department

Signature was redacted for privacy.

For the Graduate College

Iowa State University
Ames, Iowa

1989

TABLE OF CONTENTS

I. INTRODUCTION

A. Heavy Fermions

It is well known that the low temperature heat capacity, C, of an ordinary metallic material as a function of temperature, T, can be written as

$$C = \gamma T + \beta T^3. \tag{1}$$

The linear term in Equation (1) is the electronic contribution to the heat capacity, and γ is the temperature independent linear coefficient known as the electronic specific heat coefficient. The cubic term is lattice heat capacity with

$$\beta = 1944/\theta_D^3 \text{ J/gram atom K}^4, \tag{2}$$

where θ_D is the Debye temperature of the lattice [1]. When C/T is plotted against T^2 a straight line is obtained. The intercept of this straight line with C/T axis is γ, and γ is of the order of a few mJ/gram atom K^2 in an ordinary metal. β is the slope of this line.

In some intermetallic compounds where one of the constituents is a rare earth or actinide atom with a partially filled 4f or 5f electron shell, it is found that the straight line behavior in the C/T versus T^2 plot no longer holds. In contrast to common metallic materials, the γ is temperature

dependent and the resulting value for γ when T approaches 0K is extraordinarily large, about two orders of magnitude larger than in ordinary metals. Figure 1 shows the low temperature heat capacities as C/T versus T^2 of $CeAl_3$, UPt_3 and UCd_{11}, which are typical heavy fermion materials [2]. As can be seen, the $\gamma_{(T)}$ values start to increase with decreasing temperature at ~10K for $CeAl_3$ and UPt_3. This increase continues until T approaches 0K, with $\gamma_{(0)}$ = 1620 mJ/mole K^2 for $CeAl_3$ [3] and $\gamma_{(0)}$ = 450 mJ/mole K^2 for UPt_3 [4]. These huge γ values are one of the most important characteristics of this type of material. The λ-peak in UCd_{11} is due to an antiferromagnetic ordering at T_N = 5.0K [5]. Above the ordering temperature, γ is almost temperature independent and has a large value of 840 mJ/mole K^2 [5]. About 30% of this large value remains even after the system orders antiferromagnetically. Data below 1K give $\gamma_{(0)}$ = 250 mJ/mole K^2 for UCd_{11}. It is another interesting fact that a large γ is also found for magnetically ordered state. Actually a large γ (> 250 mJ/mole K^2) was also found in a magnetically ordered material UCu_5 by Ott et al. [6].

As the first step towards the understanding of the origin of these large $\gamma_{(T)}$ values at low temperature, we adopt the free electron form for the electronic specific heat coefficient [7]

$$\gamma = (\tfrac{1}{3}k_B^2\pi^2)N(\varepsilon_F) = (k_B^2 k_F/3\hbar^2)m^*, \qquad (3)$$

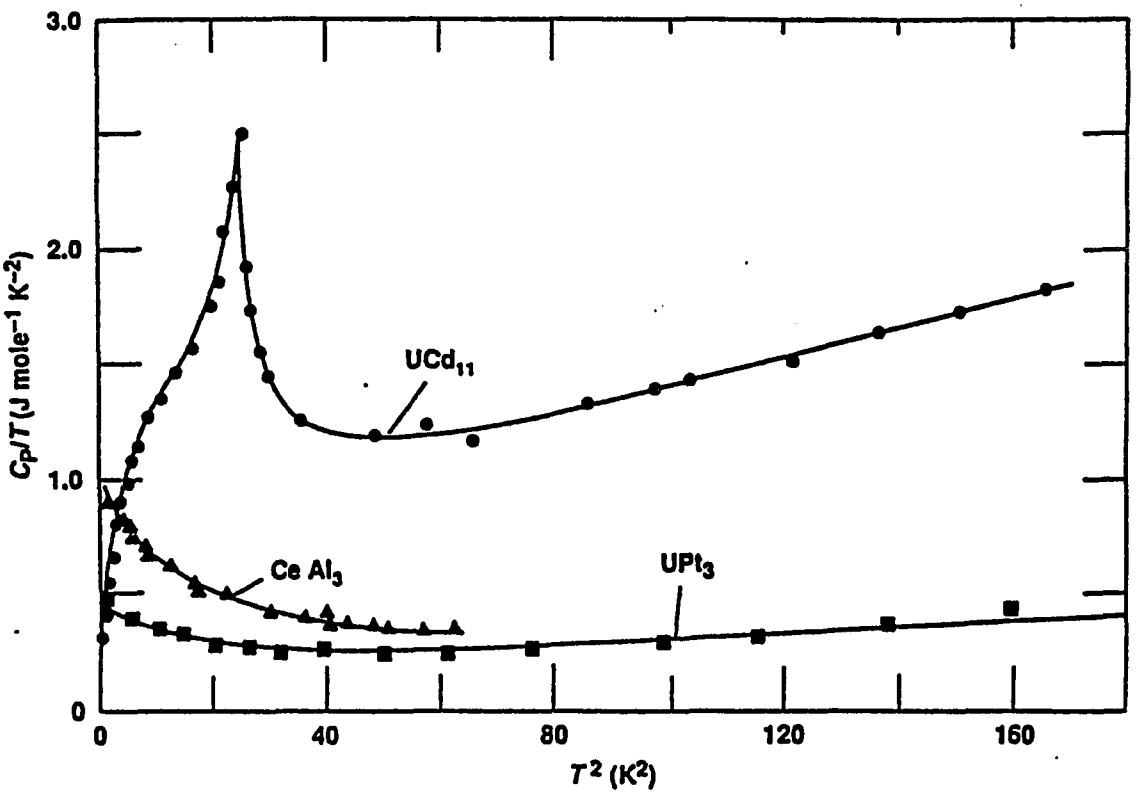

Fig. 1. C/T versus T^2 plot of $CeAl_3$, UPt_3 and UCd_{11} [2]

where k_B is the Boltzmann's constant, $N(\varepsilon_F)$ is the density of electronic states at the Fermi level ε_F, k_F is the wave vector at Fermi surface, $\hbar$ is the Planck's constant, and m* is the effective mass of electrons. We can see that a large value of γ must be interpreted as evidence for enormous density of states at ε_F. This in turn implies a large effective mass, m^*, for the electrons involved (Equation 3). Hence the name "heavy fermion" or "heavy electron" are used for these systems.

This large effective mass is also evident in low temperature magnetic susceptibility. At high temperature, the magnetic susceptibilities of the heavy fermion materials behave just like ordinary metals, following the Curie-Weiss law,

$$\chi_{(T)}=C/(T-\theta_p), \qquad (4)$$

where C is the Curie constant, and θ_p is the paramagnetic Curie temperature. θ_p is found to be negative for all the heavy fermion materials. The effective moments, p_{eff}, deduced from Curie constant, C, are usually close to those expected for the free-ion moments of respective 4f or 5f electron carrying ions. This indicates the localized and independent nature of the 4f or 5f electrons in heavy fermion materials. As temperature decreases, deviations from Curie-Weiss behavior are observed. The magnetic susceptibility, $\chi_{(T)}$, becomes almost temperature independent, a behavior which is characteristic of Pauli

paramagnetism. And χ values are quite enhanced, two or more orders of magnitude larger than Pauli paramagnetic susceptibility in ordinary metals. Again, if we adopt free electron form for the Pauli susceptibility of electrons [8],

$$\chi = \mu_B^2 N(\varepsilon_F) = (\mu_B^2 k_F/\hbar^2\pi^2)m^*, \qquad (5)$$

where μ_B is the Bohr magneton, it is obvious that the large χ comes from the large density of state at ε_F, or large effective mass, m^*, of the electrons involved. This means that both the huge electronic specific heat coefficient and the enhanced Pauli-type susceptibility at low temperature are essentially from the same origin. As a matter of fact, the ratio $\chi_{(0)}/\gamma_{(0)}$ obtained from experiments for these heavy fermion materials [9] falls indeed in the vicinity of that expected for an ordinary metal.

Electrical resistivity, $\rho_{(T)}$, is another physical property in which heavy fermion materials show distinguishing features. In ordinary metals, $\rho_{(T)}$ decreases rapidly from room temperature values, (1-10 $\mu\Omega$cm), with decreasing temperature below 300K. While in heavy fermions, the $\rho_{(T)}$ has little temperature dependence at room temperature and is usually rather high, of the order of 100 $\mu\Omega$cm [10]. Instead of dropping to lower values upon cooling, the resistivity is found to increase with decreasing temperature before it reaches a maximum at a temperature T_{max} (T_{max} is normally less than ~50K). After passing over the

maximum, ρ drops significantly to a residual value of resistivity determined by impurities and crystal lattice imperfections. At very low temperature, ρ often can be cast in the form [3,11]

$$\rho_{(T)} = \rho_o + AT^2, \tag{6}$$

where ρ_o is the residual resistivity, and A is a numerical factor. One of the most characteristic and common features for heavy fermions is this rapid drop in $\rho_{(T)}$ below T_{max}. To explain this phenomenon, it is proposed that the 4f or 5f electrons, which act as local individual scattering centers for conduction electrons at high temperature, somehow form a coherent state at low temperature so that conduction electrons can coherently propagate through the periodic f electron set in the same way that a wave propagates through a perfect lattice. This explains the drop in resistivity mentioned earlier. How and when this coherent state develops is an open question that needs to be answered.

There are many other important experimental aspects about heavy fermions, e.g., some heavy fermions go to superconducting at low temperature, and the mechanism for the superconductivity is believed to be nonconventional. Due to our primary interest, only the normal state properties were discussed above.

The essential physical picture of heavy fermions can be described as follows. At high temperature, these rare earth or

actinide intermetallic compounds act no differently than ordinary compounds with local moments arising from the partially filled 4f or 5f shell. At low temperature, instead of going to magnetically ordered state, the local f electrons and conduction electrons become more and more strongly coupled, and at the same time a coherent state is developed among the f electrons. The effective mass, m^*, describing this highly correlated electron system becomes strongly enhanced over ordinary metals. The theoretical understanding of the heavy fermion system is just at its beginning. A variety of models has been proposed. Several approaches have given some hope to finally open the door to the physics of heavy fermions.

Anderson lattice model is now under a concentrated study. Although a detailed and satisfactory result is lacking, some features are understood. In this approach [2,12], f electrons are treated as localized with energy level ~1eV below ε_F. The coupling between the local f electron and conduction electrons through their spins is of the antiferromagnetic type. This coupling induces a cloud of conduction electrons with antiparallel spin about f electron, which screens out the local moment of the f electron. This accounts for the disappearance of the local moment at low temperature in heavy fermion materials. The electron cloud shows up as a resonance state at Fermi level

ε_F and plays an important role in determining the large effective mass, m^*. This is the so called Kondo effect. Furthermore, the RKKY interaction between local f electrons mediated by the conduction electrons, which is the result of the coupling just mentioned, gives rise to an antiferromagnetic correlation among f electrons. Some believe that the fluctuation of this correlation provides a base for the interaction between the conduction electrons, and it is this interaction between conduction electrons that induces a large density of state of conduction electrons at ε_F, thus explaining the enormous electronic specific heat coefficient. According to this model, the large effective mass is not due to large density of state of f band at ε_F, rather it is from the conduction electrons themselves. This seems quite attractive because we can possibly separate the magnetic behavior of local f electrons from the itinerant heavy fermion behavior of conduction electrons. Therefore one can easily explain the coexistence of heavy fermion behavior and magnetic ordering discussed earlier.

Band structure calculations give a totally different approach. Calculations have been carried out for many heavy fermion systems. Examples are $CeSn_3$ [13,14], $CeCu_2Si_2$ [15], UAl_2 [16], UBe_{13} [17,18] and UPt_3 [18-21]. All the band structure calculations assume the narrow f band pinned at ε_F. Since the

spacings between f electrons in these heavy fermion compounds are relatively large, direct f-f overlap is absent, and the hybridization with non-f electrons of neighboring atoms dominates the f band width [22]. Although these calculations result in a relatively narrow f band width (~1eV), i.e., a relatively large density of state at ε_F, it is still much smaller than the experimental value. The inclusion of the interaction between f electrons by calculation of renormalized band structure of quasiparticles [9] seems to be necessary. In fact the view that the correlation between f electrons is responsible for the very narrow f band in heavy fermions offers the only possible solution. Here we mention the work of F. Marabelli and P. Wachter [23]. In their low energy far-infrared (FIR) and point contact spectroscopy (PCS) experiments, they find that two narrow quasiparticle bands (in meV range) with f characteristics exist at and near ε_F for various heavy fermion materials. They also demonstrated that the extraordinary heat capacities, magnetic susceptibilities and resistivities can be explained by the electronic structures consisting of two quasiparticle bands.

Fermi liquid theory is another approach that has been extensively investigated. The Pauli-type low temperature magnetic susceptibility and the T^2 behavior of resistivity both suggest the Fermi liquid behavior. The Fermi liquid theory also

predicts the $T^3 \ln T$ term in the heat capacities of some heavy fermion materials like UPt_3 [24,25]. According to this theory, spin fluctuations play an important role in determining the large effective mass, m^*. Fermi liquid theory was developed by Landau in describing liquid ^3He system [26]. The similarity between liquid ^3He and heavy fermion is that both systems consist of localized interacting Fermi particles (^3He atom in liquid ^3He and the f electron in heavy fermion). But they are different in that liquid ^3He is a isotropic system while the f electrons are influenced by crystalline anisotropy and the spin-orbit effect. So far this theory can only handle the isotropic case with no spin-orbit coupling as in ^3He. Therefore the important crystalline anisotropy and spin-orbit effects in heavy fermions have not been included in the theory. In addition, this theory provides little detail about the electronic structure of heavy fermion system compared with the other two models discussed above.

Although there are several theoretical models, we still have a long way to go to reach the complete understanding of the heavy fermion systems. First, it is obvious that three approaches gave three different physical pictures of the heavy fermion. For example, in the Anderson lattice model, the f electron level is below ε_F with a localized character, while the f electrons in

band structure calculations are assumed to be itinerant forming a narrow band at ε_F. The answers to the origin of the large effective mass, m^*, are different: in the Anderson lattice model it is from highly correlated conduction electrons; in the band structure model it is from the narrow f electron band; and in the Fermi liquid model it is from spin fluctuations. These three different pictures are surely, in some way, related, but we do not know how at the present time.

Second, no theory has given a satisfactory explanation of the transition from a independent local f electron state at high temperature to a correlated coherent state at low temperature. Little is known about how and when this coherent state develops as temperature is lowered.

Third, the competition between RKKY interaction, which favors magnetic ordering, and the f-conduction electron coupling, which favors demagnetization of local f moment, is a puzzling question. On one hand, RKKY interaction seems to be important to bring about the magnetic ordering; on the other hand, strong f-conduction electron coupling is necessary to explain the large density of state. This coexistence of the two opposite tendencies is clearly seen in the cases where heavy fermion behaviors are found in magnetic ordered materials. Although Anderson lattice model, which separates the magnetic behavior of

f electron from heavy fermion behavior of conduction electron, gives us some hope. But it only provides some expectations, and an extensive study of this model is needed.

One important reason that we do not understand so much about heavy fermion behavior is that we still do not know all the experimental aspects of this group of materials. Searching for new heavy fermion systems is an excellent way to enrich our knowledge. We can learn new experimental facts as well as testing the existing theories. Even if we do not find new heavy fermions, the comparison of the physical properties of the already known heavy fermions and those of the non-heavy fermions can provides some useful information. The primary purpose of this research is to search for heavy fermion materials in Ce intermetallic compounds.

B. Occurrence of Heavy Fermion Materials

The number of reported heavy fermion compounds has increased rapidly during the last several years. Conditions under which the formation of heavy fermion state occurs has been studied by many authors.

It was suggested by Hill [27] that the occurrence of superconductivity and magnetic ordering in rare earth or actinide

compounds depends upon the spacing between the f electron atom in the lattice. For a sufficiently short f-f spacing (less than Hill limit = 3.4Å), the overlap of neighboring f wavefunctions leads to the formation of broad f band which favors a superconducting or non-magnetic ground state. For large f-f spacing, the f electrons are essentially localized, hence magnetically ordered state occurs. All the heavy fermion materials are found to lie within the magnetic regime with f-f spacings larger than Hill limit or at least close to it. Figure 2 shows the electronic specific heat coefficient γ of some typical heavy fermion materials and related compounds versus their f-f spacings [22]. The fact that no heavy fermion was found in cases where f-f spacings are less than Hill limit suggests that the formation of broad f band by overlapping of neighboring f wavefunction prohibits heavy fermion behavior. The Hill limit provides a necessary condition, but not a sufficient one, for the occurrence of heavy fermions. Our study of some Ce intermetallic compounds confirmed this point.

The local environment about the f electron is important. Many heavy fermion materials with large f-f spacing show no sign of magnetic ordering down to the lowest temperature possible. This is because the local moment of f electron is believed to be

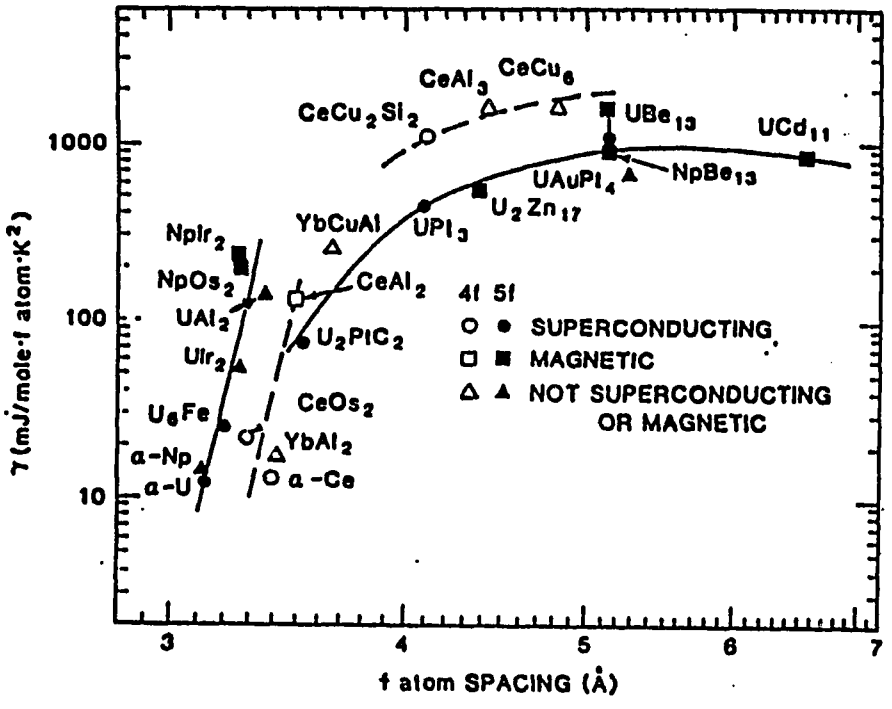

Fig. 2. The electronic specific heat coefficient versus f-f spacing of some typical heavy fermion materials and related compounds [22]

smeared out either by a cloud of conduction electrons of antiparallel spin around it as discussed in Anderson model, or by hybridization with the conduction electrons of neighboring non-f-atom [22]. Both indicate the importance of local environment about the f electron. So far, all the heavy fermion materials are found where one of the constituents is at the end of d-block such as Pt or the beginning of sp-blocks such as Al in the periodic table. The role played by these "d" or "sp" electrons of neighboring non-f-atom is still not well understood. Our interest is to investigate the low temperature properties of some Ce-Cd, Ce-Zn, Ce-Hg, Ce-Ir, Ce-Pt and Ce-Ga binary compounds and some related Ce ternary compounds.

Certain crystal structures seem to favor heavy fermion behavior. Since the local environment of f electron is important, the crystal structure, which determines this environment by changing the nearest neighbors, the symmetries and lattice parameters, is surly a big factor in the formation of the heavy fermion state. Both heavy fermions $CeAl_3$ [3] and UPt_3 [4] crystallize in hexagonal Ni_3Sn-type structure. It is of interest to study the behavior of isostructural compound $CeHg_3$. The result of our study is given in this thesis.

Another crystal structure worth mentioning is cubic $AuCu_3$-type structure. Several this type of compounds show heavy

fermion or spin fluctuation behaviors. Examples are USn_3 with γ~170 mJ/mole K^2 [28], $CeSn_3$ with γ~53 mJ/mole K^2 [29] and $CePb_3$ with γ~200-1400 mJ/mole K^2 (depending on sample preparation) [30,31]. On the other hand, several of them form antiferromagnetically ordered states, e.g., $CeIn_3$, UPb_3 and UIn_3 order at 10K, 31.8K and 108K, respectively [28]. The Ce and U based $AuCu_3$-type intermetallic compounds has provided an excellent area to explore the nature of heavy fermion, spin fluctuations, magnetism and their interrelationships.

The cubic $AuBe_5$ structure also seems to favor heavy fermion behavior. UCu_5, which crystallizes in this type of structure, shows a heavy fermion behavior within the magnetically ordered state. The coexistence of the heavy fermion state and the magnetic state in UCu_5 is an important experimental fact. UPt_5 also shows a intermediate heavy fermion behavior with γ~92 mJ/mole K^2 [32]. By replacing one Pt atom with an Au atom, $UAuPt_4$ shows a significant enhancement, γ~725 mJ/mole K^2 [33]. The isostructural $CeIr_5$ is a superconductor with T_c~1.8K [34], and its heat capacity is one of the compounds studied in this thesis.

II. EXPERIMENTAL DETAILS

A. Sample Preparation and Characterization

Samples of $CePt_5$, $CeIr_5$, $CeGa_2$, $LaGa_2$, $CePtGa_3$, $LaPtGa_3$, $CeNi_{12}B_6$, $LaNi_{12}B_6$, $CeRh_3Si_2$, $Ce_5Ni_6In_{11}$, CeNiAl and $CeNi(Al_{0.5}Ga_{0.5})$ were prepared from high purity elements (at least 99.9 at.% pure) by arc-melting in a Zr gettered argon atmosphere on water cooled Cu hearth. The weight losses during the arc-melting were determined for each cases.

Samples of $CeCd_2$, $CeCd_3$, $Ce_{13}Cd_{58}$, $CeCd_6$, $CeCd_{11}$, $LaCd_{11}$ and Ce_2Zn_{17} were prepared by melting stoichiometric amounts of the constituents in sealed tantalum crucibles under helium atomsphere using a resistance furnace due to the high vapor pressures of Cd and Zn. In the cases of incongruent melting, samples were then annealed in a sealed quartz tube under helium atomsphere to obtain homogeneous single phase compounds. The time periods and temperatures at which these samples were annealed depend on samples' melting temperatures.

$CeHg_3$ was prepared in a different way. Small pieces of Ce metal and corresponding amount of Hg were sealed under helium in a quartz tube, which was heated to ~650°C. At this temperature, which is below the melting temperature of $CeHg_3$, the Hg slowly

vaporizes and reacts with Ce to form $CeHg_x$. Heating for about two months allows the reaction between Ce and Hg to occur through diffusion and to finally form the uniform compound, $CeHg_3$.

Sample characterizations were done by both optical metallography and X-ray diffraction. Metallography is generally a better approach to determine the amount of second phase in a sample than X-ray diffraction. All of our samples except for $CeHg_3$ which is too reactive with air were examined by metallography. The magnification used is typically around 100-500X. All of the samples were essentially single phase. If in the initial preparation, the samples contained more than 1 to 2 % second phase, they were heat treated, or re-heat treated, or remade by slightly changing the Ce to M (+N) ratio to obtain a single phase material.

X-ray diffraction was done on a SCINTAG rotating diffractometer using Cu-Kα radiation. The diffractometer was controlled by a microcomputer. A small portion of sample was ground into powders before being mounted onto the sample holder. No annealing was done prior to X-ray diffraction, which might account for the poor quality in some of the diffraction patterns. X-ray diffraction patterns were taken of most of our samples. These patterns confirmed the previously reported crystal

structures. The crystal structures and lattice parameters of the compounds studied are listed in Appendix.

In case of $CePtGa_3$, a transmission electron microscope (TEM) was used to exam a tiny impurity phase, which apparently precipitated out.

B. Heat Capacity

Low temperature (1.3K to 70K) heat capacity measurements were carried out on these compounds using adiabatic heat pulse type calorimeter (Fig. 3). Samples, typically ~1 gram, were cooled down to liquid helium temperature by condensing helium in helium pot. Subsequent pumping on helium pot can cool the sample down to ~1.3K. Then sample with addenda was thermally isolated from the helium pot by a mechanical heat switch. A vacuum of $\sim 1X10^{-6}$ torr was maintained in sample chamber. A timed heat pulse is given, and the temperature rise is measured. The heat capacity of the sample C is calculated by

$$C = \left(\frac{IVt}{\Delta T} - C_{add}\right)/\text{mole}, \qquad (7)$$

where I is the heater current, V the heater voltage, t the heating time, ΔT the temperature change during the heating, C_{add} the heat capacity of addenda, and mole is the number of moles of the sample. The measuring process was controlled by a computer,

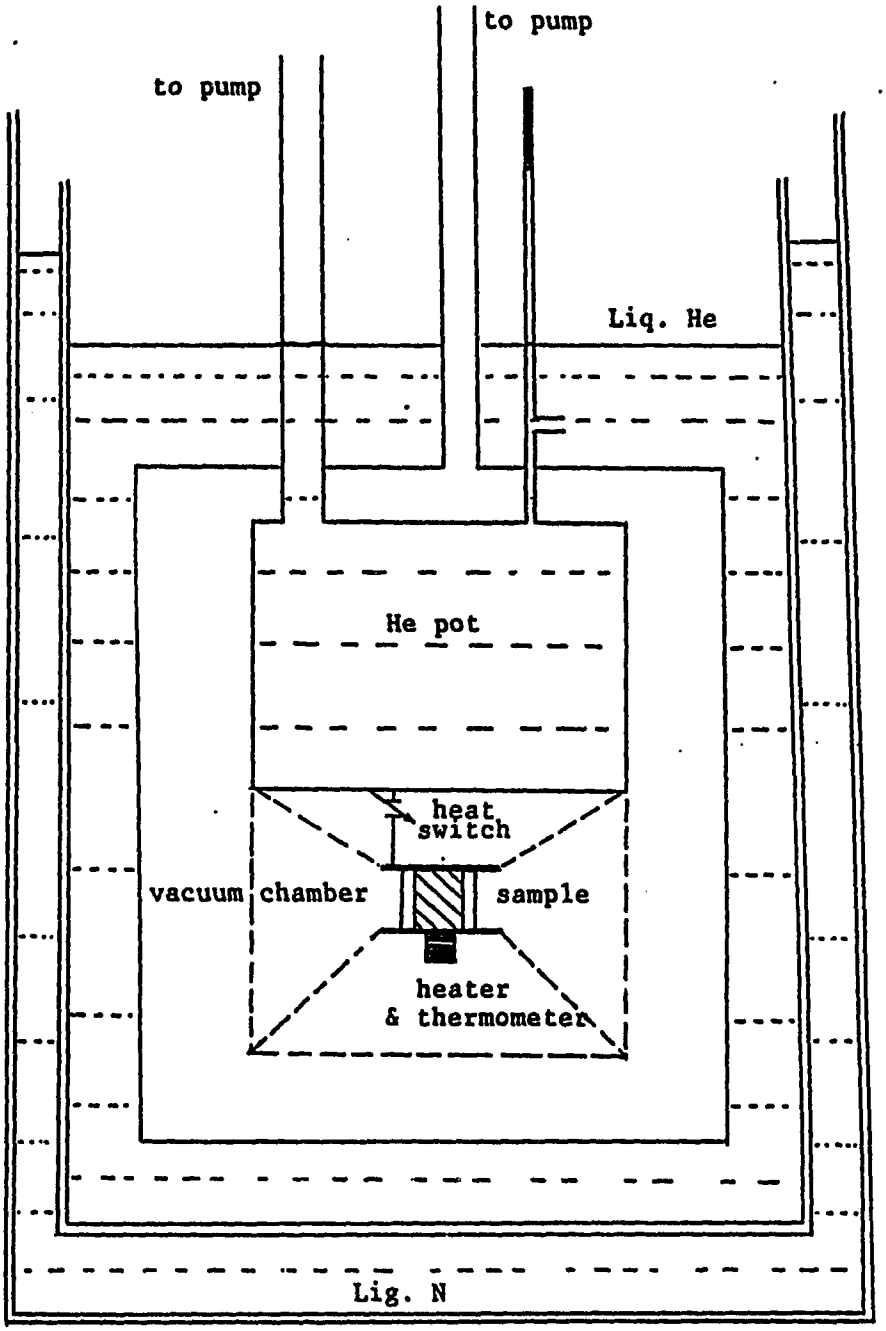

Fig. 3. Low temperature adiabatic heat pulse type calorimeter

which also collected all of the raw data and calculated the heat capacities. The details of calibration of thermometer and calorimeter are given in ref. [35].

C. Magnetic Susceptibility

Most magnetic susceptibility measurements were made from 1.3K to ~298K using a Faraday magnetometer. Figure 4 is a schematic diagram which shows the principle involved. A sample is suspended from a electromagnetic balance in a magnetic field whose field strength and field gradient are known. As the field is turned on and off, the weight of sample changes. This change is due to the force exerted on the sample by magnetic field gradient. Since this magnetic force is proportional to the susceptibility of the sample (Fig. 4), the susceptibility is calculated from the weight change. A detailed description can be found in ref. [36]. A helium atmosphere at 1-10 torr was maintained in the sample chamber. The temperatures were controlled by a resistance heater. Field strength used varied from 0.5T to 2T.

An ac susceptibility apparatus in Dr. Finnemore's group and a SQUID magnetometer in Dr. Johnston's group were also used to measure the magnetic susceptibility of some of the samples.

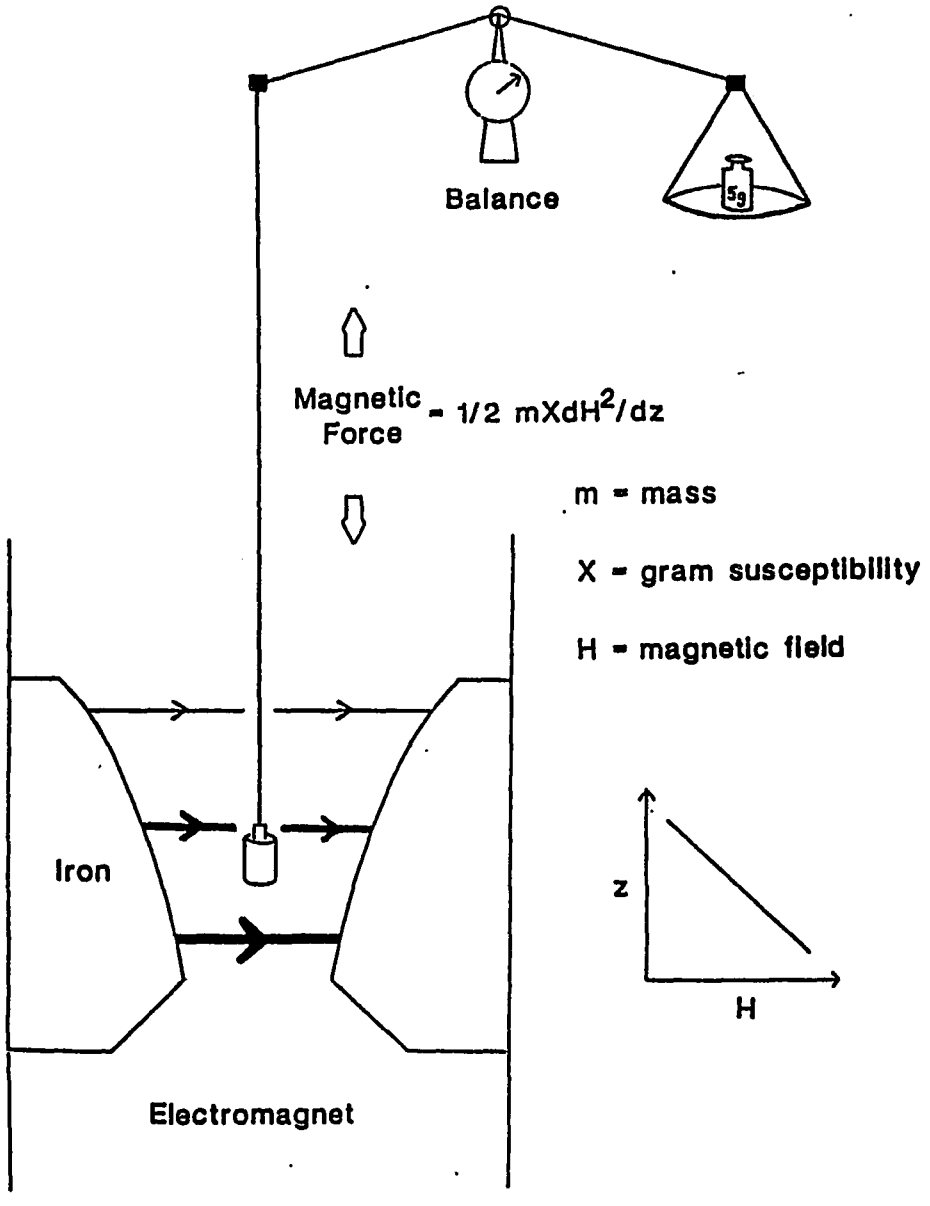

Fig. 4. Principal diagram of Faraday magnetometer

D. Electrical Resistivity

A conventional four probe technique was used for both ac and dc resistivity measurements. Samples were cut into 1x1x5 mm^3 blocks. Four Pt wires were spot-welded onto the sample, the two at the ends served as current leads and the two near the ends as voltage leads. In some cases when the material was extremely brittle, e.g., $CePtGa_3$, silver print was used to connect Pt wires to the sample. A lock-in amplifier was used in ac resistivity measurements. In dc resistivity measurement, current was applied in both directions to eliminate thermal voltages.

III. RESULTS AND DISCUSSIONS

A. Spin Glass Behavior in $CePtGa_3$

1. Introduction to spin glasses

"Classical" spin glass behavior is found in dilute metallic alloys AuFe or CuMn containing ~1 at.% of magnetic impurities Fe or Mn [37,38]. In these systems, a rather sharp cusp is observed in low field magnetic susceptibility at the freezing temperature T_f. Below T_f the spins of magnetic impurities are believed to be "frozen" in various directions that are randomly oriented. Unlike the ferromagnetic or antiferromagnetic system, in which the RKKY interaction between the nearest neighboring spins are either positive or negative, the RKKY interaction between the impurity spins in a spin glass system is random. Figure 5 shows the sketch of spins randomly diluted in a metallic matrix together with the RKKY interaction constant $J_{(\mathbf{R})}$ as a function of the distance between two spins **R** [39]. Since the RKKY interaction is a strong function of distance **R**, the random distribution of spins can cause some spins to align parallel and some spins to align antiparallel. It is because of this competition between ferromagnetic and antiferromagnetic exchange interactions that the spins can be frustrated in trying to choose

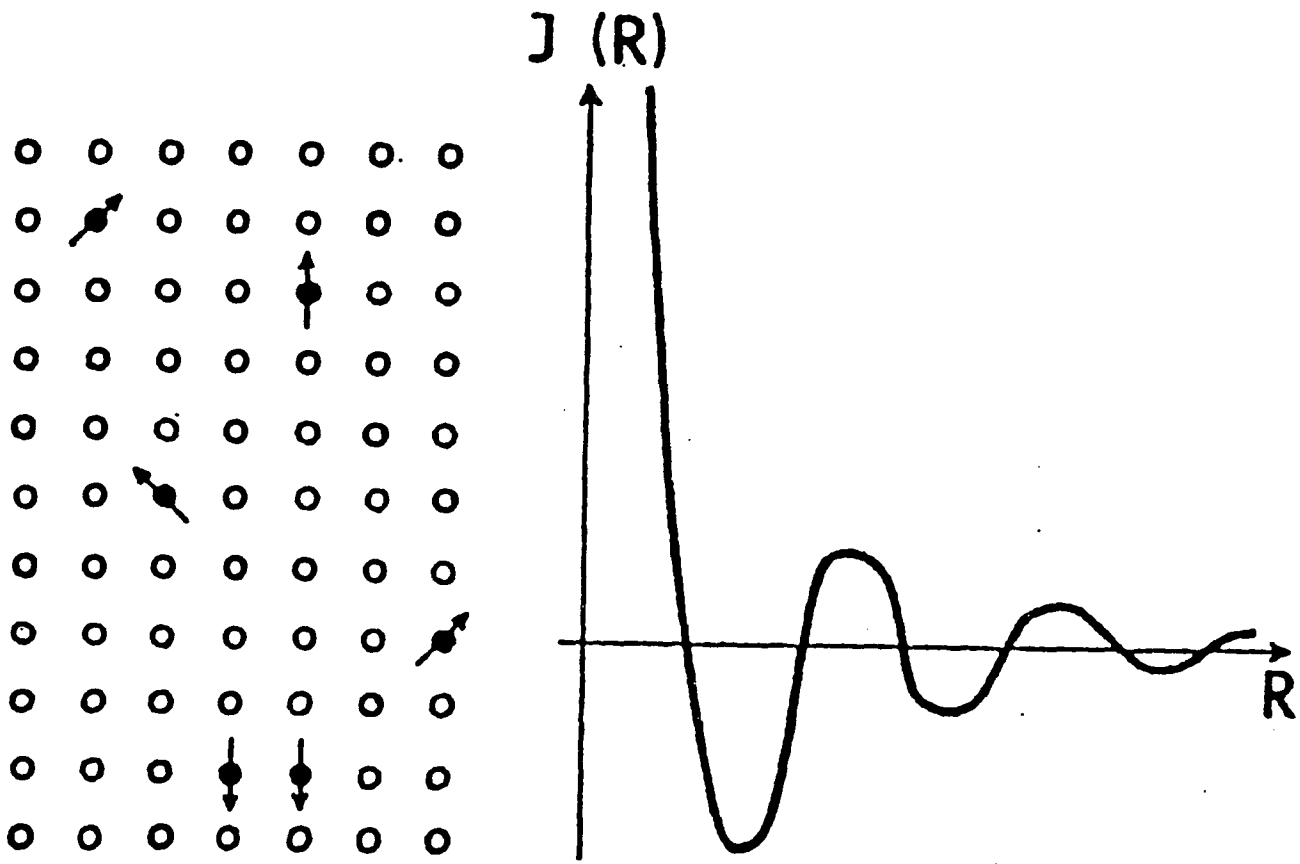

Fig. 5. The sketch of spins randomly diluted in a metallic matrix together with the RKKY interaction constant $J_{(R)}$ as a function of the distance between two spins R [39]

one state over another, and the resulting state is that spins are locked together in a configuration where they are oriented in random directions. The difference between a spin glass state and a paramagnetic state is that at long times there is a probability that a given spin will be in the same orientation where it is first observed in a spin glass state, while in a paramagnetic state, the direction of a spin changes all the time. This difference can be expressed by a local autocorrelation function in time [40],

$$q = \lim_{t \to \infty} < S_i(0)\ S_i(t) > \qquad (8)$$

where $S_i(t)$ is the spin of site i at time t, and the brackets represents the thermal average over all spins. q is finite for $T < T_f$ and is zero for $T > T_f$ when the system is in the paramagnetic state.

The spin glass behavior was also observed in concentrated metallic alloys, such as Fe_xAl_{1-x} [41], and insulators such as $Eu_xSr_{1-x}S$ [42]. In both cases, the random distribution of magnetic ions in the lattice is responsible for the spin glass behavior. Apart from crystalline alloys, the randomness, which causes spin glass behavior, can come from the non-crystallinity, i.e., amorphous solids [43,44]. Recently Rauchschwalbe et al. [45] found spin glass behavior in $CeCu_{6.5}Al_{6.5}$, which is different from the previously known spin glasses. In this case

the Ce^{3+} moments form a periodic array, and the randomness in the system is introduced by the statistical occupation of non-magnetic sites in the cage surrounding each Ce^{3+} ion. A similar situation was also found in $CePd_3B_{0.3}$ [46] where Ce^{3+} ions and Pd atoms occupy regular periodic sites in the lattice, the corners and faces, respectively, but the B atom only partially (~1/3) occupies the body-centered site. In this compound the random distribution of boron atoms and vacancies which changes the electronic environment around Ce^{3+} ions and, thus, the varying RKKY interaction between the Ce^{3+} ions is responsible for the spin glass behavior in $CePd_3B_{0.3}$.

Some of the typical spin glass behaviors can be briefly described as follows.

A sharp peak in low field ac magnetic susceptibility is found at T_f which can be smeared and transformed into a broadened peak by an applied dc magnetic field [47].

The static susceptibility χ reveals a cusp at T_f only when the sample is cooled in zero field. If the sample is cooled through T_f with the field applied, a plateau in χ will be found due to the alignment of spins by the field which are frozen in as T passes through T_f [40].

Near and below T_f, irreversible behavior including remanence and coercivity appears, and the remanent magnetization decays slowly with time in a logarithmic way [48].

A broad peak in heat capacity appears at a temperature about 20% above T_f, which is progressively rounded and pushed to a higher temperature by an applied magnetic field [49]. The interesting fact is that no singularity in heat capacity is found at T_f.

In many cases, the entropy associated with the peak is about 70% of the expected value, e.g., 70% of Rln2 for a doublet ground state such as is normally found in Ce systems [50,51]. This indicates the presence of correlated spins at temperature high above T_f.

At high temperature the magnetic susceptibility obeys the Curie-Weiss law with a relatively small Curie temperature θ_p [38].

The theoretical understanding of spin glass behavior is still underway. Many models have been proposed. It is one of the most active areas in solid state physics.

2. Sample characterization

Samples $CePt_{1.1}Ga_{2.9}$, $CePtGa_3$ and $CePt_{0.9}Ga_{3.1}$ together with their corresponding La partners were prepared by arc-melting.

The samples were then heat treated at 600°C for about 2 weeks. While samples $CePt_{1.1}Ga_{2.9}$ and $CePt_{0.9}Ga_{3.1}$ were clean single phase alloys (Fig. 6), metallographic examination of $CePtGa_3$ showed many parallel black strips distributed in the grains which at one time were thought to be twins (Fig. 7). To verify this a portion of the $CePtGa_3$ sample was examined by transmission electron microscope (TEM) in Ames Laboratory. Careful analysis shows that these black strips are an impurity phase. In addition an electron diffraction pattern showed that some of the diffracted beams are due to a second phase. The magnetization measurements also revealed the existence of the second phase (see below).

The crystal structures of these Ce-Pt gallides were first reported by Grin et al. [52]. They found that $CePt_xGa_{4-x}$ ($0.2 < x < 1.15$) crystallizes in body-centered tetragonal $BaAl_4$-type structure. In this structure the Ce atoms occupy 2(a) positions (0,0,0); (1/2,1/2,1/2). The Pt and Ga atoms randomly occupy the 4(e) [(0,0,z); (0,0,$\bar{z}$); (1/2,1/2,1/2+z); (1/2,1/2,1/2+$\bar{z}$)] and the 4(d) positions [(0,1/2,1/4); (1/2,0,1/4); (1/2,0,3/4); (0,1/2,3/4)]. It is this random distribution of Pt and Ga atoms that provides a random environment around Ce which may cause spin glass behavior in these systems as will be discussed below. Grin et al. [52] also observed, within the homogeneous range of the

Fig. 6. Metallography of $CePt_{0.9}Ga_{3.1}$ (upper) and $CePt_{1.1}Ga_{2.9}$ (lower). Magnification: 250X

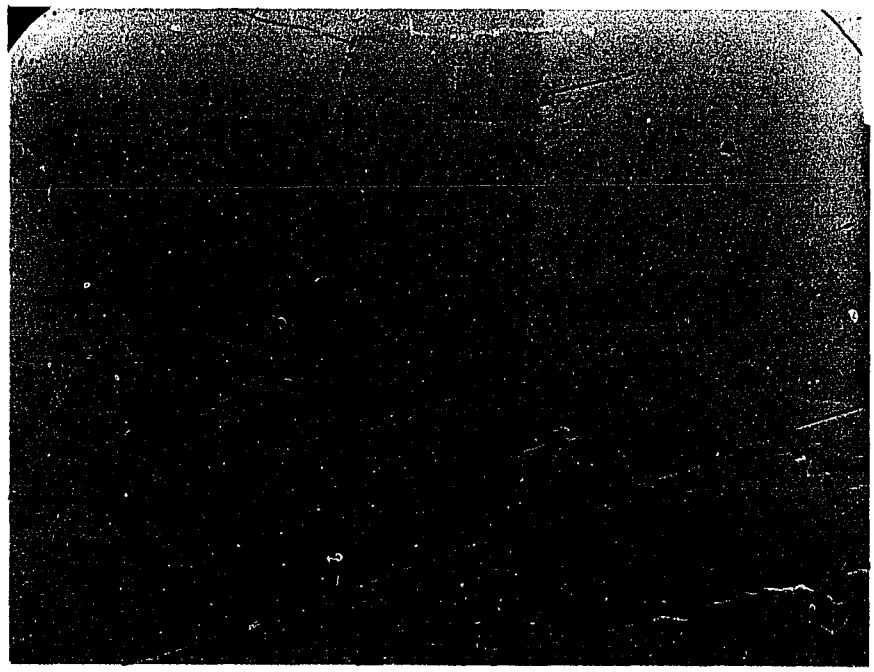

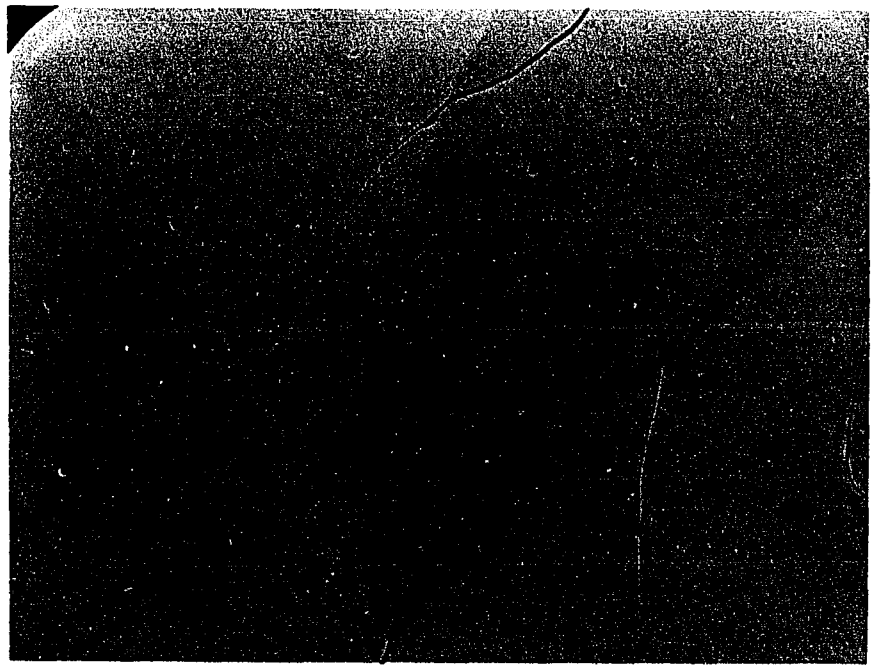

Fig. 7. Metallography of $CePtGa_3$. Magnification: 500X

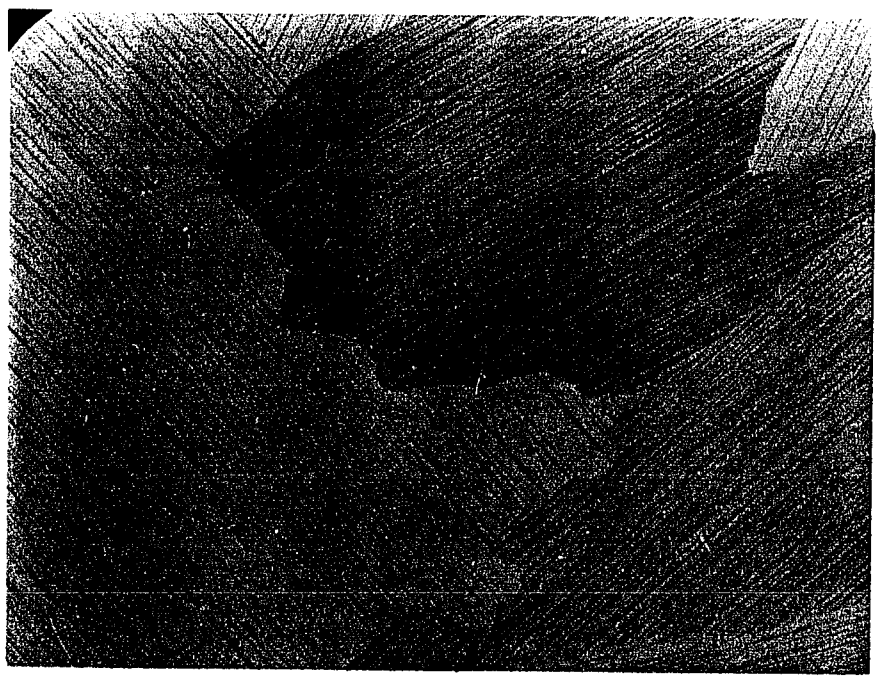

$BaAl_4$-type structure, the existence of a phase with a small orthorhombic deviation from $BaAl_4$ structure at the composition $CePtGa_3$.

X-ray diffraction experiments were performed on our samples. The $CePt_{1.1}Ga_{2.9}$ sample crystallizes in $BaAl_4$-type structure in agreement with the report of Grin et al. $CePtGa_3$ also has the $BaAl_4$ structure in contrast to the report of Grin et al. which stated that $CePtGa_3$ has a face-centered orthorhombic structure. We believe that the reason for this difference is as follows. Since our sample contains some second phase, which might be Ga rich (see below), the real composition of our sample can be slightly different from the nominal composition, i.e., $CePt_{1+\delta}Ga_{3-\delta}$ (where δ is a small positive value). Therefore, its crystal structure is the $BaAl_4$-type. $CePt_{0.9}Ga_{3.1}$ had a face-centered orthorhombic structure as indicated by the double peaks in X-ray pattern associated with planes like (h,k,l) and (k,h,l). It also indicates that the face-centered orthorhombic structure exists at least over the composition range between $CePt_{0.9}Ga_{3.1}$ and $CePtGa_3$. The crystal structures and lattice parameters of these compounds are listed in the Appendix.

3. Heat capacity

The heat capacity of $CePtGa_3$ as a function of temperature at three different magnetic fields is shown in Fig. 8. The heat capacity at zero field starts to increase with decreasing temperature when temperature passes through 7K, and then it reaches a maximum at ~1.7K. The maximum shifts to a higher temperature if a magnetic field is applied. This suggests that the maximum is due to a magnetic phase change and not heavy fermion behavior, such as has been observed in $CeCu_2Si_2$. The significant feature for this compound is that this maximum in zero field heat capacity is not a sharp but a broad one. While for an ordinary ferromagnetic or antiferromagnetic phase transition, a sharp λ-type peak is normally found. One possible explanation is that the system undergoes a spin glass type transition since a rounded peak is one of the characteristics of spin glass system [49]. The heat capacity under magnetic field also suggests the spin glass behavior. As just mentioned, the peak is shifted to a higher temperature and becomes even more rounded in an applied field. This shift of the peak is typical of spin glass behavior [49], although a shift to higher temperature also occurs in ferromagnetic materials (e.g., see below $CeGa_2$ - Fig. 28). As will be seen in magnetic susceptibility, the peak is not due to a ferromagnetic ordering.

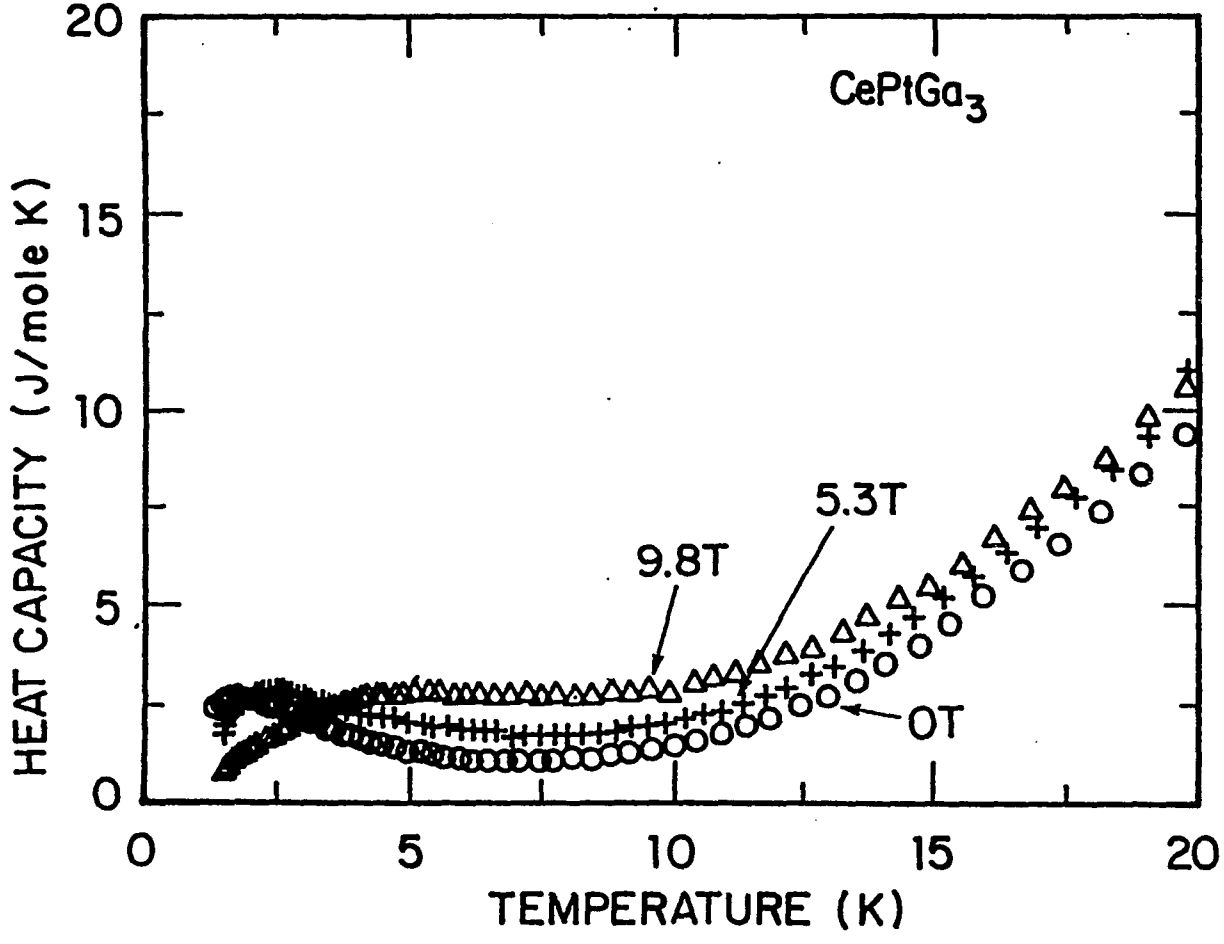

Fig. 8. Heat capacity of $CePtGa_3$ under fields of H = 0, 5.3T and 9.8T

The heat capacity of $LaPtGa_3$ which also crystallizes in $BaAl_4$-type structure was measured in order to estimate the lattice and nuclear contributions to the heat capacity of $CePtGa_3$. The heat capacity of $LaPtGa_3$ and $CePtGa_3$ and the difference ($C_{CePtGa3} - C_{LaPtGa3}$) for temperature T < 10K are shown in Fig. 9. As seen, the rounded peak is obvious. The entropy associated with the peak in ($C_{CePtGa3} - C_{LaPtGa3}$) was estimated to be ~4.7 J/mole K, which is ~80% of the expected value Rln2 = 5.76 J/mole K, and is what is typically found in other spin glass systems [50,51]. It is believed that at temperatures above T_f, the spins in the system are already somewhat correlated with each other, and accounts for the 20% loss of the entropy. This is the so called "frozen-in entropy".

Figure 10 shows the heat capacity of $CePt_{1.1}Ga_{2.9}$, $CePtGa_3$ and $CePt_{0.9}Ga_{3.1}$. The peak in $CePtGa_3$ is shifted to a lower temperature by replacing some Ga atoms with Pt atoms as in the case of $CePt_{1.1}Ga_{2.9}$, while the opposite is true when replacing some Pt atoms with Ga atoms. Although the crystal structure of $CePt_{0.9}Ga_{3.1}$ is different from the other two (see Sec. 2), the magnetic properties are practically unchanged as indicated by the similar peak at ~2K in the heat capacity. This conclusion has also been stated by Grin et al. as based on their susceptibility data. It is not surprising that the change of crystal structure

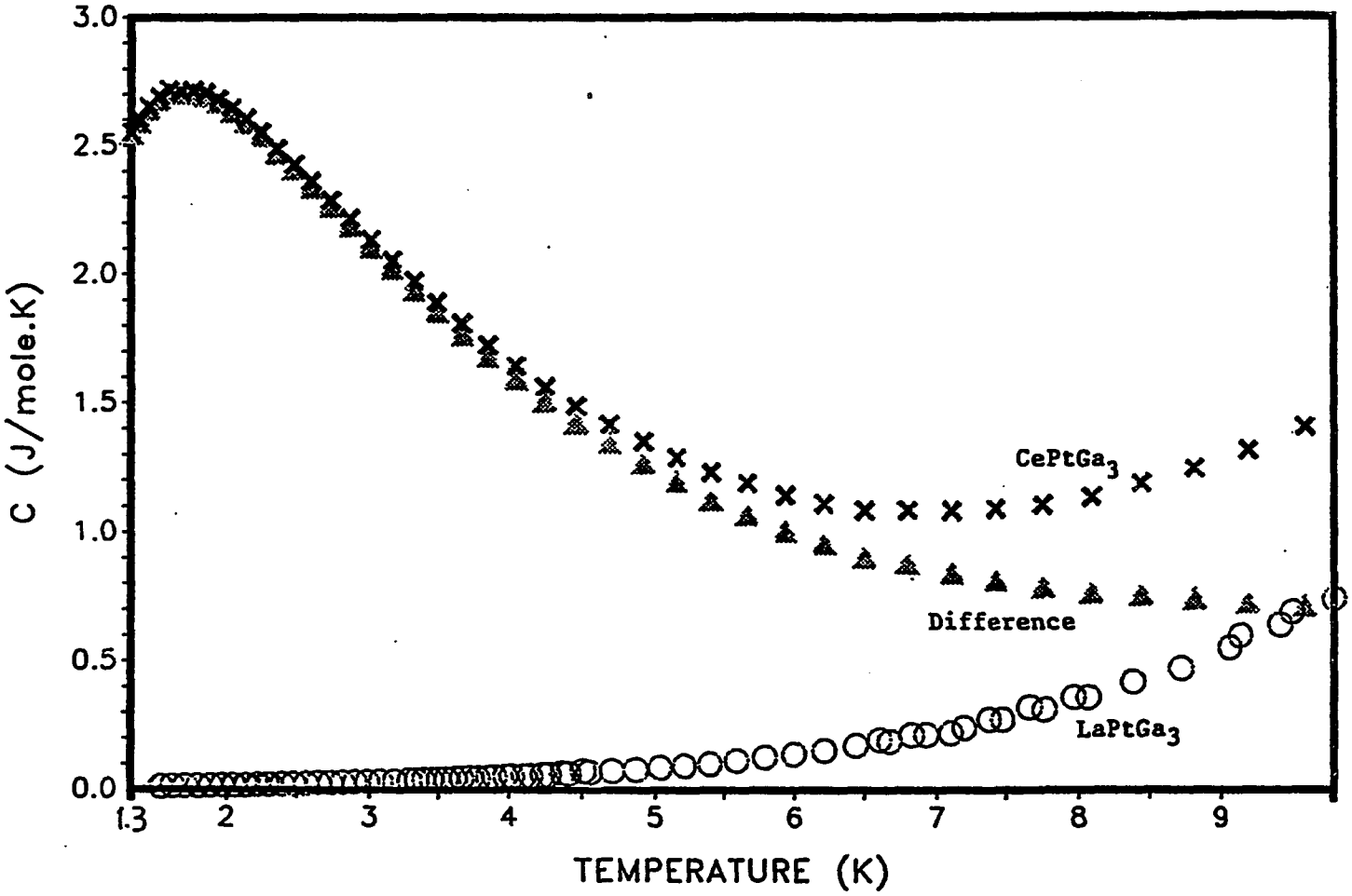

Fig. 9. Heat capacity of $CePtGa_3$ and $LaPtGa_3$ and their difference $C_{CePtGa3} - C_{LaPtGa3}$

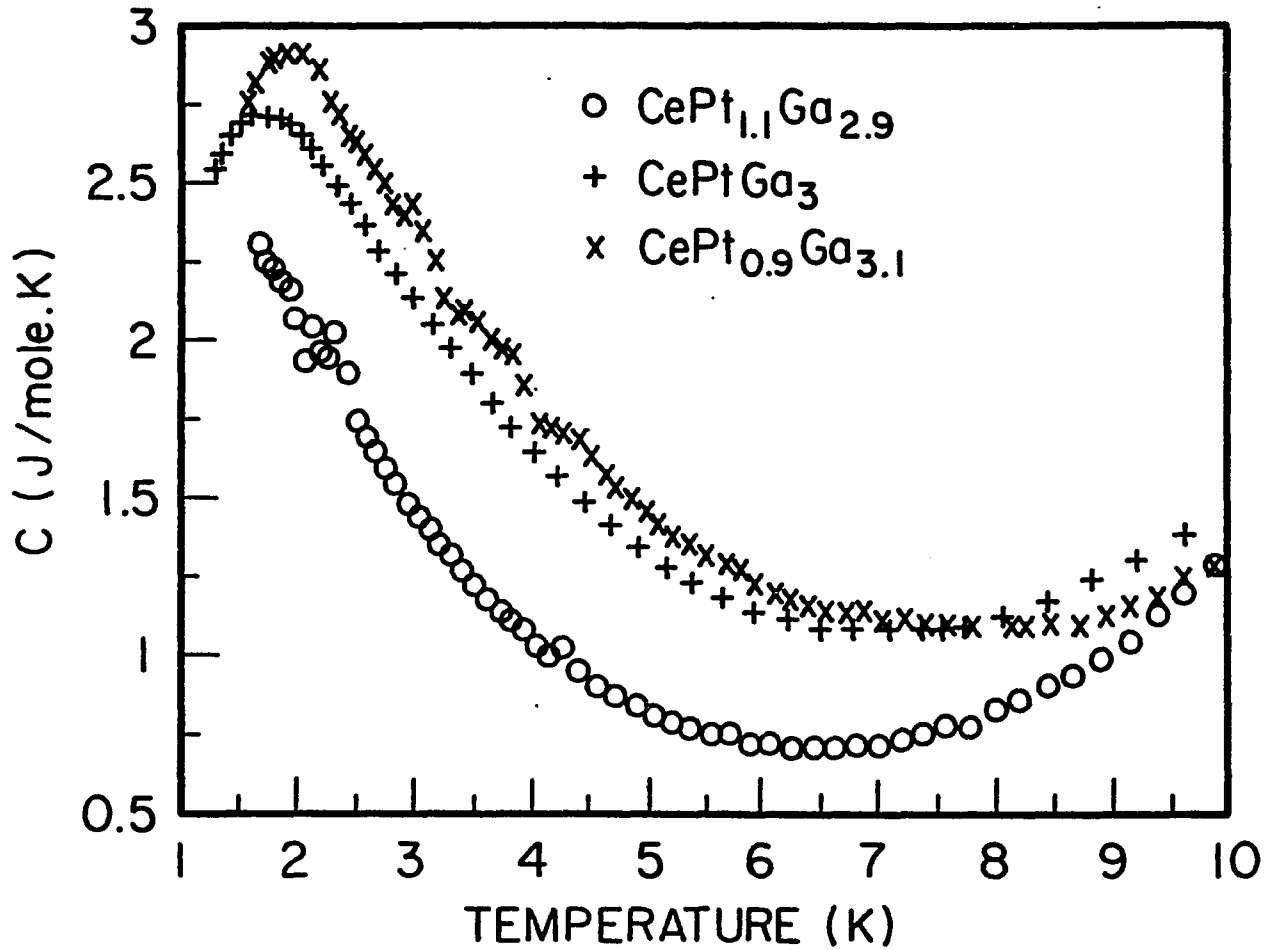

Fig. 10. Heat capacity of $CePt_{1.1}Ga_{2.9}$, $CePtGa_3$ and $CePt_{0.9}Ga_{3.1}$

has little influence on the magnetic behavior if we notice that the face-centered orthorhombic structure is only a slight distortion from the $BaAl_4$-type structure [52].

Shown in Fig. 11 is the C/T versus T^2 plot for $CePtGa_3$ and $LaPtGa_3$ and their difference over temperature range $10K < T < 20K$ ($100K^2 < T^2 < 400K^2$). This difference is the electronic specific heat coefficient of $CePtGa_3$ in excess of that of $LaPtGa_3$ since it is assumed that $CePtGa_3$ and $LaPtGa_3$ have the same lattice and nuclear contributions to the heat capacity and thus these two contributions to the heat capacity of $CePtGa_3$ have been subtracted off. The specific heat coefficient of $CePtGa_3$, γ = ~71 mJ/mole K^2, was determined by adding the average value of this difference to the γ of $LaPtGa_3$, which was determined in the usual way (C/T versus T^2) at much lower temperatures (1.3K to 4.5K). The Debye temperature was estimated from that of $LaPtGa_3$, see the Appendix.

The electronic specific heat coefficients of $CePt_{1.1}Ga_{2.9}$ and $CePt_{0.9}Ga_{3.1}$ were determined in the same way by assuming that their Debye temperatures are the same as that of $LaPtGa_3$.

A portion of our sample was sent to Prof. F. Steglich and his student R. Caspary (Inst. Festkörperphysik, Darmstadt, FRG) to study the heat capacity and susceptibility at extremely low temperature (down to ~60mK) using dilution refrigerator. Their

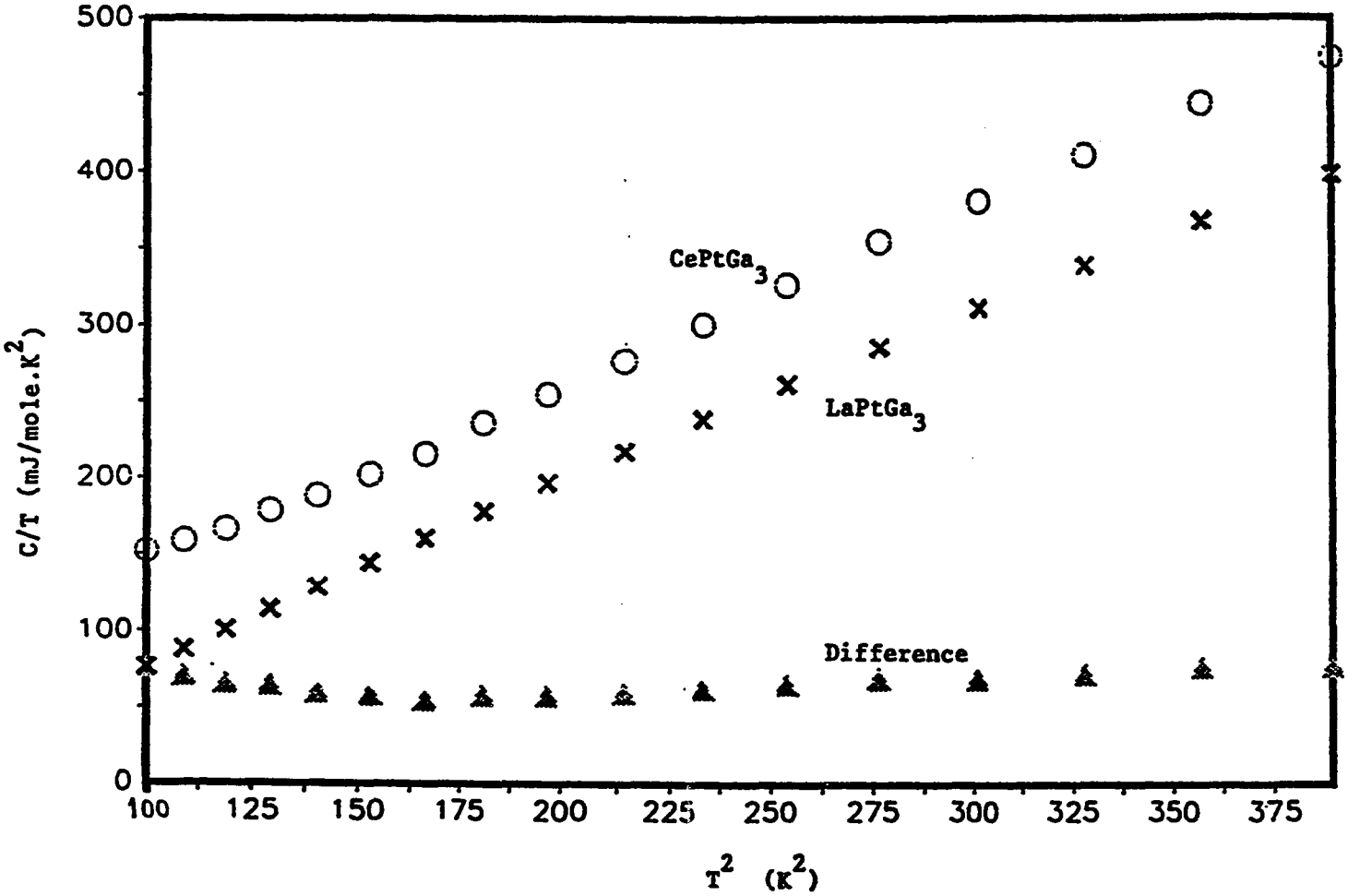

Fig. 11. C/T versus T^2 plot of $CePtGa_3$ and $LaPtGa_3$ and their difference ($100K^2$ to $400K^2$)

heat capacity results agree with ours, where the data overlap, and clearly show the rounded peak which was just evident in our zero field data (compare Fig. 9 and Fig. 12). At temperatures below 1K, the $\Delta C/T = (C - C_{nucl})/T$ versus T plot of heat capacity after the nuclear hyperfine contribution (a T^{-2} term) has been subtracted out is shown in Fig. 13. In the case of H = 8T, the electronic specific heat coefficient can be obtained from the $\Delta C/T$ value at ~0.2K where $\Delta C/T$ becomes temperature independent. Unfortunately, γ can not be extracted for the low-field and zero-field cases. If we assume that γ is field independent, γ at H = 8T can be taken as γ at H = 0T, which is ~120 mJ/mole K^2. This value is substantially larger than the value obtained from above the peak temperature.

The entropy associated with the peak for zero field data seems to saturate at 90% of Rln2 above ~6K. Although it is slightly larger than our entropy value (80% of Rln2 at ~8K), still, 10% of the total entropy is frozen in. The smaller entropy value from our measurements are probably due to the lack of data points below the peak temperature. The shape of the C/T versus T curve used to calculate the entropy was estimated for temperatures below the peak in our case, because the Steglich Caspary results were not available at the time.

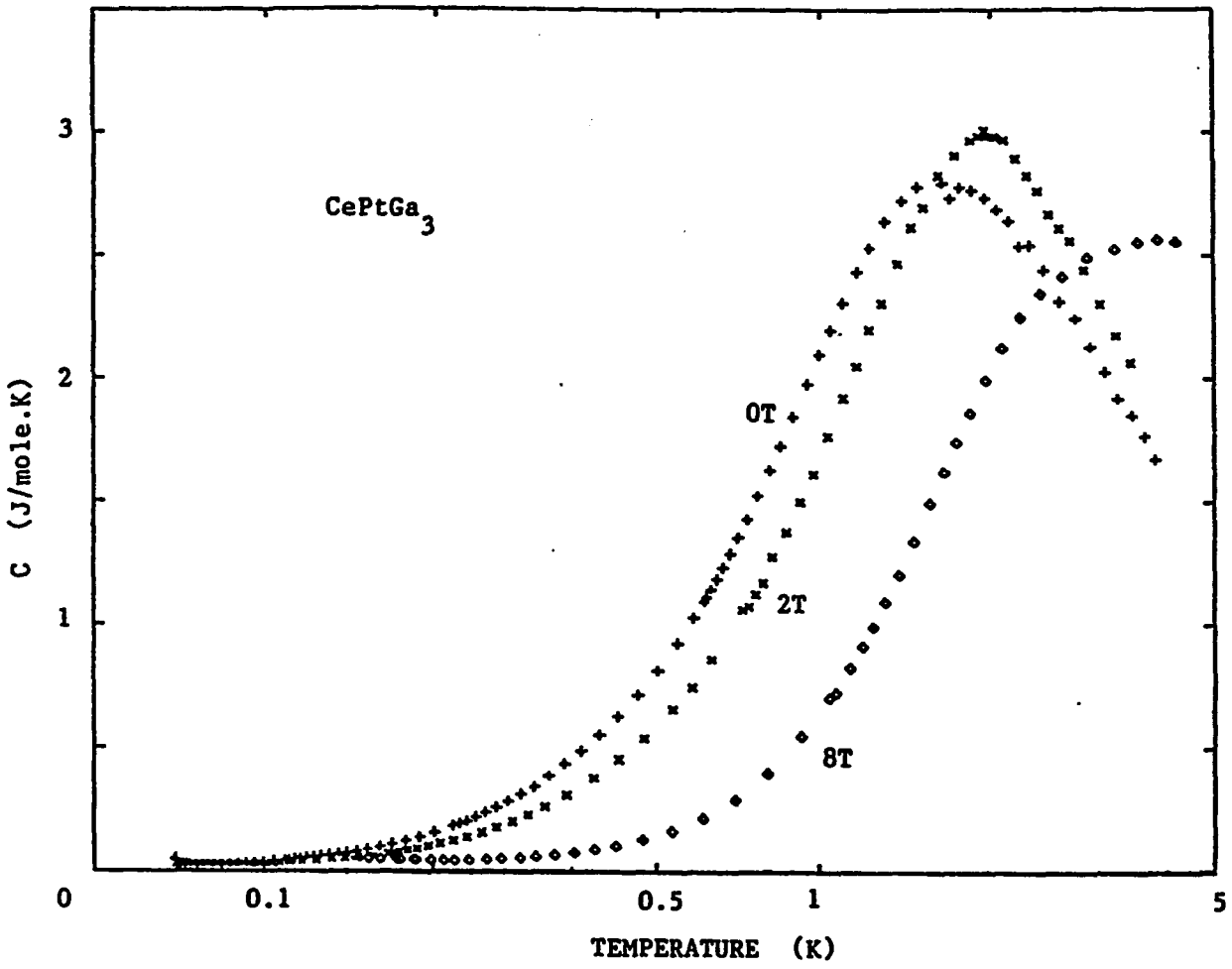

Fig. 12. Heat capacity of $CePtGa_3$ in fields of H = 0T, H = 2T and H = 8T at lower temperatures

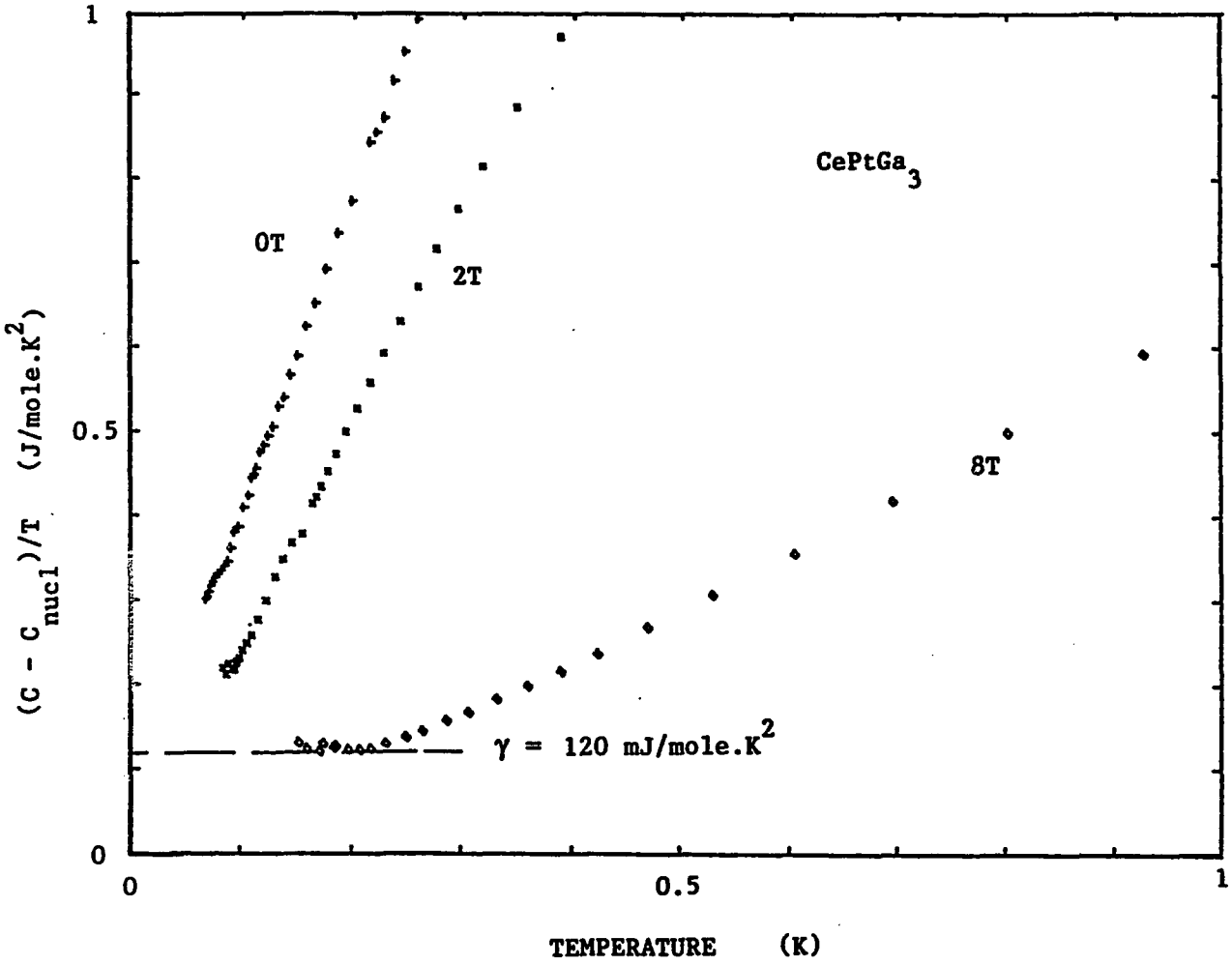

Fig. 13. $(C - C_{nucl})/T$ versus T in fields of H = 0T, H = 2T and H = 8T, see text

4. Magnetic susceptibility

The ac magnetic susceptibility χ_{ac} of $CePtGa_3$ from ~0.4K to 3K is shown in Fig. 14. The absence of a peak around 1.7K in χ_{ac} suggests that the peak in heat capacity at the same temperature is not due to an ordinary magnetic phase transition, e.g., ferromagnetic phase transition, since the peaks in χ_{ac} and heat capacity occur at about the same temperature for an ordinary magnetic phase transition. On the other hand, we did not find the spin glass derived peak below 1.7K which is supposed to be broadened and wiped out by a static magnetic field. Instead, an apparent plateau in χ_{ac} is found at ~0.5K, which may actually be the top of a broad peak (Fig. 15). Measurements to lower temperatures in this regard would be useful. The behavior of this plateau under applied magnetic field is at least partially consistent with spin glass behavior, however the existence of some antiferromagnetic ordering at T_N = ~0.5K in the sample could account for the unusual temperature and field dependences.

Combining the data on ac susceptibility and heat capacity, the following conclusion can be made. Most of the Ce spins freeze into a "glassy state", but a small part of the sample forms an antiferromagnetic cluster which is evident in the χ_{ac} data. The possibility that this antiferromagnetic behavior is from the second phase black strips present in the sample is quite

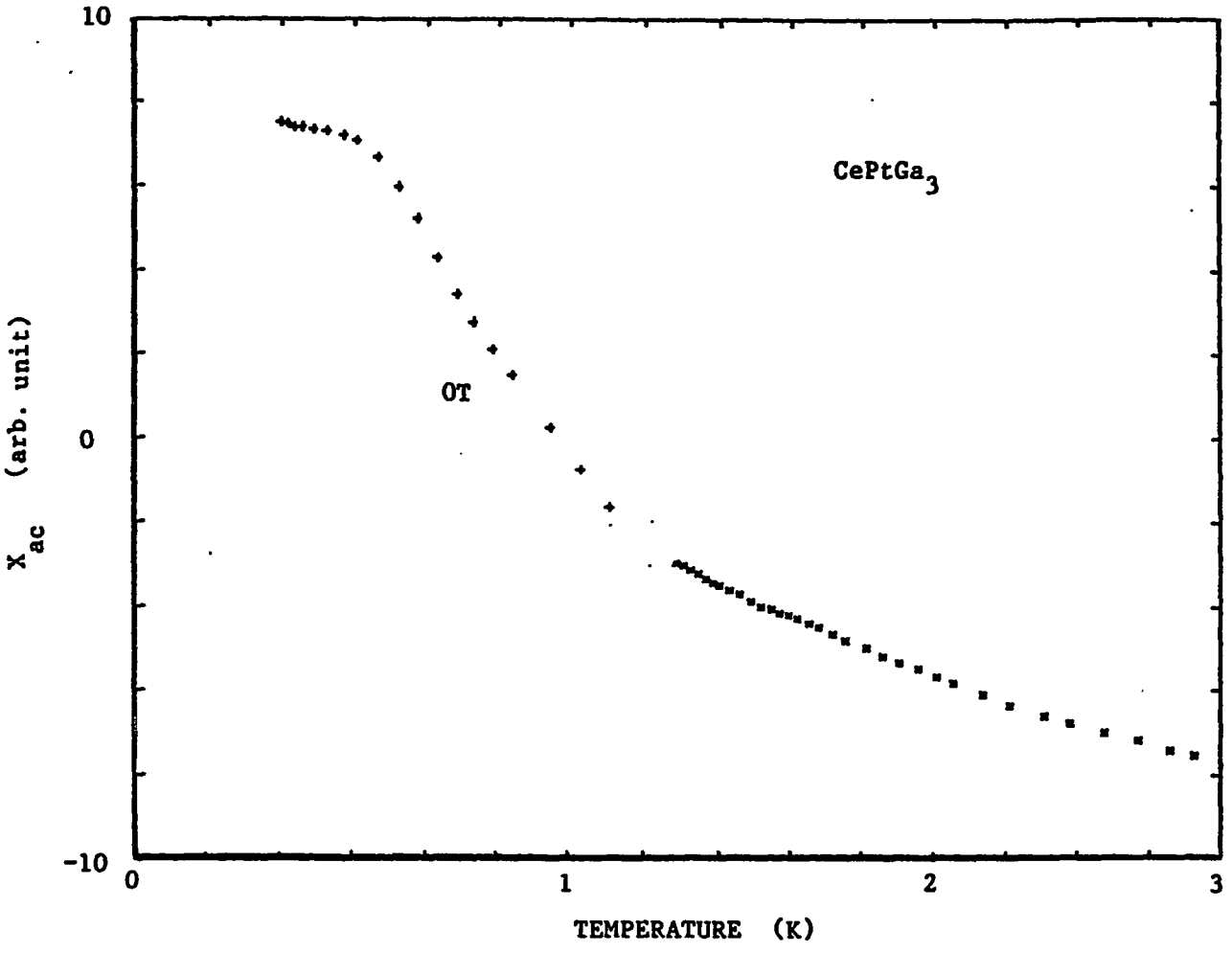

Fig. 14. The ac magnetic susceptibility χ_{ac} of CePtGa$_3$

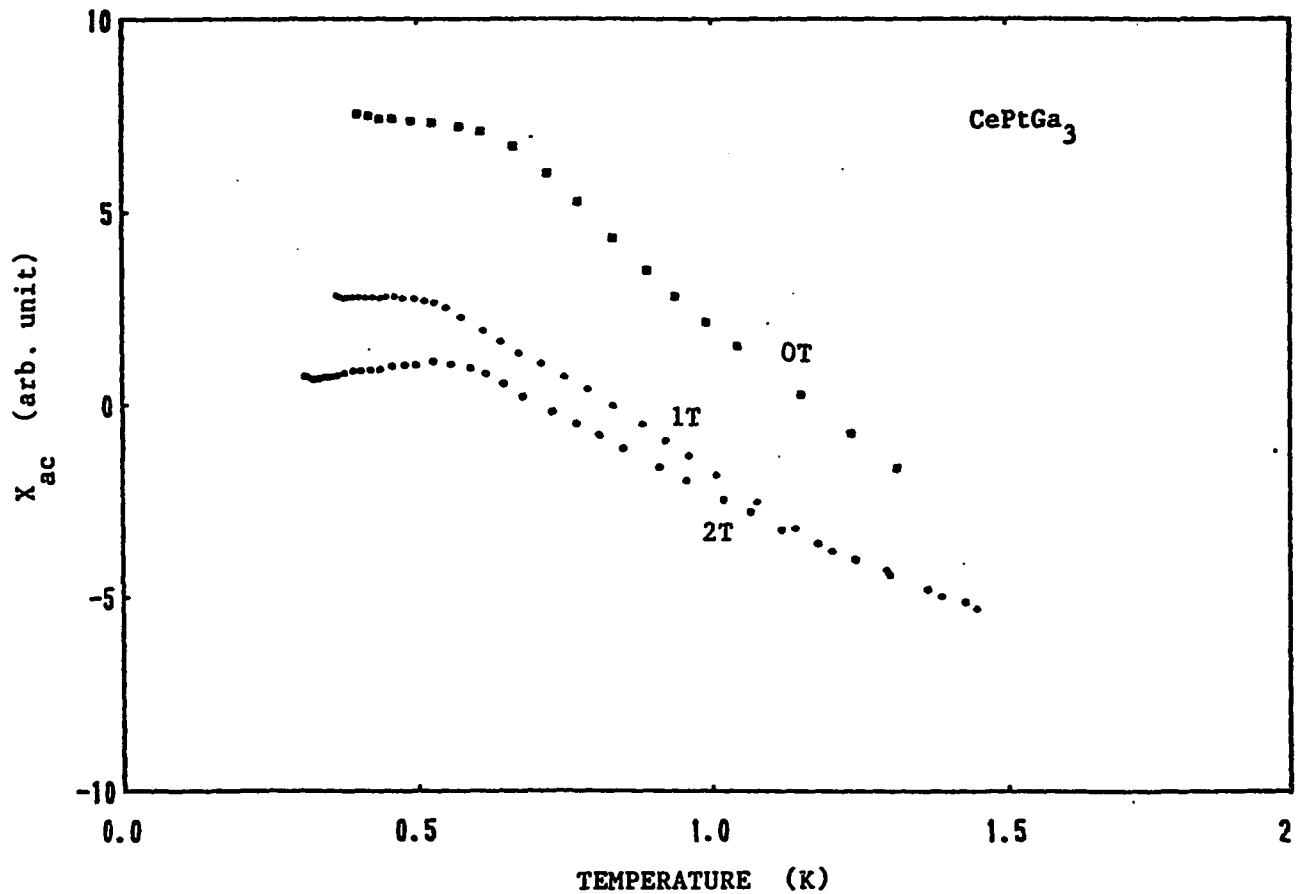

Fig. 15. The ac magnetic susceptibility χ_{ac} in different applied fields

strong. Additional measurements on the other two $CePtGa_{\sim 3}$ samples, which are free of this second phase, would be helpful.

Surprisingly, a peak was found in ac susceptibility ~8K (Fig. 16), which was also confirmed in the Faraday magnetic susceptibility measurement (see below). In a previous report [53] we were unable to explain the origin of this peak. But it is now believed that this peak is due to a magnetic impurity. As we mentioned, many black strips were found in $CePtGa_3$ sample which turned out to be impurity phase. Since $CePt_{1.1}Ga_{2.9}$ and $CePt_{0.9}Ga_{3.1}$ are clean single phase samples, we conducted the ac susceptibility measurements on both of them from 1.4K to 20K. As shown in Fig. 17, no peak can be seen in χ_{ac} around 8K in either samples. This comparison suggests that the impurity in $CePtGa_3$ is responsible for the peak at ~8K. One curious fact is that there is no indication of a peak ~8K in heat capacity of $CePtGa_3$. Normally the heat capacity is more sensitive to a magnetic impurity than the magnetic susceptibility.

The data of $CePt_{1.1}Ga_{2.9}$ and $CePt_{0.9}Ga_{3.1}$ are less scattered than that of $CePtGa_3$. It is much more obvious that there is no peak around 2K in χ_{ac} (Fig. 17).

The dc susceptibility of $CePtGa_3$ is shown in Fig. 18 as χ^{-1} versus T for temperature range $1.3K < T < 300K$. Above 70K, it follows Curie-Weiss law. The effective moment and Curie

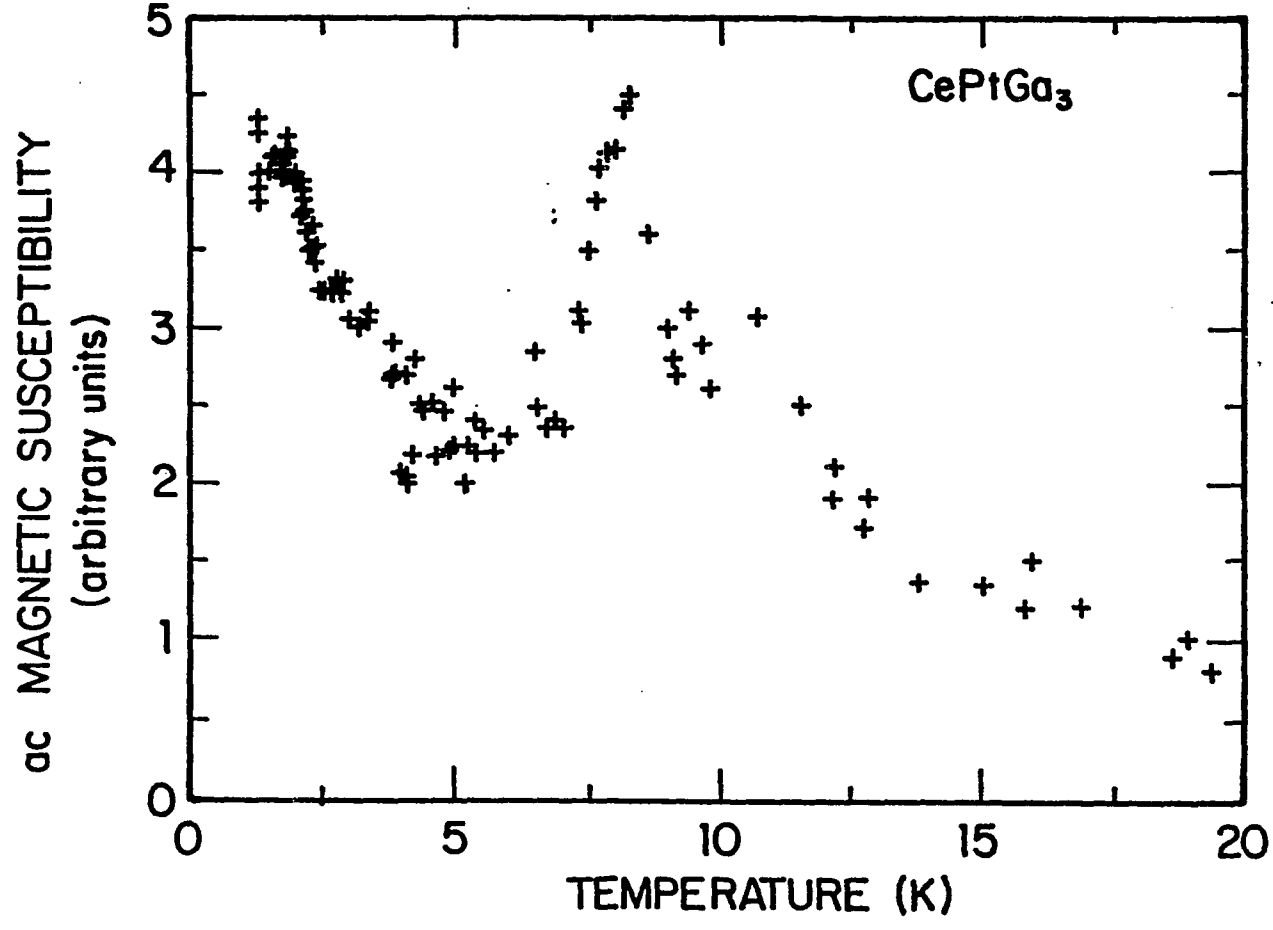

Fig. 16. The ac magnetic susceptibility χ_{ac} in zero field at higher temperatures (measuring field H = 1 Oe, frequency f = 100 Hz)

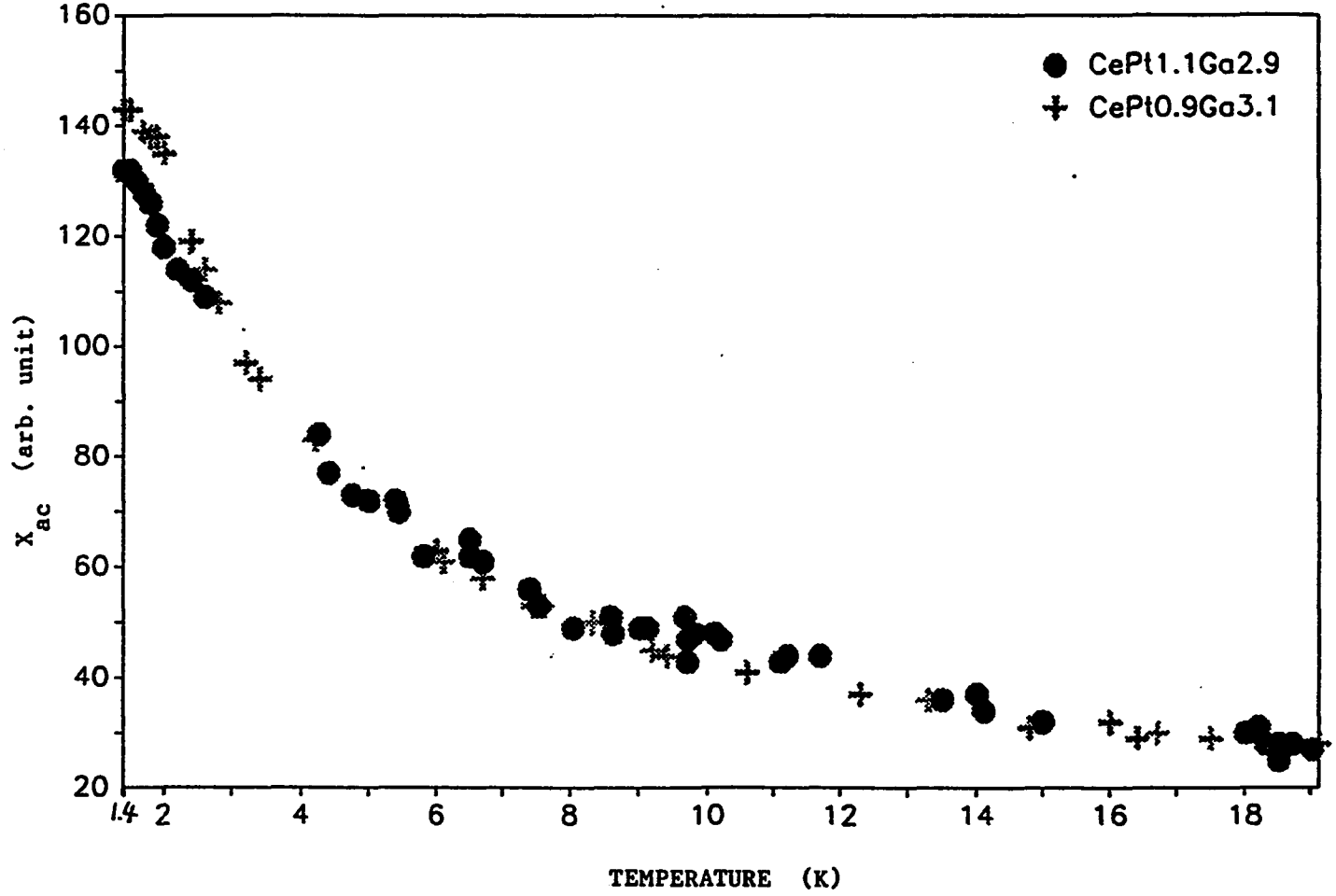

Fig. 17. χ_{ac} of $CePt_{1.1}Ga_{2.9}$ and $CePt_{0.9}Ga_{3.1}$

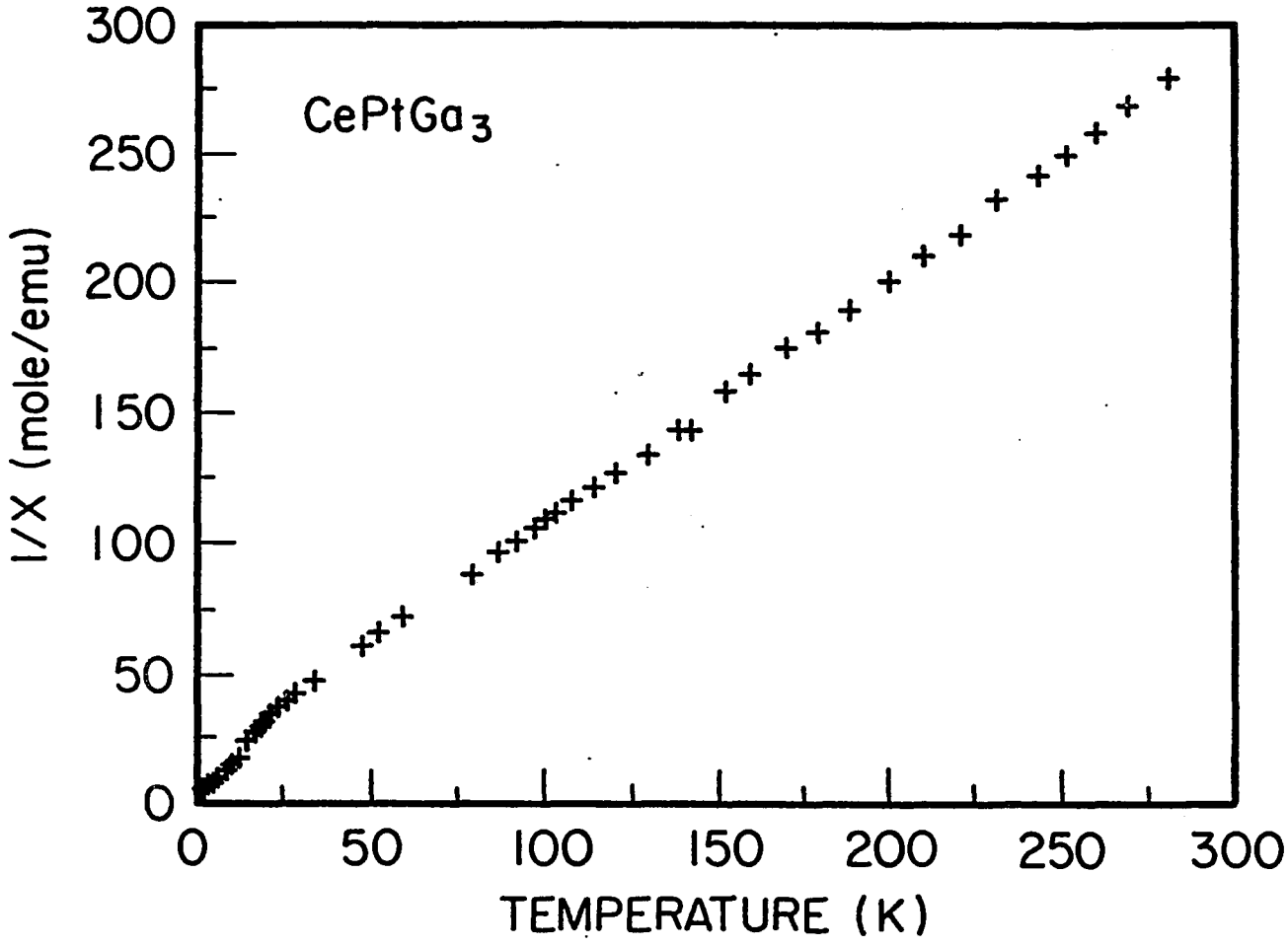

Fig. 18. The inverse dc magnetic susceptibility $1/\chi$ as a function of temperature

temperature were found to be $\mu_{eff} = 2.89\mu_B$ and $\theta_p = -14K$, respectively. The negative θ_p value for a spin glass system does not mean that the interaction between the spins is antiferromagnetic. In fact, the θ_p value can be either positive or negative depending on the deviation from random mixing [49]. χ^{-1} shows a drop above 8K which is believed to be related to the peak in ac susceptibility at ~8K.

The linear response of magnetization M to the applied magnetic field H of $CePtGa_3$ at different temperatures (Fig. 19) implies the paramagnetic behavior of $CePtGa_3$ above ~9K. At high temperature the extrapolations of the straight lines to zero field have zero intercept with M axis. As temperature is lowered below ~8.6K, non-zero intercept appears. This is an indication of the presence of magnetic impurity phase in the sample. Compared with the ac susceptibility data, there seems to be no doubt that this non-zero intercept and the peak in χ_{ac} at ~8K are from the same magnetic impurity. In order to find out what the impurity phase could be, we went through the literature to see if there is a $CePt_x$ or $CeGa_x$ or another $CePt_xGa_y$ which orders magnetically at ~8K. It was found that $CeGa_2$ (also see Sec. B) is a ferromagnet with $T_c = 8.4K$. Assuming that the impurity compound is $CeGa_2$, the amount of impurity can be estimated from the non-zero intercept M_o at H = 0. Since the saturation moment

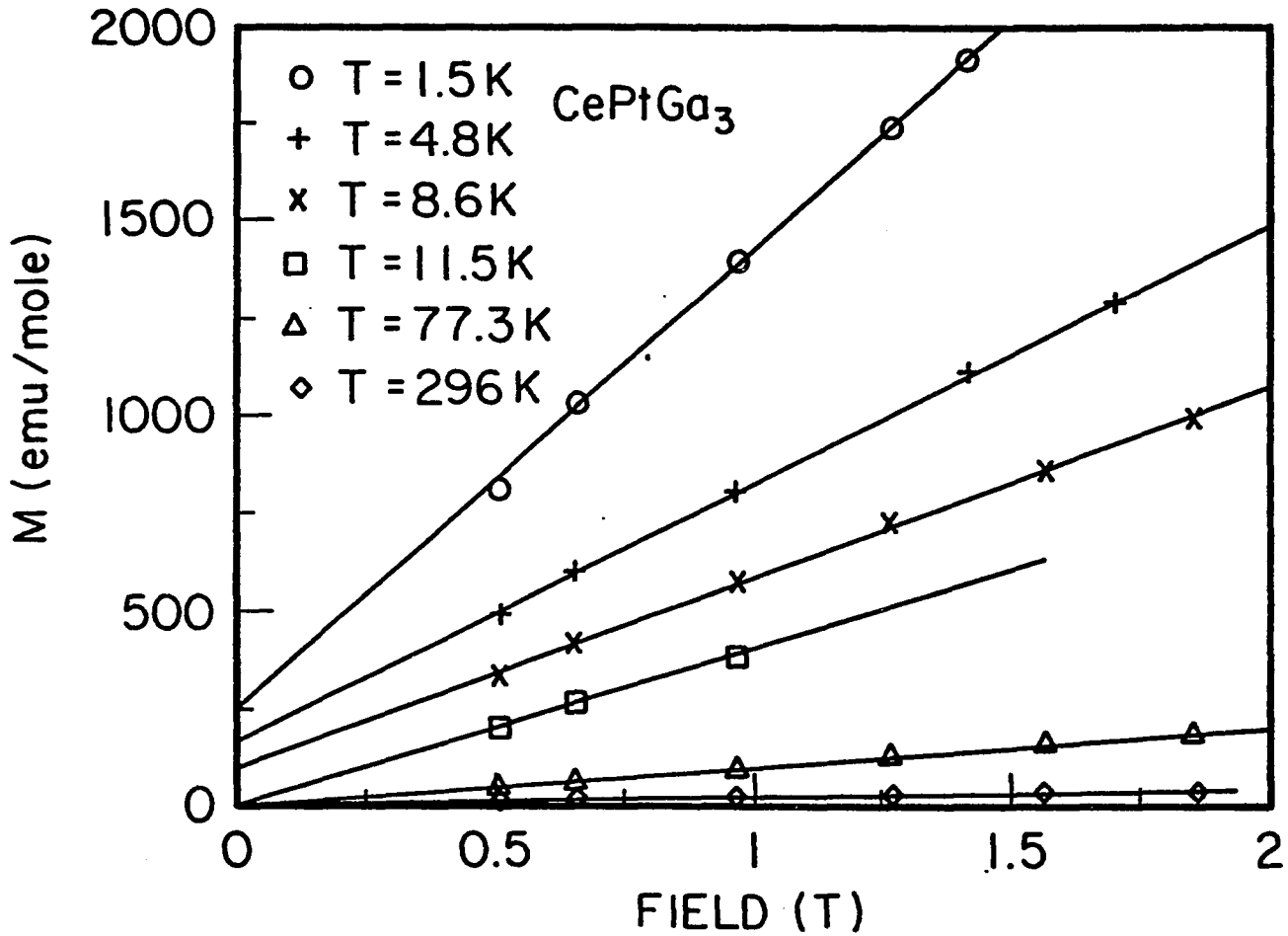

Fig. 19. Magnetization M versus applied field at different temperatures

of $CeGa_2$ is ~1.3 μ_B/Ce (Sec. B), the M_o value at 1.5K, ~250 emu/mole.Ce, infers that ~3.4% of the total Ce atoms are in $CeGa_2$, i.e., the amount of $CeGa_2$ impurity present is ~3.4%, which is consistent with the metallographic results, see Fig. 7.

5. Summary

The rounded peak in heat capacity, which was once considered as a heavy fermion behavior, is due to spin glass type transition. Unlike the ordinary spin glasses, the spin-carrying Ce^{3+} ions in $CePtGa_3$ occupy the periodic lattice sites. The random RKKY interaction between the spins which provides the basis for spin glass behavior is induced by the random distribution of Pt and Ga atoms around Ce^{3+} ions. The heat capacity and susceptibility data support this conclusion.

B. Crystalline Electric Field (CEF) Effect in $CeCd_{11}$ and $CeGa_2$

1. $CeCd_{11}$

a. Crystal structure and CEF $CeCd_{11}$ crystallizes in cubic $BaHg_{11}$-type structure, with lattice constant a = 9.319Å [54]. Detailed examination of the structure reveals that a Ce atom is surrounded by 12 nearest neighboring Cd atoms and 8 second nearest neighboring Cd atoms. Figure 20 shows the atomic

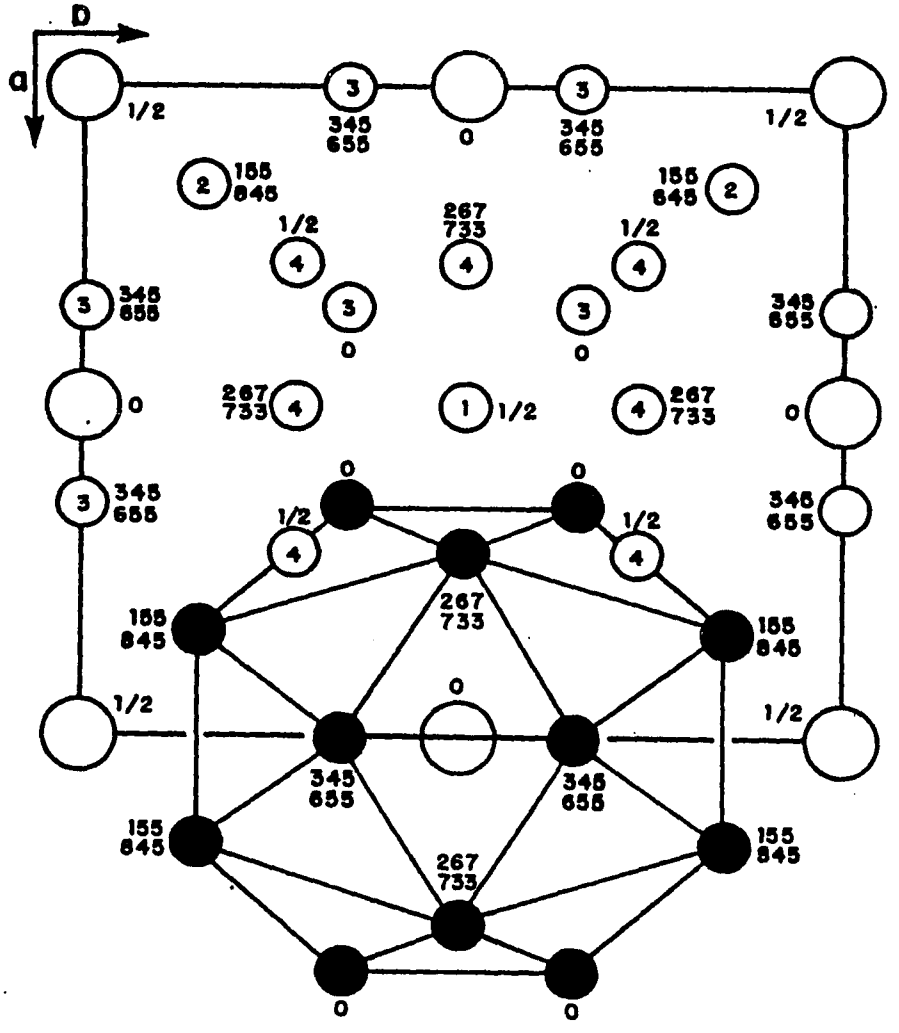

Fig. 20. A projection along the c-axis of the atomic arrangement of $CeCd_{11}$. The solid circles show the arrangement of Cd atoms about a Ce atom. The big cirles represent the Ce atoms and the small ones the Cd atoms

arrangement in $CeCd_{11}$. The neighboring Cd form a polyhedron of tetragonal symmetry about the Ce atom. Under the crystalline electric field (CEF), the 6-fold degenerate ground state of Ce^{3+} ion, $^2F_{5/2}$, will be split into three doublets. According to the CEF Hamiltonian for Ce^{3+} ion (J = 5/2) with tetragonal symmetry [55],

$$H_{CEF} = B_2^0 O_2^0 + B_4^0 O_4^0 + B_4^4 O_4^4 \qquad (9)$$

where coefficients B_n^m and operators O_n^m were defined in Hutchings [56]. The final eigenstates consist of three doublets $|\pm 1/2\rangle$, $a|\pm 5/2\rangle + b|\mp 3/2\rangle$ and $b|\pm 5/2\rangle - a|\mp 3/2\rangle$. The actual energy levels of these doublets and the values of a and b depend upon the coefficients B_n^m. This CEF splitting will influence the behaviors of heat capacity, magnetic susceptibility and electrical resistivity of $CeCd_{11}$ over the temperature range comparable to the energies of splitting. Low temperature property measurements, especially the heat capacity, allowed us to determine the energies of this 3-level CEF in $CeCd_{11}$.

b. Heat capacity The heat capacity of $CeCd_{11}$ was measured over the temperature range 1.5K < T < 70K, and it is shown in Fig. 21. Also shown in Fig. 21 is the heat capacity of $LaCd_{11}$, which is isostructural with $CeCd_{11}$. The more typical C/T vs. T^2 is shown in Fig. 22. The temperature dependence is quite unusual and the magnitude above 6K ($36K^2$) is quite large (~800

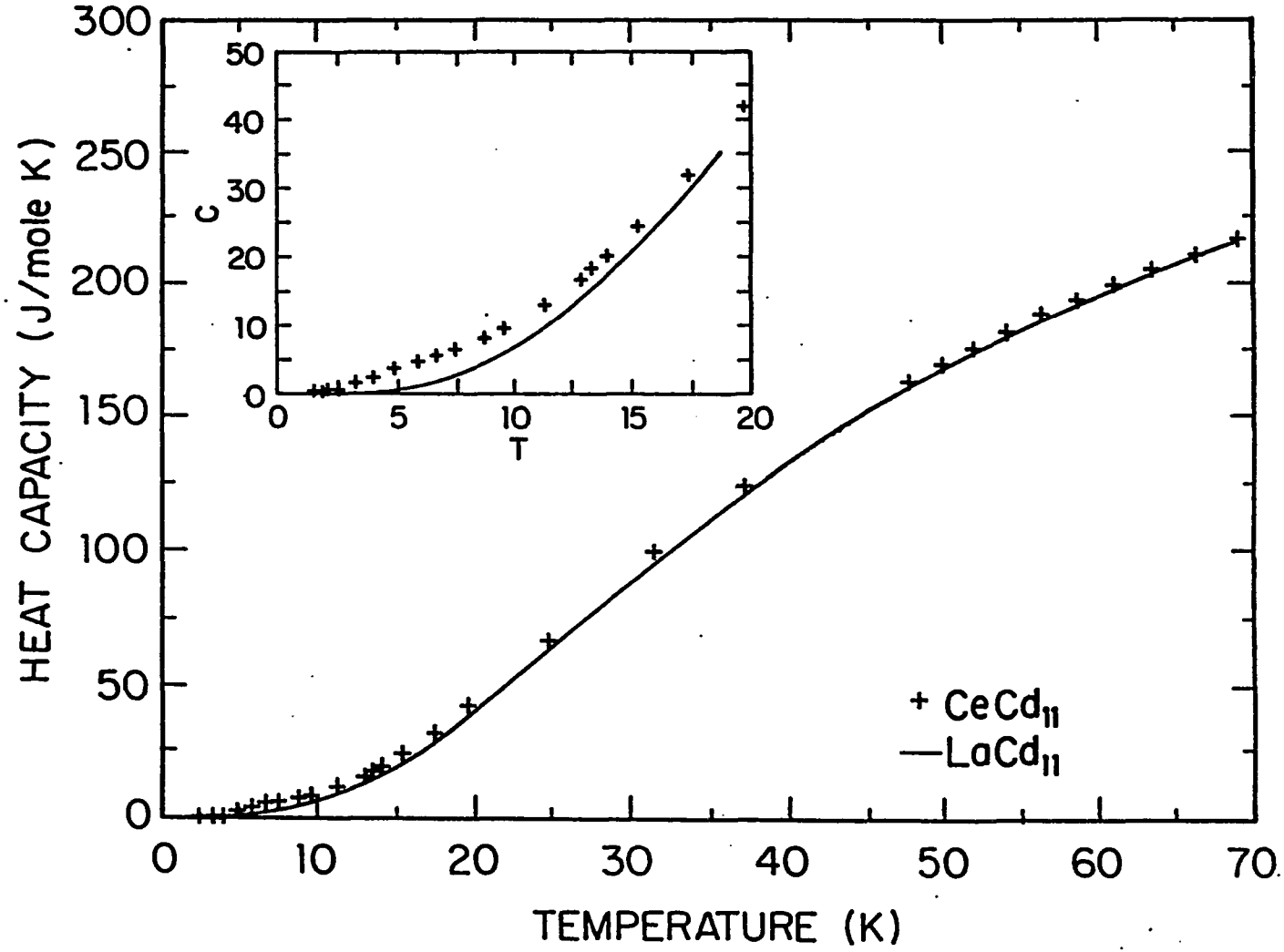

Fig. 21. Heat capacities of $CeCd_{11}$ and $LaCd_{11}$ from 1.5K to 70K. The inset shows an expanded version of the data below 20K

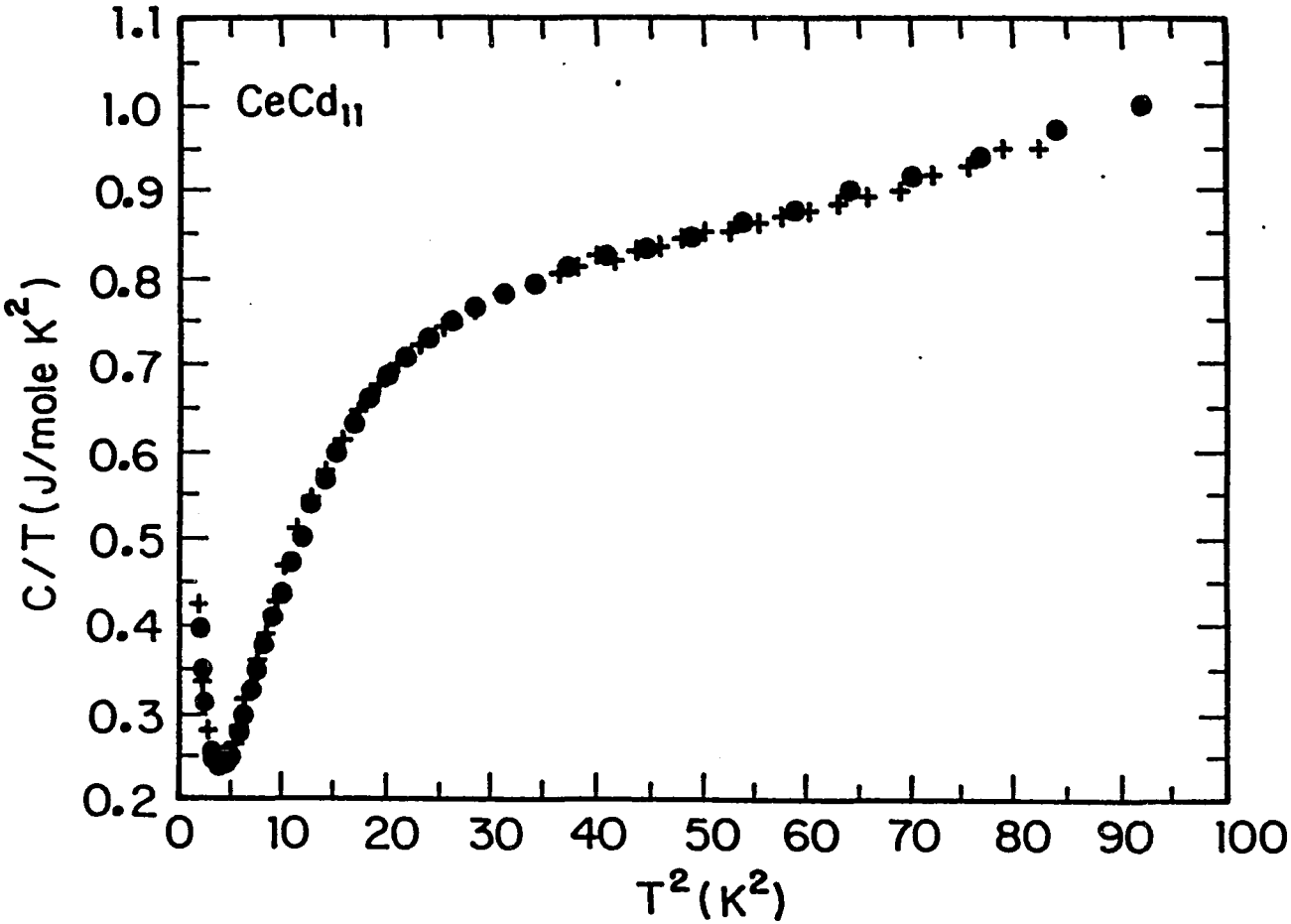

Fig. 22. C/T versus T^2 plot for $CeCd_{11}$. The crosses are for a sample weighing 1.58 g and the dots are for a sample weighing 14.27 g

mJ/mole K^2). Below 2K, it appears that $CeCd_{11}$ may be tending towards ordering magnetically. In order to understand this behavior we have assumed that the electronic and lattice heat capacities of $CeCd_{11}$ are the same as that of $LaCd_{11}$. This is quite reasonable because of the similar lattice constants (a = 9.339Å for $LaCd_{11}$ [54] and 9.313Å for $CeCd_{11}$) and the same outer electronic configurations of the two compounds (Ce is trivalent, see 1.4. Magnetic susceptibility, below). Therefore, the difference between the two heat capacities ($C_{CeCd11} - C_{LaCd11}$) should represent the contributions essentially due to the 4f electrons in Ce^{3+} ion. The shape of curve ($C_{CeCd11} - C_{LaCd11}$) versus temperature (see Fig. 23) shows a fairly sharp bump at ~7K and a broader bump at ~25K, suggesting the existence of 3-level CEF effect. The main peak near T = 7K is due to the excitation of 4f electron from ground state level to the 1st excited level and the 25K shoulder could be due to the excitation from the 1st excited level to the 2nd excited level. To make sure this interpretation is correct we calculated the magnetic heat capacity of a 3-level CEF system, which takes the form

$$C_{CEF} = \frac{R[E_1^2\exp(-E_1/T)+E_2^2\exp(-E_2/T)+(E_2-E_1)^2\exp(-(E_1+E_2)/T)]}{T^2[1+\exp(-E_1/T)+\exp(-E_2/T)]^2} \quad (10)$$

where R is the universal gas constant, E_1 and E_2 are the energies

Fig. 23. The difference of the two heat capacities ($C_{CeCd11} - C_{LaCd11}$) (+) and $C_{CEF} + \gamma' T$ (line). Inset: energy levels of the CEF

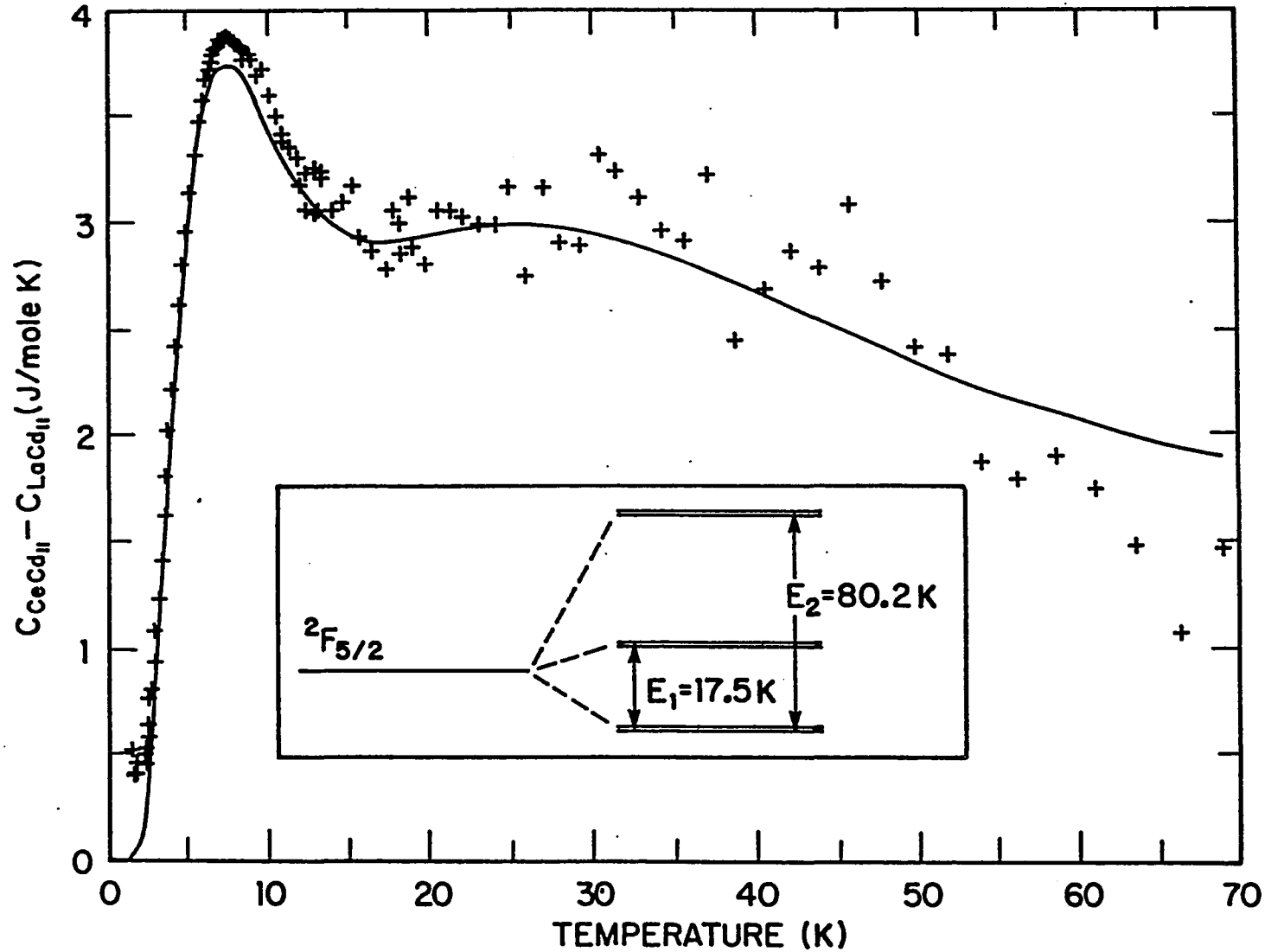
4
3
2
1
0
0
10
20
30
40
50
60
70
TEMPERATURE (K)
$C_{CeCd_{11}} - C_{LaCd_{11}}$ (J/mole K)
$^2F_{5/2}$
E_2=80.2 K
E_1=17.5 K

(in K) of the 1st and 2nd excited levels, respectively. After several trials of fitting, C_{CEF} to $C_{CeCd11} - C_{LaCd11}$, good agreement between the two was obtained when we added a small linear term $\gamma' T$ to the calculated C_{CEF}. Shown in Fig. 23 (solid line) is the function $C_{CEF} + \gamma' T$. The agreement between this function and the experiment is obvious. Energy levels and the constant γ' obtained in this manner are:

$$E_0 = 0, \tag{11}$$

$$E_1 = 17.5K, \tag{12}$$

$$E_2 = 80.2K, \tag{13}$$

$$\gamma' = 9.0 \text{ mJ/mole } K^2. \tag{14}$$

$E_1 = 17.5K$ is one of the lowest CEF splittings found in Ce compounds. The only Ce compound having a lower CEF splitting, that we know of, is cerium ethylsulphate with $E_1 = 6.6K$ [57]. Usually CEF splittings occur at temperatures 5 times to an order of magnitude higher.

$\gamma' T$ is the electronic contribution to heat capacity of $CeCd_{11}$ in excess of that of $LaCd_{11}$. The electronic specific heat constant, γ, and the Debye temperature θ_D of $LaCd_{11}$ are 17 mJ/mole K^2 and 280K, respectively, and were obtained from a least squares fit of the data to a C/T versus T^2 plot between 1.3K and 2.5K. Adding γ' to the γ of $LaCd_{11}$, the electric specific heat

constant is estimated to be 26 mJ/mole K^2 for $CeCd_{11}$. The Debye temperature of $CeCd_{11}$ is assumed to be 280K.

The magnetic entropy, S_m, associated with our heat capacity data was also calculated. Near T = 70K, S_m reaches a value close to 9.13 J/mole K (Fig. 24), which is the expected value for a 3-level CEF system

$$S_{CEF} = R\ln(m) = R\ln 3 = 9.13 \text{ J/mole K.} \qquad (15)$$

In the above expression, m is the number of doublets in a CEF system [58], where m = 3 in our case. The agreement between the experimental entropy and the theoretical value confirms the splitting of a 3-level CEF. Since J = 5/2 for Ce^{3+}, we expect the total magnetic entropy $S_m^{tot} = R\ln(2J + 1) = R\ln 6$. Knowing the entropy associated with CEF is Rln3, we believe that the difference (Rln6 - Rln3 = Rln2) is associated with magnetic ordering below T = 1.3K. Because of the low temperature limit of our apparatus we were unable to make measurements below 1.3K, but the tendency toward magnetic ordering at a lower temperature can be clearly seen from the upturn in heat capacity at T ~2K (and is also evident in the magnetic susceptibility, see 1.4.). Also it is not difficult to understand that the offset between the experiment and $C_{CEF} + \gamma' T$ (Fig. 23) below ~10K is due to the non-zero tail of the magnetic ordering peak.

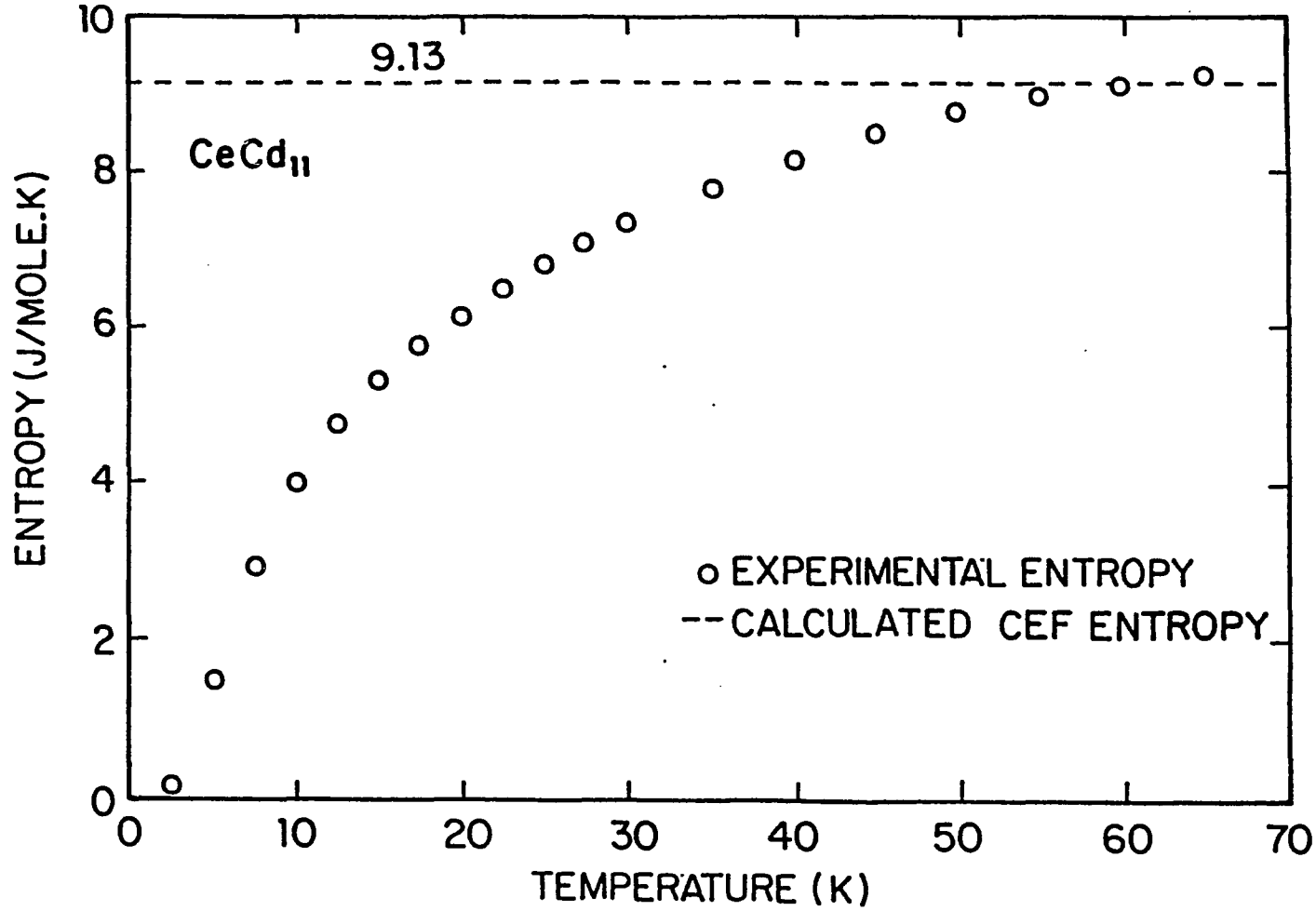

Fig. 24. Entropy associated with the CEF

c. ac resistivity The ac resistivity of our $CeCd_{11}$ sample is shown in Fig. 25. The resistivity data over a wider temperature range is also shown in the Fig. 25 inset. We can see that there is a resistivity drop near T = 7K as temperature decreases. We believe this is associated with the spin-disorder resistivity of a CEF system. Since the 2nd excited level lies high above both the ground and the 1st excited levels, we assume that the 2nd excited level remains unoccupied over the temperature of concern and treat resistivity as a 2-level system. According to V. Rao and W. Wallace [59], the spin-disorder resistivity of a 2-level CEF system can be derived from the first Born approximation. It follows below:

$$\rho_s = \frac{A + B\exp(-E_1/T)}{1 + \exp(-E_1/T)} + \frac{C}{(1 + \exp(-E_1/T))(1 + \exp(E_1/T))} \quad (16)$$

where A, B and C can be determined from fitting the experimental data to this equation. The total resistivity is composed of three parts. One is the spin-disorder resistivity ρ_s as discussed above, another comes from the phonon scattering of conduction electrons ρ_{ph}, and the third part is the temperature independent residual resistivity due to impurities ρ_o. Since the phonon scattering resistivity near liquid helium temperature is about two orders of magnitude smaller than experimental

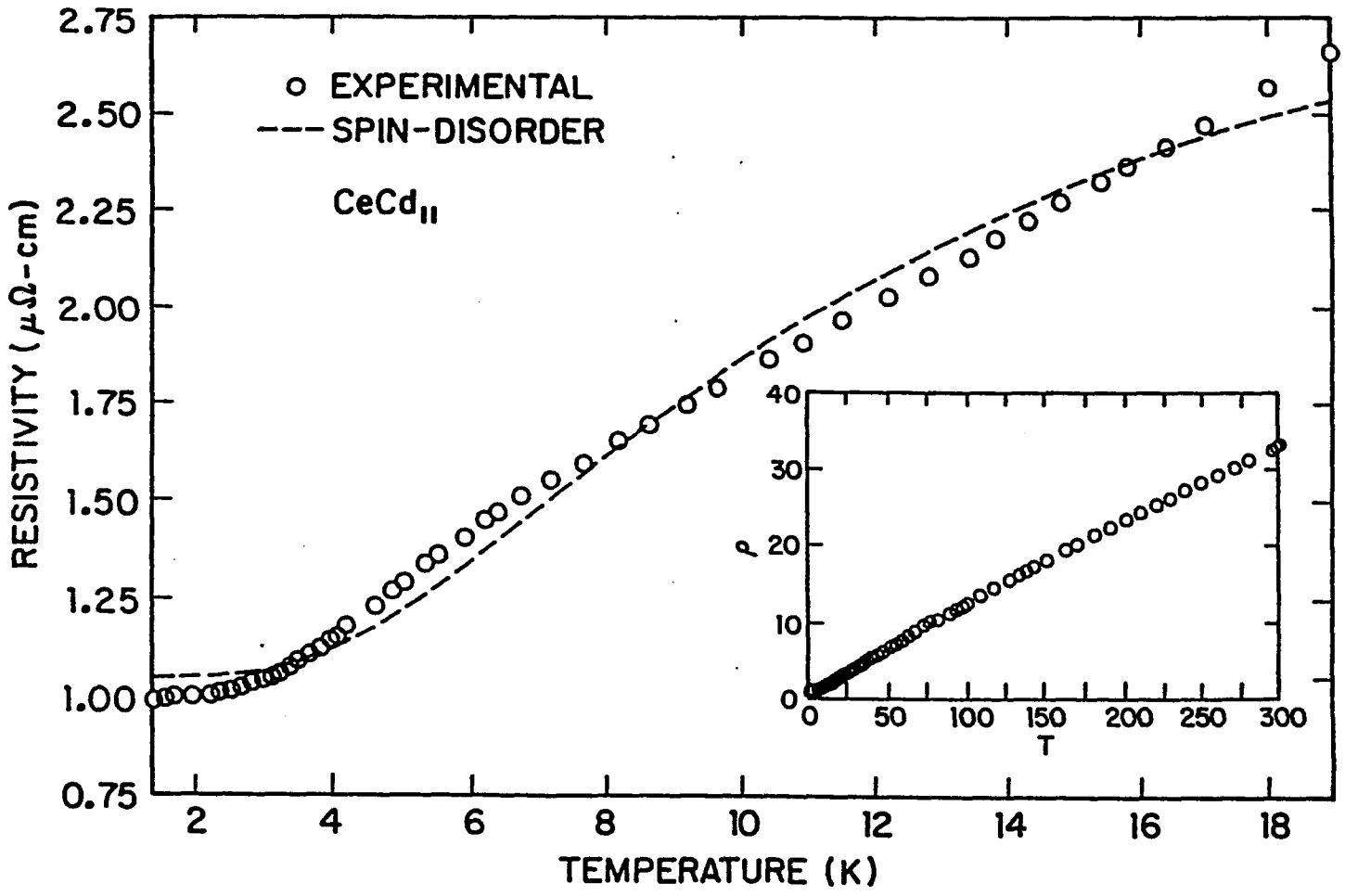

Fig. 25. Experimental resistivity of $CeCd_{11}$ (circles) and $\rho_{tot} = \rho_o + \rho_s$ (line), with A = 0.394, B = 4.04, C = 2.20 and ρ_o = 0.655 μΩcm. Inset: experimental data over a wider temperature range

resistivity (estimated from Debye temperature) [60], we neglected phonon scattering resistivity ρ_{ph}. Therefore, the total resistivity is the sum of two parts

$$\rho_{tot} = \rho_o + \rho_s \tag{17}$$

This equation was taken to fit the experimental data for temperature 1.5K < T < 20K, and the constants A, B, C and ρ_o were determined. Such a determined equation is shown in Fig. 25 together with the experimental data. The values of A, B, C and ρ_o are given in the caption of Fig. 25. We see that, in spite of a slight difference between experiment and Equation (17), the drop of resistivity near T = 7K can be explained with spin-disorder resistivity as expressed by Equation (17).

d. Magnetic susceptibility The magnetic susceptibility measurement was carried out at a field H = 0.96T over the temperature range 1.5 < T < 250K. The experimental data can be expressed by the following equation for T > 4K

$$\chi = \frac{C}{(T-\theta)} f + \alpha, \tag{18}$$

where C = 0.830 emu K/mole, (19)

θ = -5.5K, (20)

$\alpha = -5.7 \times 10^{-4}$ emu/mole, (21)

Fig. 26. Magnetic susceptibility times the temperature versus temperature for $CeCd_{11}$ - a comparison of experiment with theory. The inset shows the low temperature region on an expanded scale

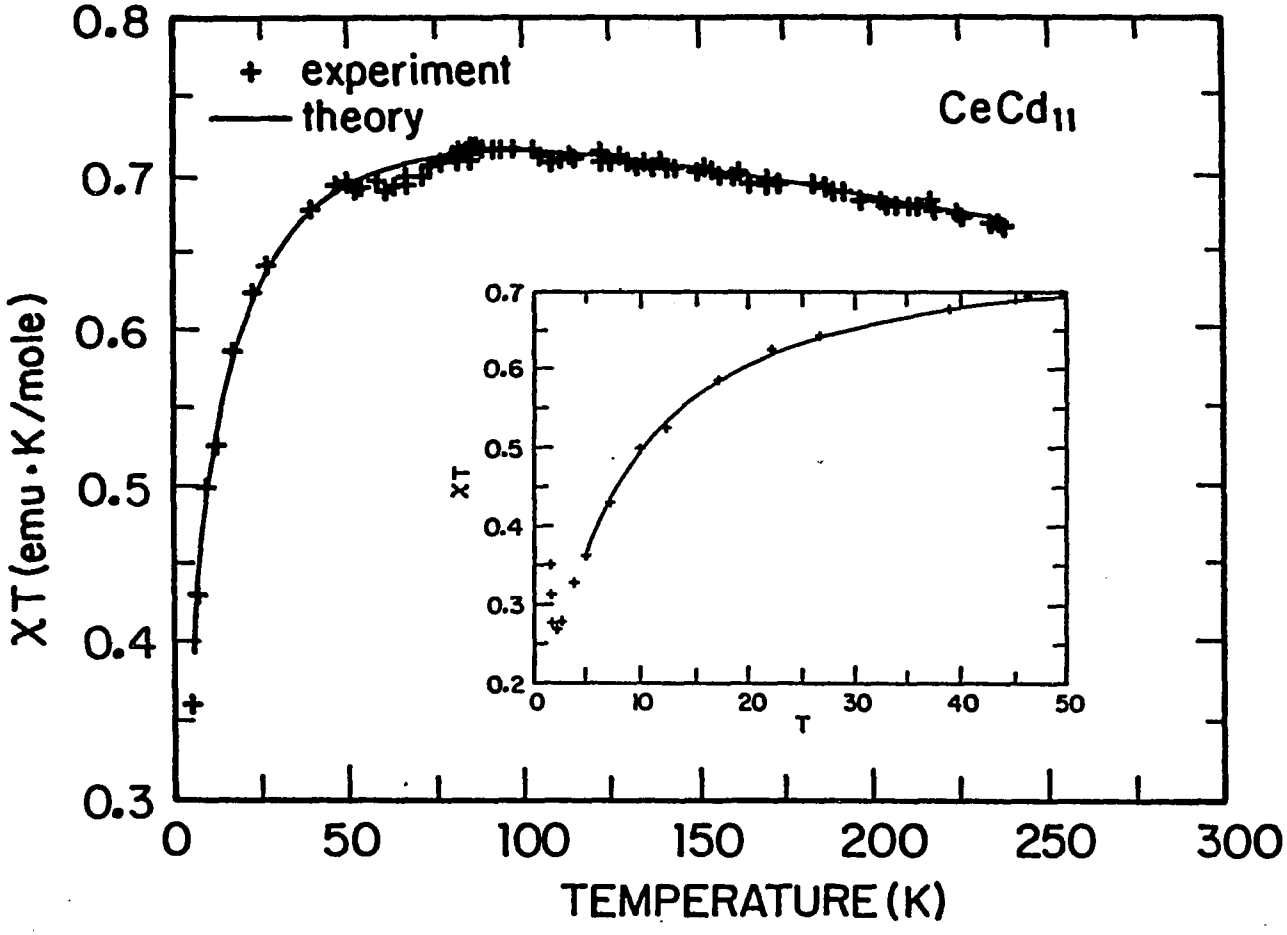
+ experiment
— theory
CeCd11
χT (emu·K/mole)
TEMPERATURE (K)
0.8
0.7
0.6
0.5
0.4
0.3
0
50
100
150
200
250
300
χT
T
0.7
0.6
0.5
0.4
0.3
0.2
0
10
20
30
40
50

and f is the modification factor due to CEF (see below). The experimental susceptibility (in the form as χT) and the fit of the data to Equation (18) are shown in Fig. 26. The term $C/(T-\theta)$ in Equation (18) is the Curie-Weiss paramagnetic contribution from 4f electrons of Ce^{3+} ions. The value of C = 0.830 corresponds to an effective moment $p_{eff} = 2.57\mu_B$, which is close to the expected theoretical value of a free Ce^{3+} ion $p_{eff} = 2.54\mu_B$ [61]. This indicates that the 4f electrons in $CeCd_{11}$ are well localized in agreement with a large Ce-Ce distance d = 6.59Å. The negative paramagnetic Curie temperature θ = -5.5K infers that the system will order antiferromagnetically at low temperature. Actually, the tendency toward magnetic ordering was seen from heat capacity data at T < 2K, as mentioned earlier (1.2.), and is seen in the inset of Fig. 26.

The 2nd term in Equation (18), α comes from the orbital motion of core electrons. Since the diamagnetic susceptibility of Cd metal is about -20×10^{-6} emu-per-gram-atom [62], we expect that the Larmor diamagnetic susceptibility of $CeCd_{11}$ would have a value of the same magnitude. The experimental value $\alpha = 5.7\times10^{-4}$ emu-per-mole, which is -52×10^{-6} emu-per-gram-atom of Cd, is in fair agreement with the value for pure Cd metal.

Under the influence of CEF, the magnetic susceptibility of a 3-level system will be modified by multiplying a factor

$$f = \frac{p_1^2 + p_2^2 \exp(-E_1/T) + p_3^2 \exp(-E_2/T)}{1 + \exp(-E_1/T) + \exp(-E_2/T)} \qquad (22)$$

to Curie-Weiss term (see Equation 18) [63], where constants p_1, p_2 and p_3 depend on the values of coefficients B_n^m in Equation (9). These constants have been determined from our experiment, $p_1 = 0.97$, $p_2 = 0.99$ and $p_3 = 1.05$. Since all of them are in the vicinity of unity, the factor f has a weak temperature dependence, which explains why the influence of CEF is hardly observed in magnetic susceptibility. Note, the large temperature dependence shown in Fig. 26 is due to the Curie-Weiss portion of Equation (18) $[C/(T-\theta)]$ and not f.

e. Summary The existence of CEF effect in $CeCd_{11}$ was established. The heat capacity data and associated magnetic entropy confirmed the splitting of a 6-fold degenerate ground state into three doublets. AC resistivity showed a drop near T = 7K which can be explained by spin-disorder resistivity in presence of CEF. Both the heat capacity and magnetic susceptibility indicate that $CeCd_{11}$ orders slightly below 2K.

2. $CeGa_2$

a. Some background $CeGa_2$ has been studied by several research groups [64-69]. It crystallizes in hexagonal AlB_2-type

structure with Ce at (0,0,0) and Ga at ±(1/3,2/3,1/2). Tsai et al. [65] and Tsai and Sellmeyer [66] described $CeGa_2$ as an antiferromagnetic compound with T_N = 9.5K in which long-range ferromagnetic interaction also exists. No Kondo-like behavior was observed. Dijkman [67] reported a peak at ~9.9K in heat capacity which was broadened and shifted to a higher temperature by an applied magnetic field. The possibility of the existence of short range order above 9.9K was suggested by Dijkman from the fact that entropy associated with the peak in heat capacity is considerably smaller than Rln2. He also excluded the occurrence of intermediate valence of Ce. Burlet et al. [68] reported the neutron study of single crystal $CeGa_2$. One sample showed antiferromagnetic ordering at 9.5K with a sine wave modulated incommensurate structure. Another sample showed the incommensurate structure below 9.5K followed by a ferromagnetic ordering at 8.5K. It seems that the behavior of $CeGa_2$ is very sensitive to sample preparation and the presence of impurities. In contrast to the previous reports, they concluded that $CeGa_2$ is a Kondo lattice in which anisotropic exchange interactions are important. The CEF splitting was also determined from their inelastic neutron scattering spectra. Lately Takahashi et al. [69] studied a single crystal prepared by floating-zone technique. The resistivity data show no Kondo-like behavior,

which agrees with the reports of Tsai et al. and Dijkman. The heat capacity and magnetic measurement indicate that $CeGa_2$ undergoes a series of antiferromagnetic phase transitions between 8.4K and 11.4K before it finally orders ferromagnetically below 8.4K. Total entropy associated with these multiple phase transitions is estimated to be about Rln2.

b. Our results As a part of an effort to clarify the inconsistency of the previous reports, our experimental data on a polycrystalline sample are given here. Metallography of the sample prepared by arc-melting is shown in Fig. 27. As seen, it is a fairly clean single phase sample (The black spots are cracks on surface of the sample).

The heat capacities of $CeGa_2$ were measured from 1.3K to 20K under different magnetic fields ($1.5T < H < 10T$), and the data are shown in Fig. 28. One large combined peak at ~10K in zero field, which might be the result of the conjunctive magnetic phase transitions between 8.4K and 11.4K mentioned earlier [69], is obvious, and the peak is broadened and shifted to higher temperatures by the applied fields. This behavior seems to support the result of Takahashi et al. that $CeGa_2$ undergoes several conjunctive antiferromagnetic states of low spin-flip field ($< 0.1T$) between 8.4K and 11.4K before it reaches a ferromagnetic ground state at 8.4K. Actually, the broadening and

Fig. 27. Metallography of $CeGa_2$. Magnification: 100X.

(see text for explanation)

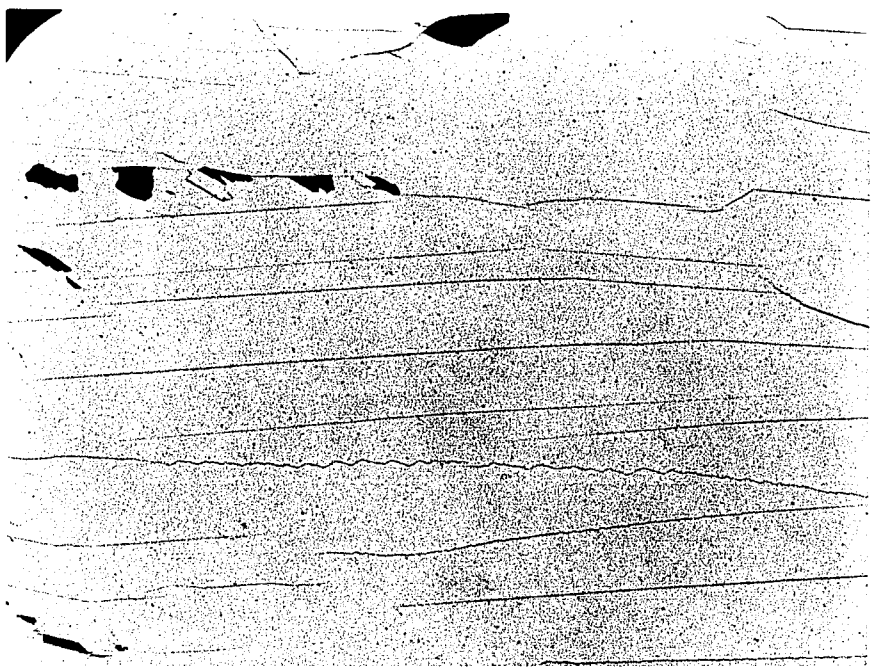

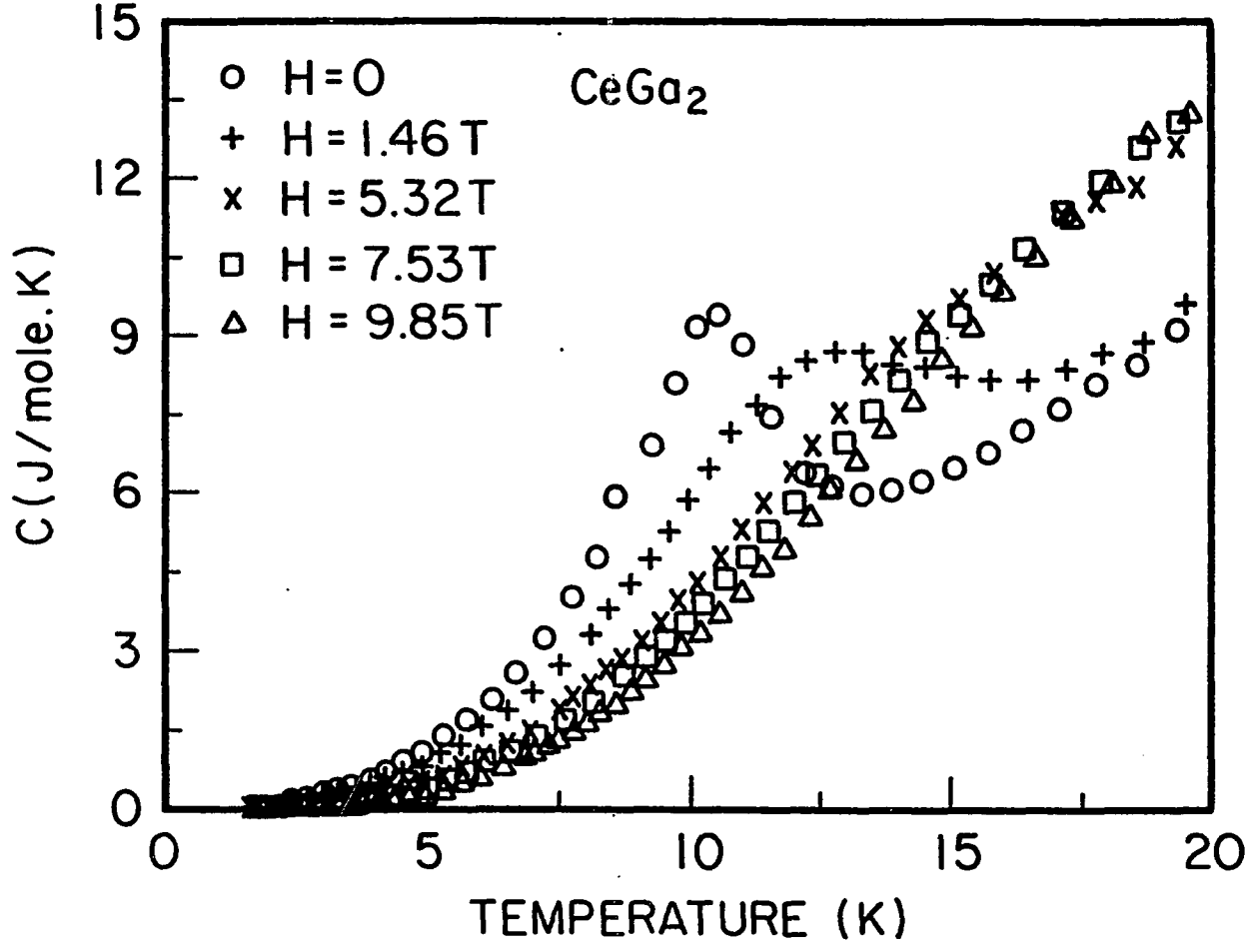

Fig. 28. Heat capacity of $CeGa_2$ in different magnetic fields

the shift of the combined peak implies that the antiferromagnetic states between 8.4K and 11.4K are unstable and destroyed by the large applied fields. It also implies that the ground state of the system is ferromagnetic in nature. This shift was seen in Dijkman's data also, but no conclusion about the nature of the ordering was given at the time.

Magnetic susceptibility measured from 1.3K to 280K under field H = 0.5T is shown in Fig. 29 as χ^{-1} versus T. It has a Curie-Weiss behavior with effective moment $\mu_{eff} = 2.85\mu_B$ and Curie temperature $\theta_p = +1.8K$. Compared with other reported θ_p values, $\theta_p = -18K$ [64], +12.5K [65] and -5K [67], it can be seen that θ_p depends very much on each individual sample. Understanding of these differences in θ_p is important because the sign of θ_p (+ or -) usually predicts the type of magnetic interaction (ferromagnetic or antiferromagnetic),

$$\theta_p = \frac{S(S+1)}{3} \frac{J_o}{k_B}, \tag{23}$$

where S is the spin quantum number, and J_o is the coupling constant [70]. A positive J_o corresponds to a ferromagnetic coupling, and a negative J_o corresponds to an antiferromagnetic coupling. We believe that the differences in the measured θ_p are due to the different grain orientations in the samples. As a matter of fact, susceptibility measurement on a single crystal

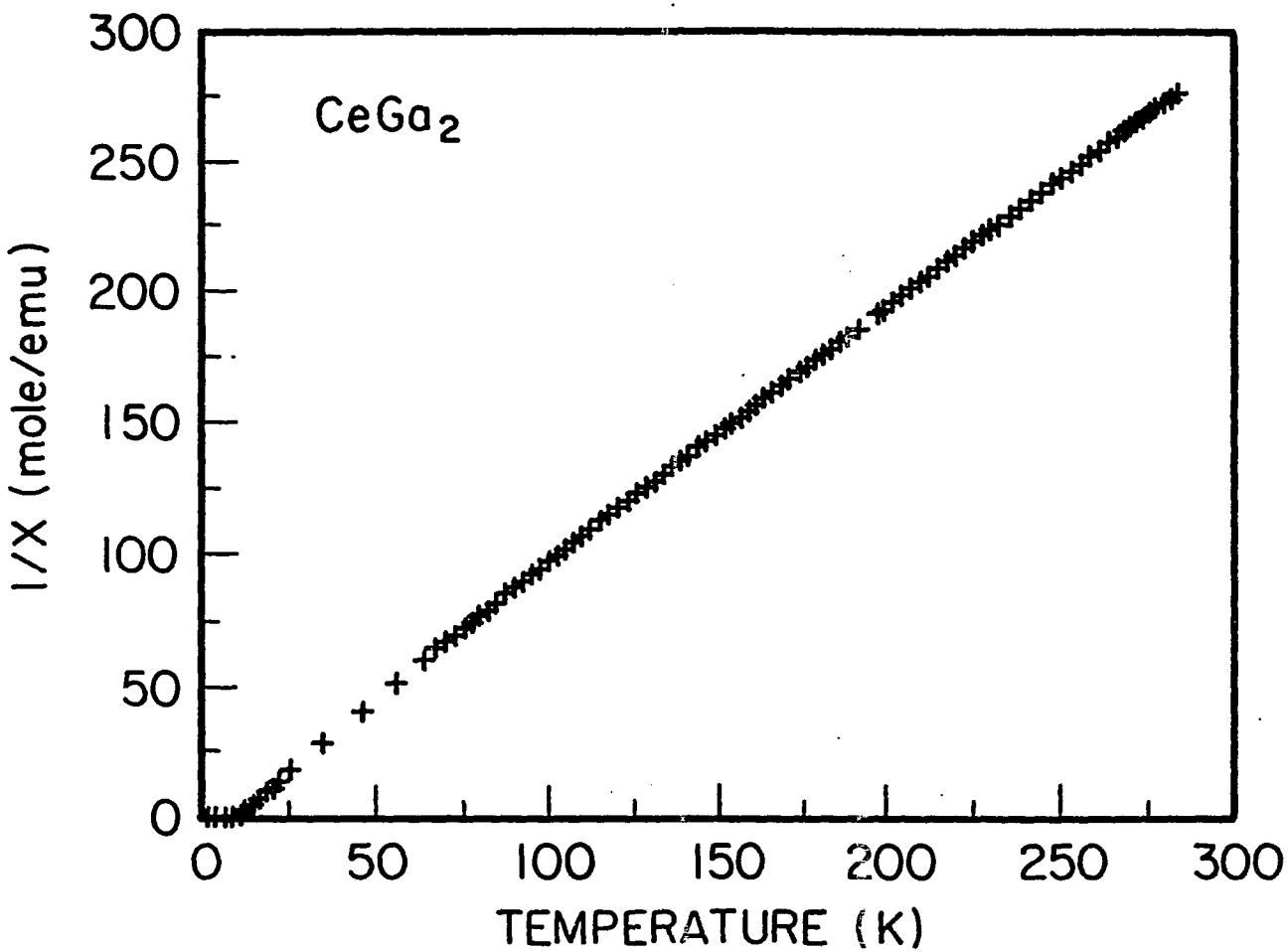

Fig. 29. The inverse magnetic susceptibility as a function of temperature

sample in both parallel to c axis and perpendicular to c axis gave θ_p(para) = -107K and θ_p(perp) = 22K [68,69]. It is not difficult to understand that, depending on the orientations of each individual grain, theoretically we can have any value of θ_p between -107K and 22K for a polycrystalline sample. Clear indication of ferromagnetic ground state can be seen from the saturation behavior in low temperature magnetic moment M versus T plot (Fig. 30).

c. CEF in $CeGa_2$ Shown in Fig. 31 is the heat capacities of $CeGa_2$ and isostructural $LaGa_2$ as C/T versus T^2 in zero field. Data are taken from another independent experiment, in which temperature range is expanded to (1.3-70K). Above the peak temperature, the C/T versus T^2 curve of $CeGa_2$ follows nearly a straight line. The extrapolation of the straight line to 0K gives a moderately large C/T value (~340 mJ/mole K^2), which might suggest heavy fermion (Kondo lattice) behavior. The origin of this moderately large heat capacity is now believed to be due to CEF effect in $CeGa_2$ rather than a Kondo lattice effect. The CEF in a hexagonal structure of $CeGa_2$ will split the 6-fold degenerate ground state of Ce^{3+} ion, $^2F_{5/2}$ into three doublets $<\pm 1/2|$, $<\pm 3/2|$ and $<\pm 5/2|$ [71]. According to the inelastic neutron scattering experiment on $CeGa_2$ by Burlet et al. [68], the CEF energy levels of the three doublets are 0, 62.5K and 310K,

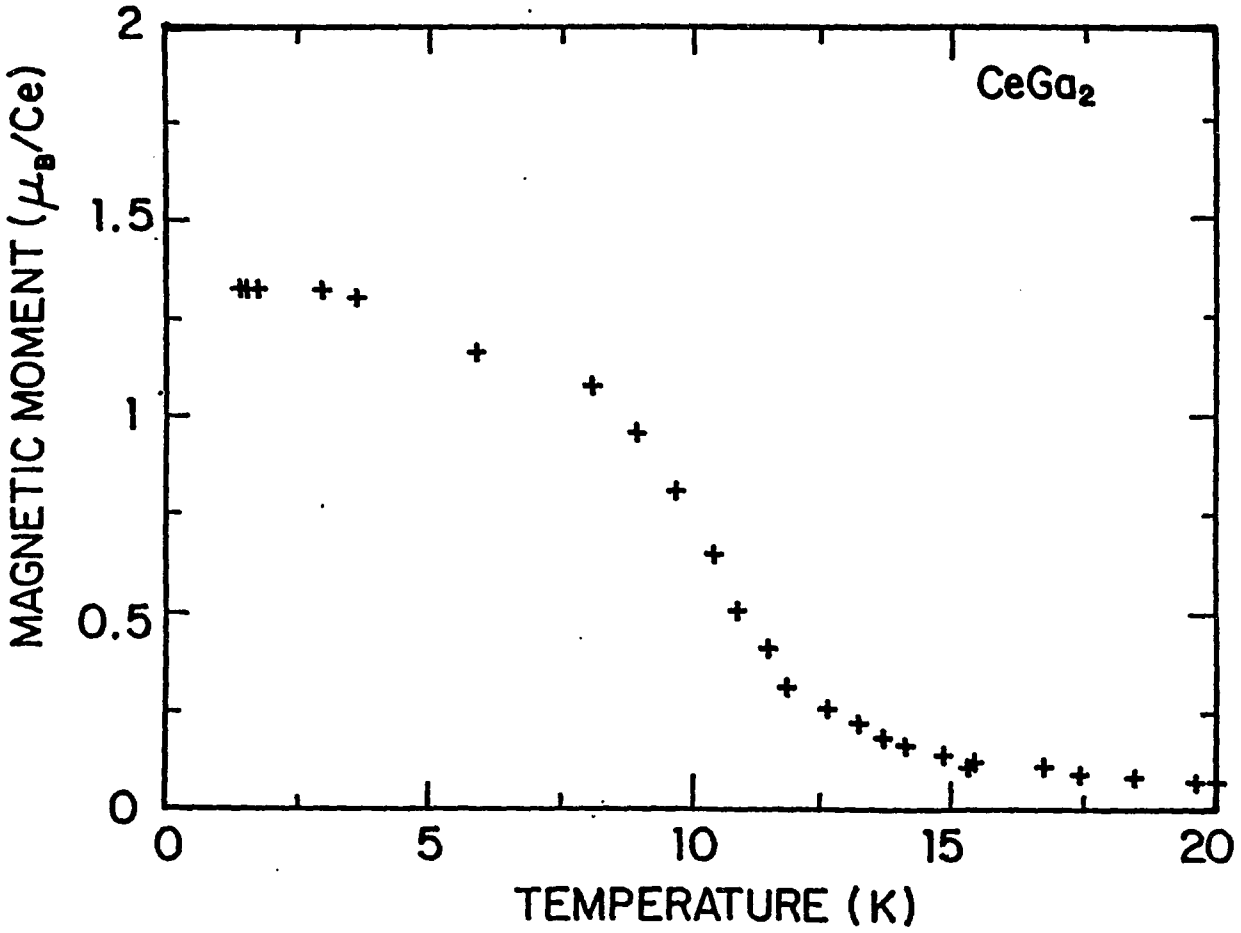

Fig. 30. Low temperature magnetic moment of $CeGa_2$

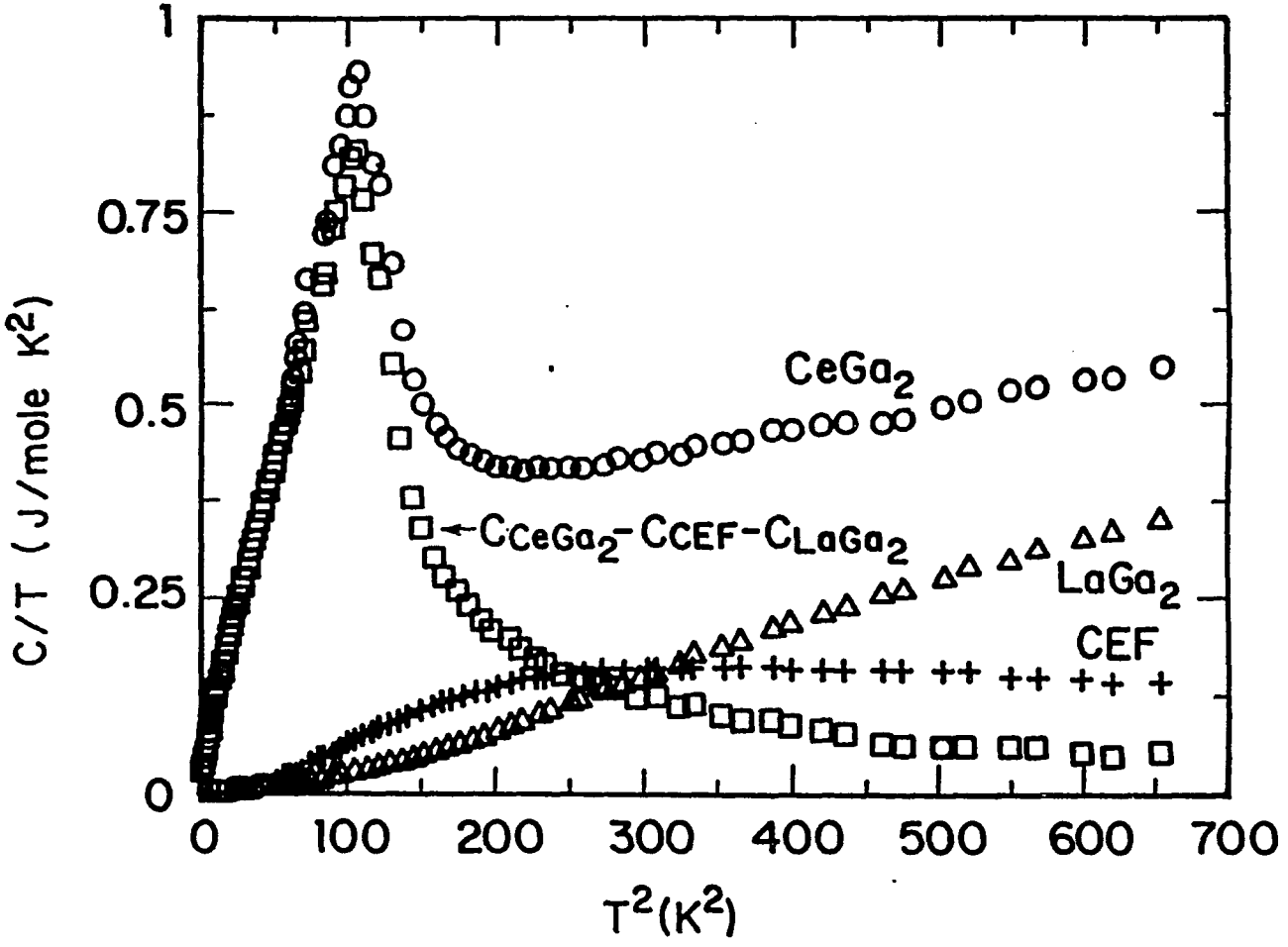

Fig. 31. C/T versus T^2 of C_{CeGa2}, C_{CEF}, C_{LaGa2} and $(C_{CeGa2} - C_{CEF} - C_{LaGa2})$

respectively. The contribution to the heat capacity from this 3-level CEF system, which takes exactly the same form as that used for $CeCd_{11}$ (Equation 10), is significant and is shown in Fig. 31. As seen, after subtraction of the heat capacity of CEF and that of isostructural $LaGa_2$ from the heat capacity of $CeGa_2$ the difference is only a magnetic peak, in C/T values, from 0K to ~20K (i.e., ~400K^2). The entropy associated with the peak reaches Rln2 at ~25K. This suggests that the moderately large heat capacity in $CeGa_2$ is due to the CEF effect.

The electronic specific heat coefficient of $CeGa_2$ is 32.6 mJ/mole K^2, which was estimated by adding C/T value of(C_{CeGa2} C_{CEF} - C_{LaGa2}), which is a constant from 25K to 40K (500K^2 to 1600K^2, only part of this region is shown in Fig. 31), to the electronic specific heat coefficient of $LaGa_2$. The low temperature part of the C/T versus T^2 plot for $LaGa_2$ is shown in Fig. 32. It follows a straight line. The electronic specific heat coefficient and Debye temperature of $LaGa_2$ are determined from the straight line, and they are listed in the Appendix. The Debye temperature θ_D of $CeGa_2$ is assumed to be the same as that of $LaGa_2$.

In summary, our heat capacity data show no sign of heavy fermion behavior in $CeGa_2$. Magnetic behavior of the compound supports the conclusion that the ground state of the system is a

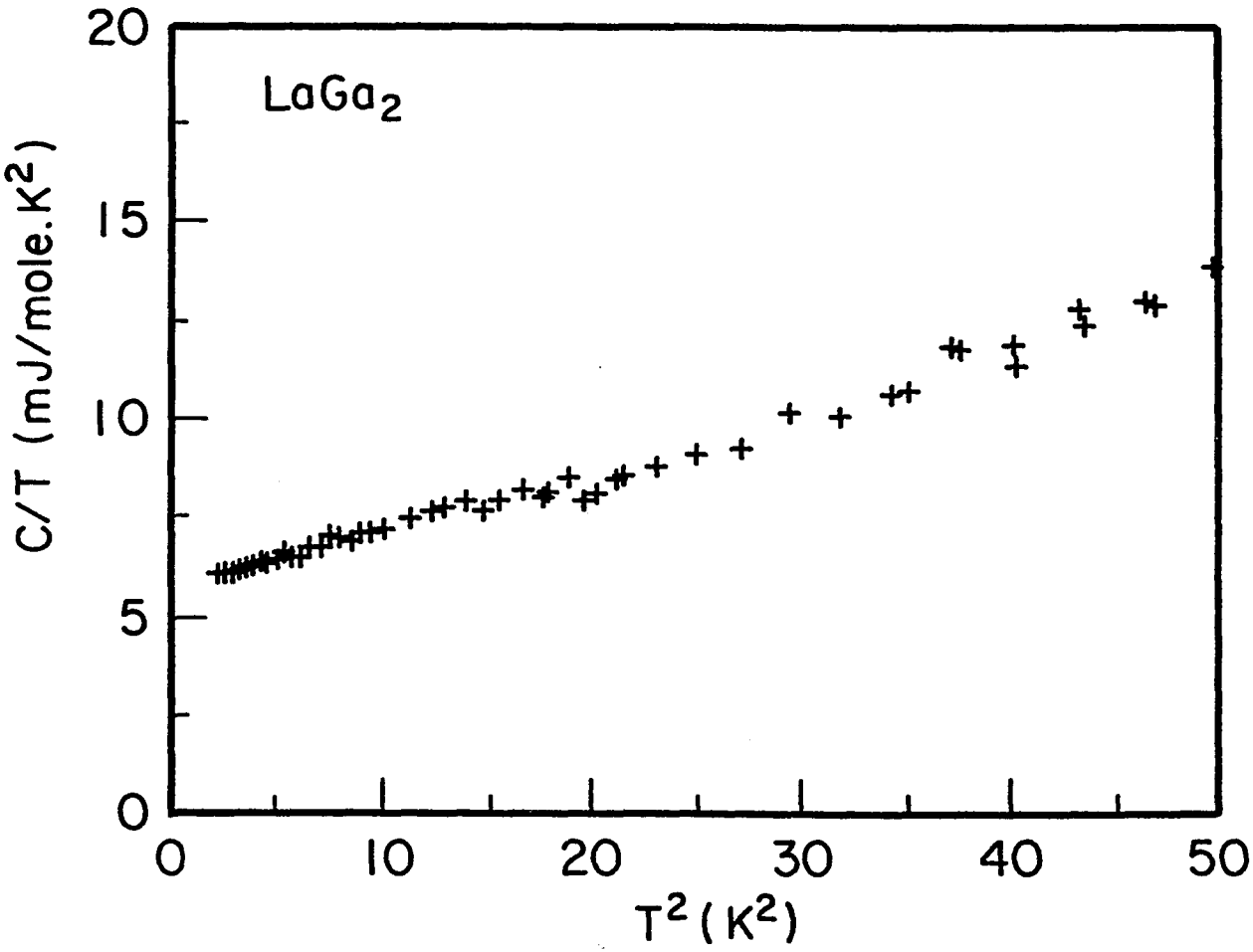

Fig. 32. C/T versus T^2 plot for $LaGa_2$

ferromagnetic one. A interesting point is that CEF effect, which plays an important role in the heat capacity of both $CeGa_2$ and $CeCd_{11}$, sometime can show up as a false signal of heavy fermion behavior when the CEF splittings are small. Precaution is recommended.

C. Some Other Ce Binary Compounds

1. $CeHg_3$

$CeHg_3$ has a hexagonal Ni_3Sn-type structure with lattice parameters a = 6.760Å and c = 4.941Å [72]. The Ce-Ce spacing in $CeHg_3$ d_{CeHg3} = 4.62Å is just slightly larger than Ce-Ce spacing in the isostructural $CeAl_3$ d_{CeAl3} = 4.43Å [10]. Since $CeAl_3$ is a typical heavy fermion, it would be interesting to study the low temperature behavior of $CeHg_3$.

$CeHg_3$ is a very unstable compound and reacts readily with air. In order to avoid its reaction with the air, the heat capacity was measured by sealing a $CeHg_3$ sample in a small brass container under helium atmosphere, then the heat capacity of the sample together with the container were measured and finally the heat capacity of the container was subtracted off. Figure 33 shows the low temperature portion of the heat capacity of $CeHg_3$ as C/T versus T^2. The magnetic peak at ~1.6K is obvious in the C

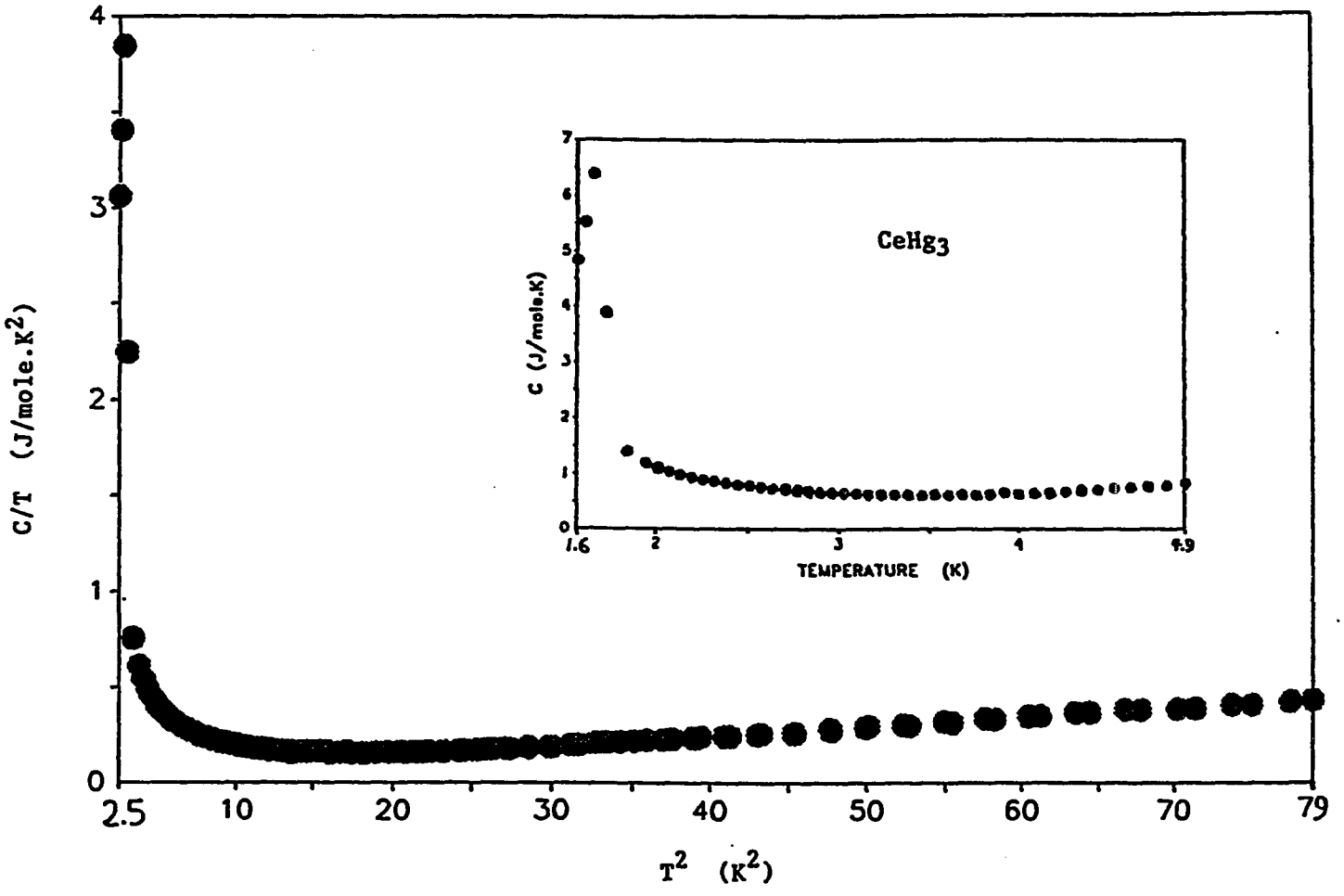

Fig. 33. C/T versus T^2 plot for $CeHg_3$. The inset shows the heat capacity as a function of T for lower temperatures

versus T plot (Fig. 33, inset). The entropy associated with this peak was estimated to be ~2.4 J/mole K, which is ~40% of the expected value Rln2 = 5.76 J/mole K. This tells us that the magnetic peak is an intrinsic property but not a impurity effect. The reason that the experimental entropy is so far off the expected value is perhaps due to the lack of experimental data below the ordering temperature. Actually we were only able to reach a temperature just below the peak (~1.5K). Therefore, the extrapolated values of the heat capacity used to calculate the entropy below the peak temperature can be significantly different from the real situation. The nature of the peak will be discussed later. Above the peak temperature, the C/T versus T^2 plot shows a straight line. The Debye temperature θ_D and electronic specific heat coefficient γ were determined and are listed in the Appendix. The γ value of 52 mJ/mole K^2 indicates that $CeHg_3$ is not a heavy fermion material. Compared with $CeAl_3$, we may conclude that by increasing the Ce-Ce spacing from 4.43Å for $CeAl_3$ to 4.62Å for $CeHg_3$ the non-magnetic heavy fermion behavior is destroyed and a magnetically ordered state is created. Although a large Ce-Ce spacing is necessary for the formation of heavy fermion state, it is not, as noted in the Introduction, a sufficient condition. Probably the 4f-p state

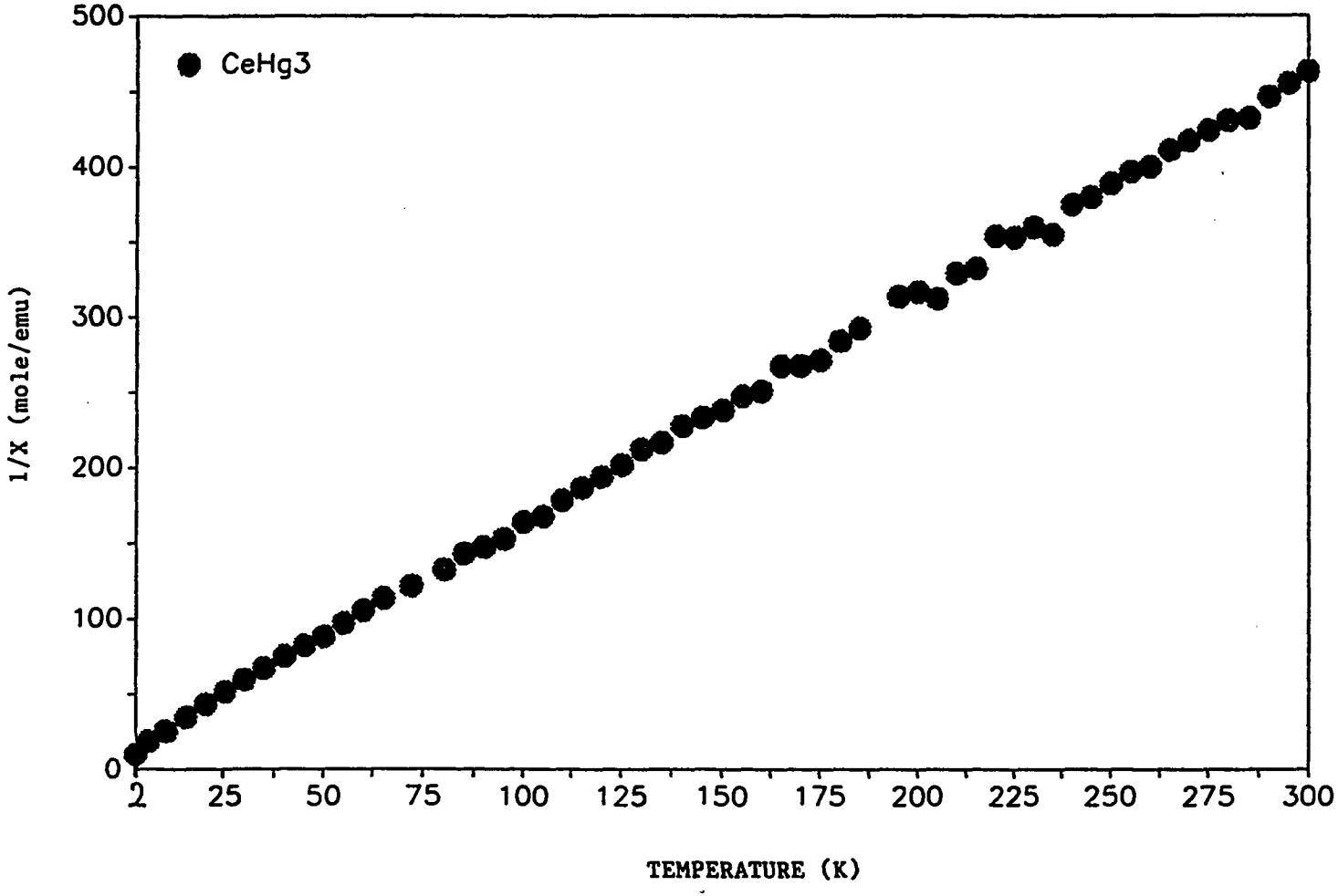

Fig. 34. The inverse magnetic susceptibility of $CeHg_3$

interaction (hybridization) changes sufficiently between Al and Hg in these CeM_3 compounds to give these different behaviors.

The inverse of magnetic susceptibility of $CeHg_3$ is shown in Fig. 34 for temperature range $2K < T < 300K$. The Curie-Weiss behavior is indicated by the straight line in this plot. The effective moment and Curie temperature were found to be $\mu_{eff} = 2.32\mu_B$ and $\theta_p = -10K$, respectively. These values are quite different from the ones of Olcese [72], who reported $\mu_{eff} = 2.93\mu_B$ and $\theta_p = -53K$. One point that both experiments agree on is the negative Curie temperature θ_p, which implies that the peak in heat capacity at ~1.6K is due to an antiferromagnetic phase transition.

2. $CeIr_5$ and $CePt_5$

a. $CeIr_5$ The superconductivity in $CeIr_5$ was first reported by Geballe et al. in 1965 [34]. Our heat capacity data confirmed this transition at T_c ~1.8K. Shown in Fig. 35 are the heat capacities of $CeIr_5$ under zero field and under field H = 1.46T. The zero-field heat capacity clearly indicates the superconducting transition at T_c ~1.8K. This critical temperature is suppressed to below 1.5K under the applied field. The value of $(C_s - C_n)/C_n$ at T_c is ~1.3, which is close to the predicted value of 1.43 from BCS theory [73].

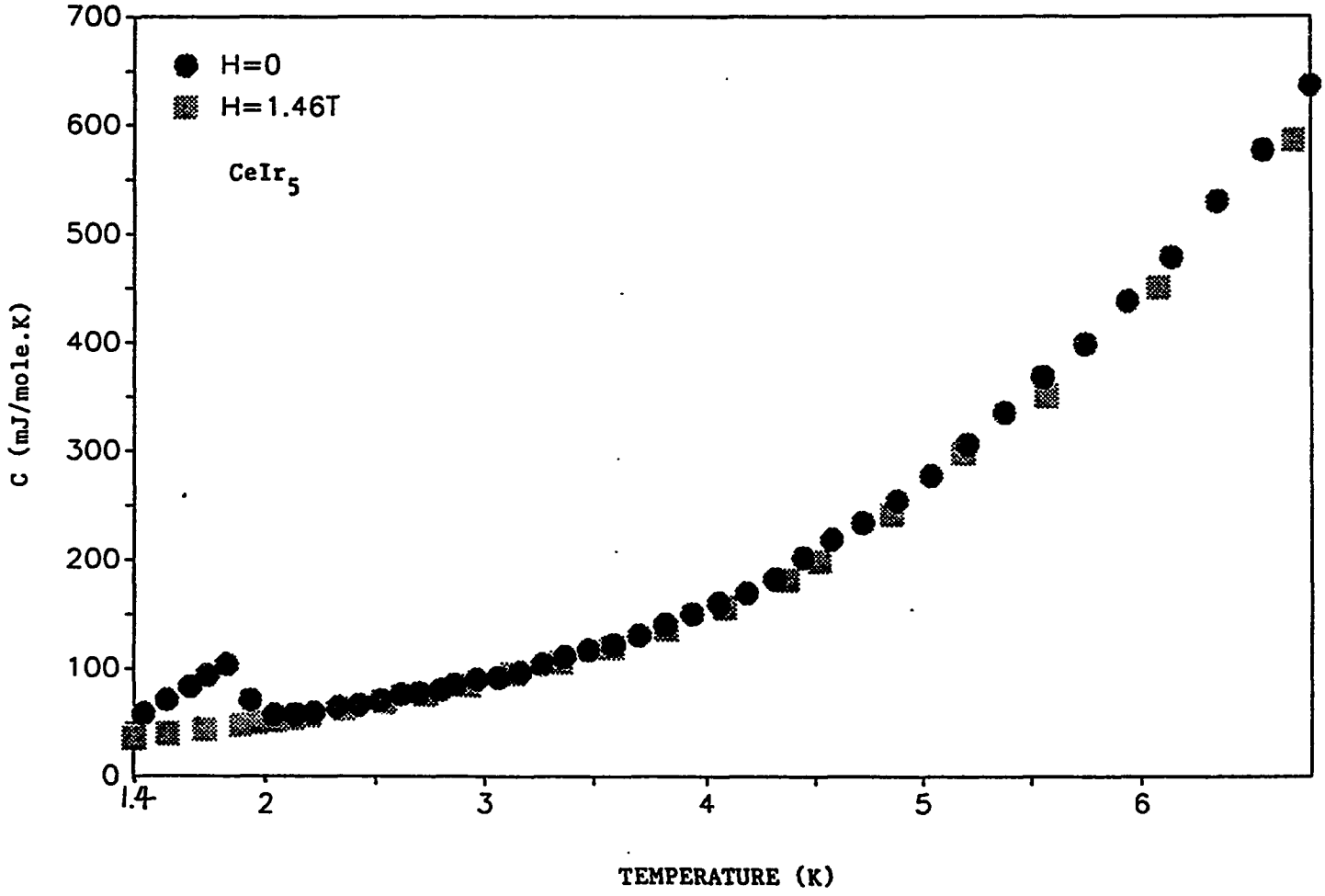

Fig. 35. Heat capacity of $CeIr_5$ in zero field and in field H = 1.46T

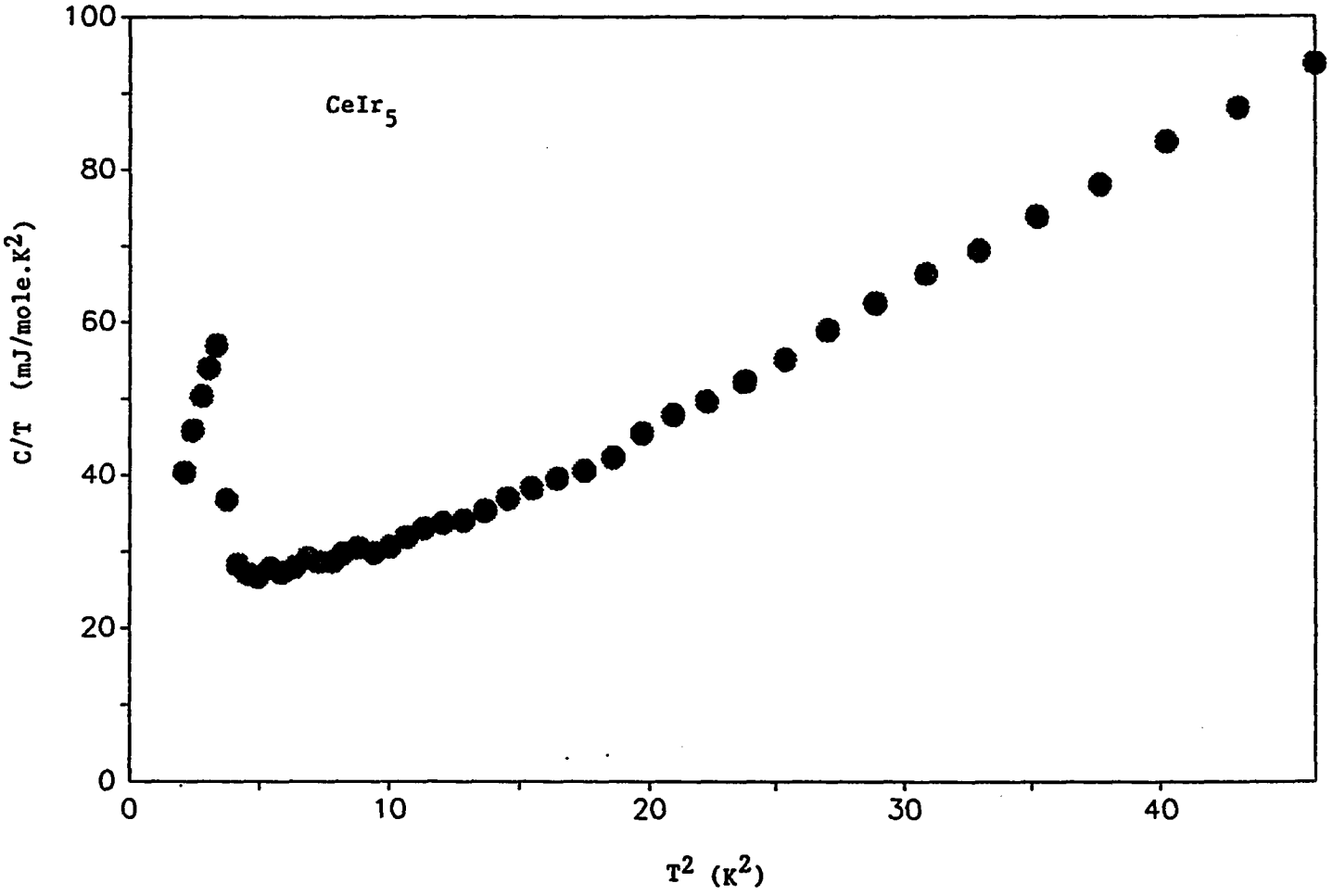

Fig. 36. C/T versus T^2 plot for $CeIr_5$ in zero field

The C/T versus T_2 plot for $CeIr_5$ (Fig. 36) follows a straight line from ~4K to ~10K (i.e., ~$15K^2$ to ~$100K^2$, only part of this region is shown). The Debye temperature θ_D and electronic specific heat coefficient γ were determined from this linear region. γ is found to be 19 mJ/mole K^2, which means that $CeIr_5$ is another ordinary non-heavy fermion compound.

The crystal structure of $CeIr_5$ is cubic $AuBe_5$-type with Ce-Ce spacing d_{Ce-Ce} = 5.31Å [74]. Although it lies high beyond the Hill limit [27], $CeIr_5$ is a superconductor. This was explained by Huber [75] who suggested that it is the transition metal (Ir), not Ce, which carries the superconductivity. Therefore Hill's criterion does not apply to this system.

It is interesting to compare $CeIr_5$ with UNi_5 and UCu_5, which also have cubic $AuBe_5$-type structures [76]. While UNi_5, with a U-U spacing of d_{U-U} = 4.796Å, has an essentially temperature independent magnetic susceptibility below room temperature and stays paramagnetic, UCu_5, with d_{U-U} = 4.973Å, orders antiferromagnetically below 15K and has a C/T value of 86 mJ/mole K^2 below 0.5K. On one hand, the magnetic ordering in UCu_5 is due to the presence of f electron carrying U atoms. On the other hand, the non-magnetic behavior of UNi_5 is determined by an almost filled Ni 3d band [76]. The transition from magnetic UCu_5 to non-magnetic UNi_5 arises from the disappearance

of U^{3+} ions in the compound. The behavior of superconductor $CeIr_5$ seems to be similar to that of UNi_5 in the sense that both of them are non-magnetic and have the characteristics of transition metal. Since Ni and Cu are immediate neighbors in periodic table, it would be interesting to replace Ir in $CeIr_5$ by its immediate neighbor Pt in order to see if the UCu_5-like behaviors, i.e., the appearance of Ce^{3+} ions, magnetic ordering and the relatively large C/T value can be found in $CePt_5$. Unfortunately, $CePt_5$, which is supposed to have a slightly larger d_{Ce-Ce} than $CeIr_5$, crystallizes in a different structure (see below). Therefore we were unable to study this trend.

Our sample contained some second phase. X-ray diffraction pattern showed that the second phase could be Ce_2Ir_7. However, the fact that $(C_s - C_n)/C_n$ at T_c is so close to the BCS theoretical value indicates that the influence of the second phase on heat capacity can be ignored.

b. $CePt_5$ $CePt_5$ has been studied by Schroder et al. [77]. It crystallizes in hexagonal $CaCu_5$-type structure. Although $CePt_5$ has a much smaller Ce-Ce spacing (d_{Ce-Ce} = 4.38Å) than $CeIr_5$ (d_{Ce-Ce} = 5.31Å, cubic $AuBe_5$ structure), it undergoes a magnetic transition at T_N = 1.0K into an antiferromagnetic structure [77]. The tendency toward magnetic ordering is clearly

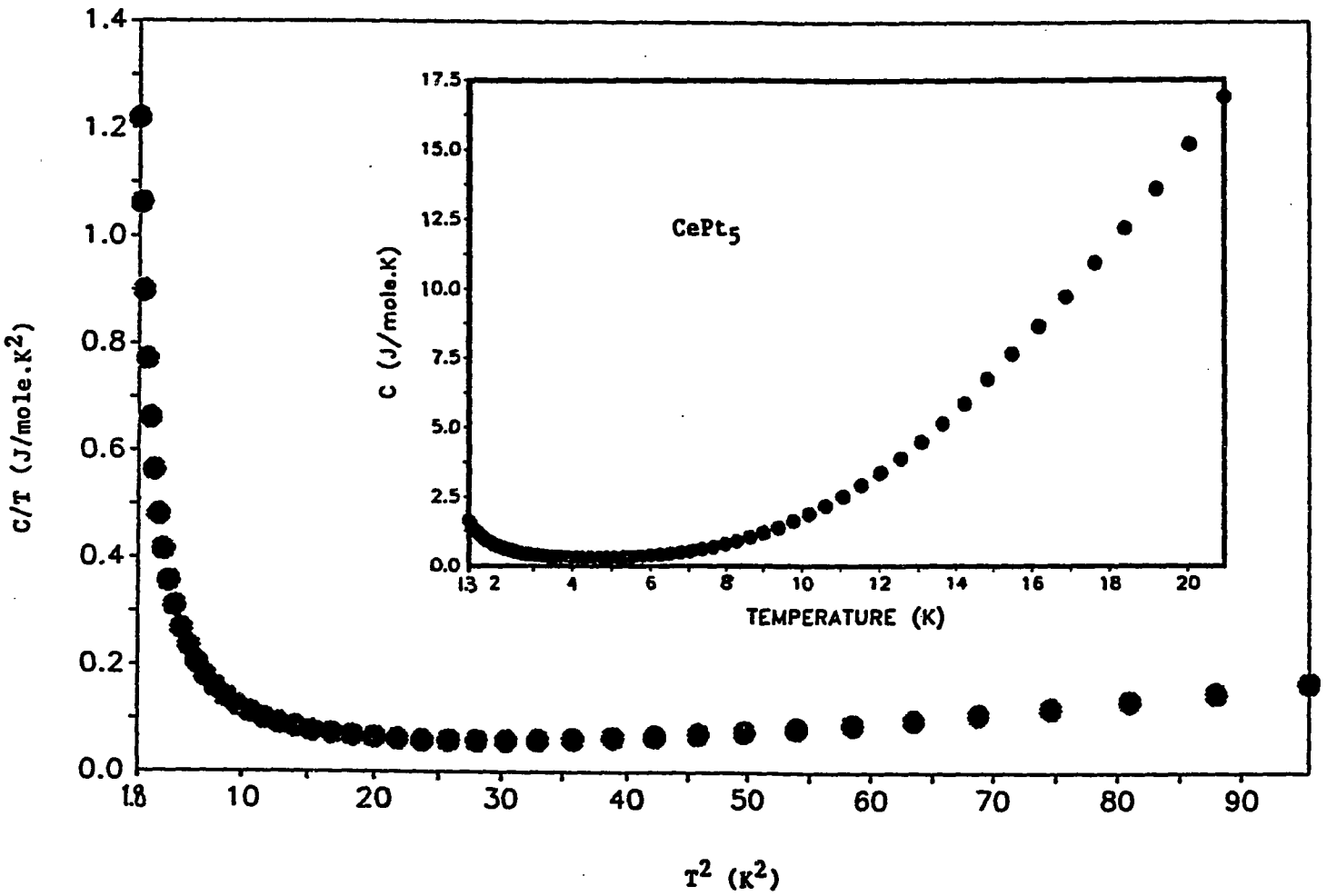

Fig. 37. C/T versus T^2 of $CePt_5$. Inset: heat capacity as a function of temperature T

seen from the upturn in our heat capacity data at ~3K (Fig. 37, inset). Because of the low temperature limit of our apparatus we were unable to make measurements below 1.3K. The electronic specific heat coefficient γ determined from the linear region of C/T versus T^2 plot ($20K^2 < T^2 < 100K^2$) (Fig. 37) is ~15 mJ/mole K^2.

3. Ce_2Zn_{17}

Ce_2Zn_{17} has been extensively studied by both Olivier et al. [78] and Sato et al. [79]. The former concluded that Ce_2Zn_{17} is a Kondo lattice (or 4f instability) from the resistivity and magnetic susceptibility behaviors. While the latter suggested that there was no evidence of dense Kondo effect for resistivity and Ce_2Zn_{17} is a stable trivalent cerium compound. They also suggested that some short range ordering occurred before the system undergoes an antiferromagnetic ordering at T_N ~1.6K from the entropy calculation.

The experiments conducted on a polycrystalline sample in our laboratory revealed that the compound showed no sign of Kondo lattice behavior and no short range ordering above T_N was evident in our sample. Figure 38 shows the heat capacity of Ce_2Zn_{17} as C/T versus T^2. The peak at ~1.7K (Fig. 38, inset) is due to the antiferromagnetic ordering just mentioned. The entropy

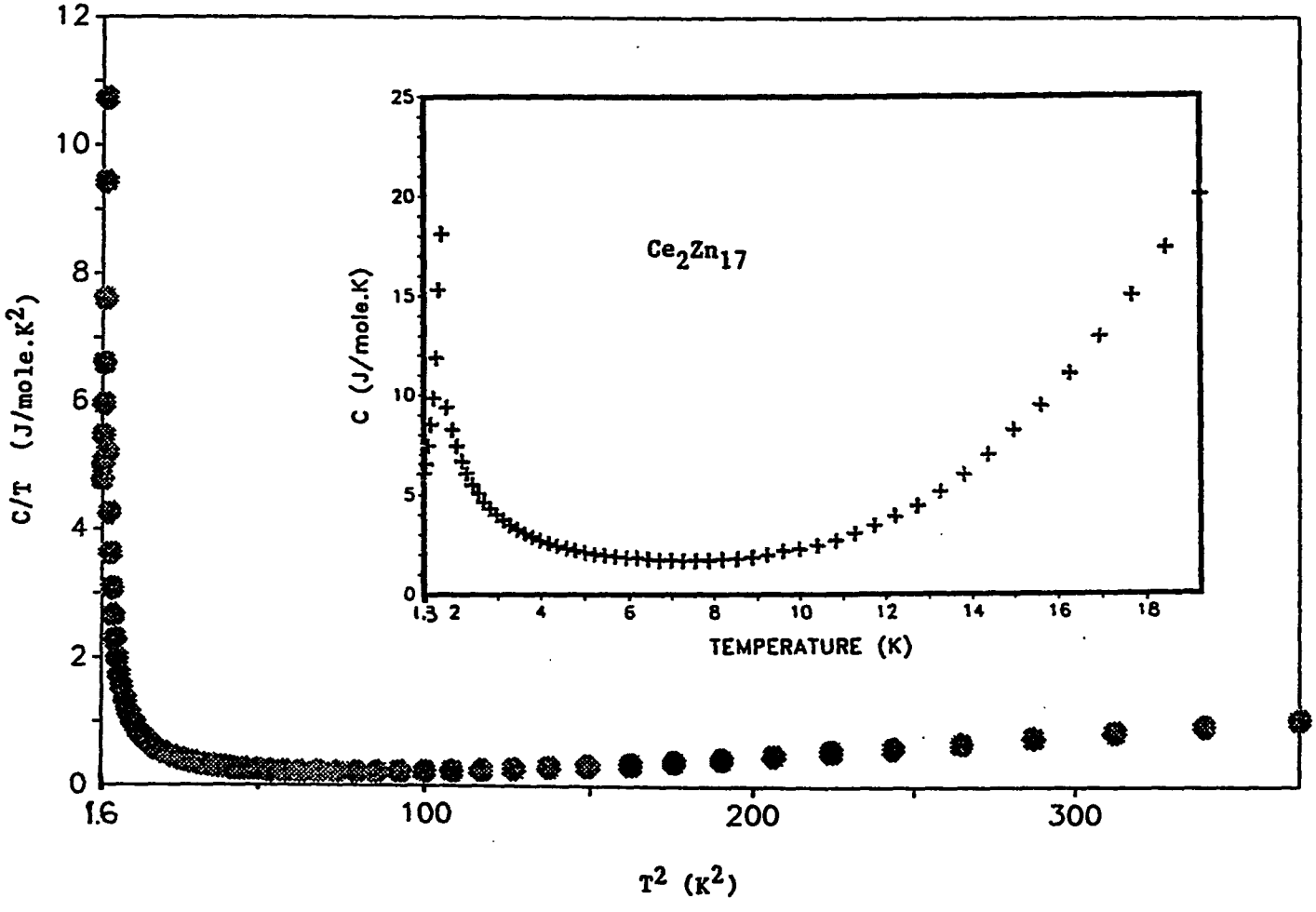

Fig. 38. C/T versus T^2 of Ce_2Zn_{17}. Inset: heat capacity as a function of temperature T

associated with this peak was calculated, and it reached Rln2 per mole-Ce at ~5K. No large tail was found above the ordering temperature in heat capacity. All these suggest that there is no short range order above T_N. The conclusion made by Sato et al. that short range ordering exists was based on the fact that entropy up to T_N is less than half of the total entropy Rln2 per mole-Ce [79], which is not quite convincing because the rest of the entropy might be recovered above T_N. Above ~7K, (~50K^2), C/T versus T^2 follows a straight line, and the electronic specific heat coefficient γ and Debye temperature θ_D were determined. The small value of γ = 15 mJ/mole Ce K^2 is typical of an ordinary metallic compound. No sign of heavy fermion behavior was seen.

The inverse of magnetic susceptibility is plotted against temperature in Fig. 39. The susceptibility χ can be expressed as

$$\chi = C/(T - \theta_p) + \alpha \qquad (24)$$

where

$$C = 1.06 \text{ emu K/mole Ce} \qquad (25)$$

$$\theta_p = -1.7K \qquad (26)$$

$$\alpha = -1.8 \times 10^{-3} \text{ emu/mole.} \qquad (27)$$

The effective moment derived from Curie constant C is $2.91\mu_B$, which is somehow larger than the expected value $2.54\mu_B$. The small Curie temperature θ_p = -1.7K is consistent with the θ_p values of the other rare earth R_2Zn_{17} compounds according to

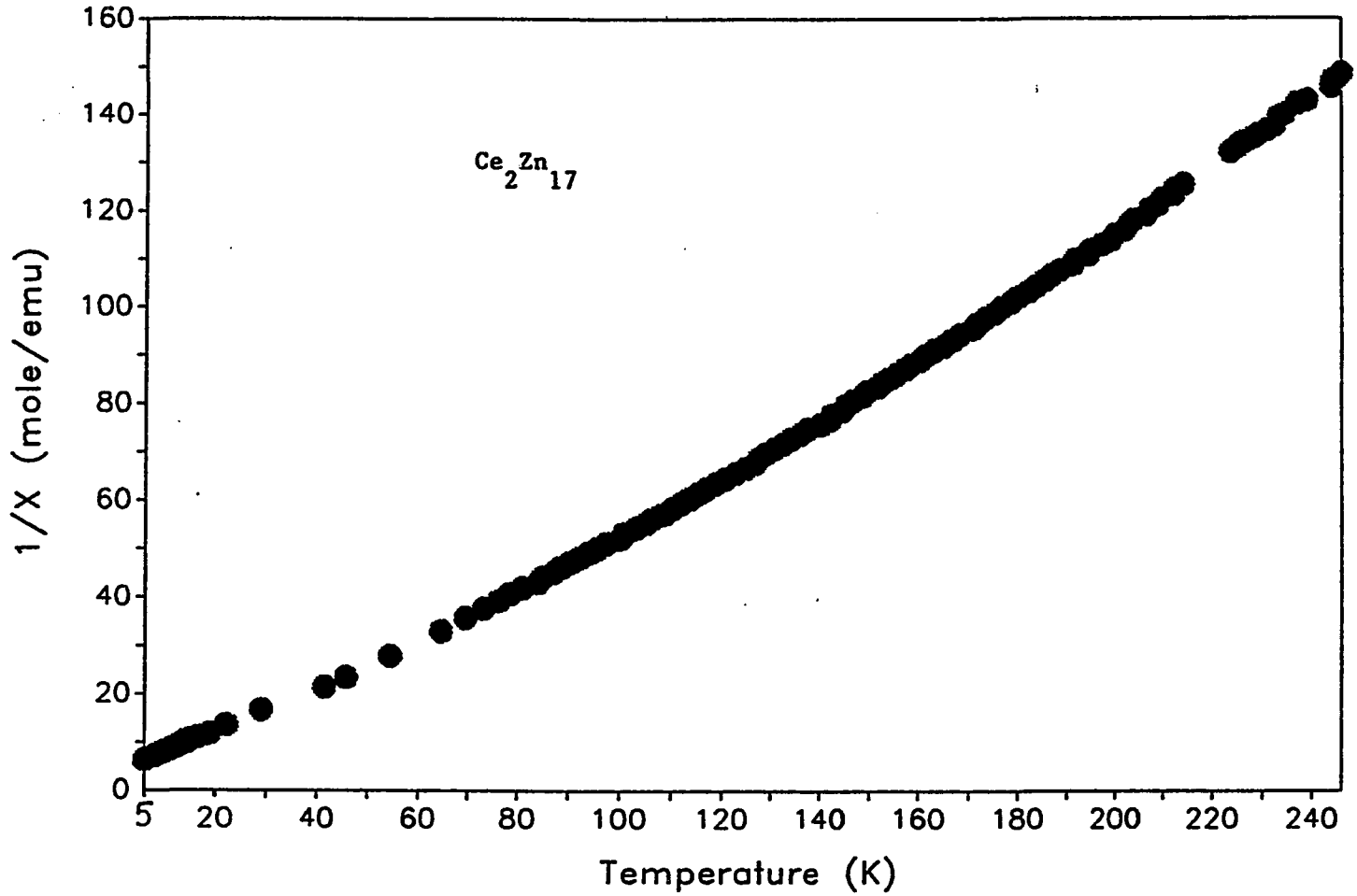

Fig. 39. The inverse susceptibility as a function of temperature

DeGennes' scaling [78]. While in Olivier's report, θ_p = -25K for Ce_2Zn_{17}, which is inconsistent the θ_p values of other R_2Zn_{17} compounds, was attributed to either a 4f instability or Kondo effect [78]. Our results support the conclusion that Ce_2Zn_{17} is an ordinary stable trivalent compound. The relatively large Larmor diamagnetism as indicated by α value explains the obvious deviation from the Curie-Weiss law.

4. Ce-Cd compounds

As mentioned in the introduction of this thesis, the interaction between f electron and conduction electrons of the neighboring non-f atoms is important in determining the behaviors of a system. It seems to be necessary that one of these neighboring elements is from the end of d-block or the beginning of the sp-block in the periodic table for a heavy fermion system. Since Cd is an early sp-block member, we studied the low temperature properties of some Ce-Cd binary intermetallic compounds. Among them, $CeCd_{11}$ has been discussed earlier in Section B.

a. $CeCd_2$ The crystal structure and low temperature susceptibility data above ~80K have been reported [80,72]. Other information is lacking. In studying the low temperature properties of this compound, two samples had been prepared. The

first one has a small amount of impurity phase in it, while the other is a clean single phase sample. The original measurements were conducted on the first sample before the second one was made.

The heat capacity of the first sample showed some interesting features. As shown in Fig. 40, two conjunctive peaks were found at ~18.5K and ~22K, respectively. To find out the origin of the two peaks, we measured the dc magnetic susceptibility χ using a field of H = 0.5T. Figure 41 shows the χ as a function of temperature from 1.3K to 50K. One local maximum was found at ~23K. This maximum suggests that the transition associated with the peak(s) in heat capacity is an antiferromagnetic one.

The question is why there is only one peak in χ while there are two peaks in heat capacity. There are two possible answers to this question. One possibility is that the system undergoes two conjunctive antiferromagnetic phase transitions. Since the measuring field (H=0.5T) is large, one of the transitions is smeared out due to a small spin-flip field. Therefore, we see only one peak in susceptibility. Another possibility is that one of the peak in heat capacity is from the impurity present in the sample and actually there is only one magnetic phase transition at ~22K. This latter suggestion is supported by the

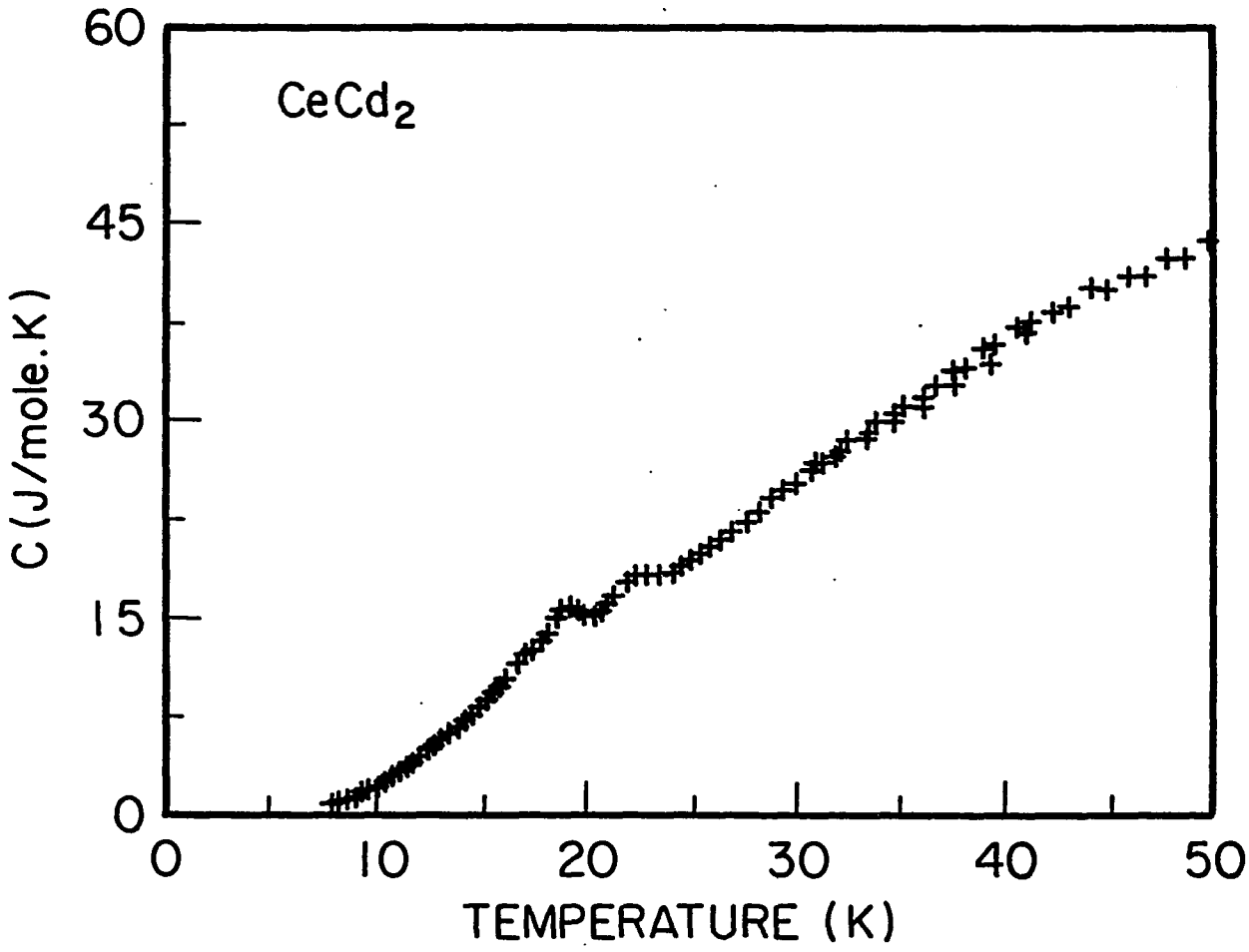

Fig. 40. Heat capacity of $CeCd_2$ over temperature range 8K < T < 50K

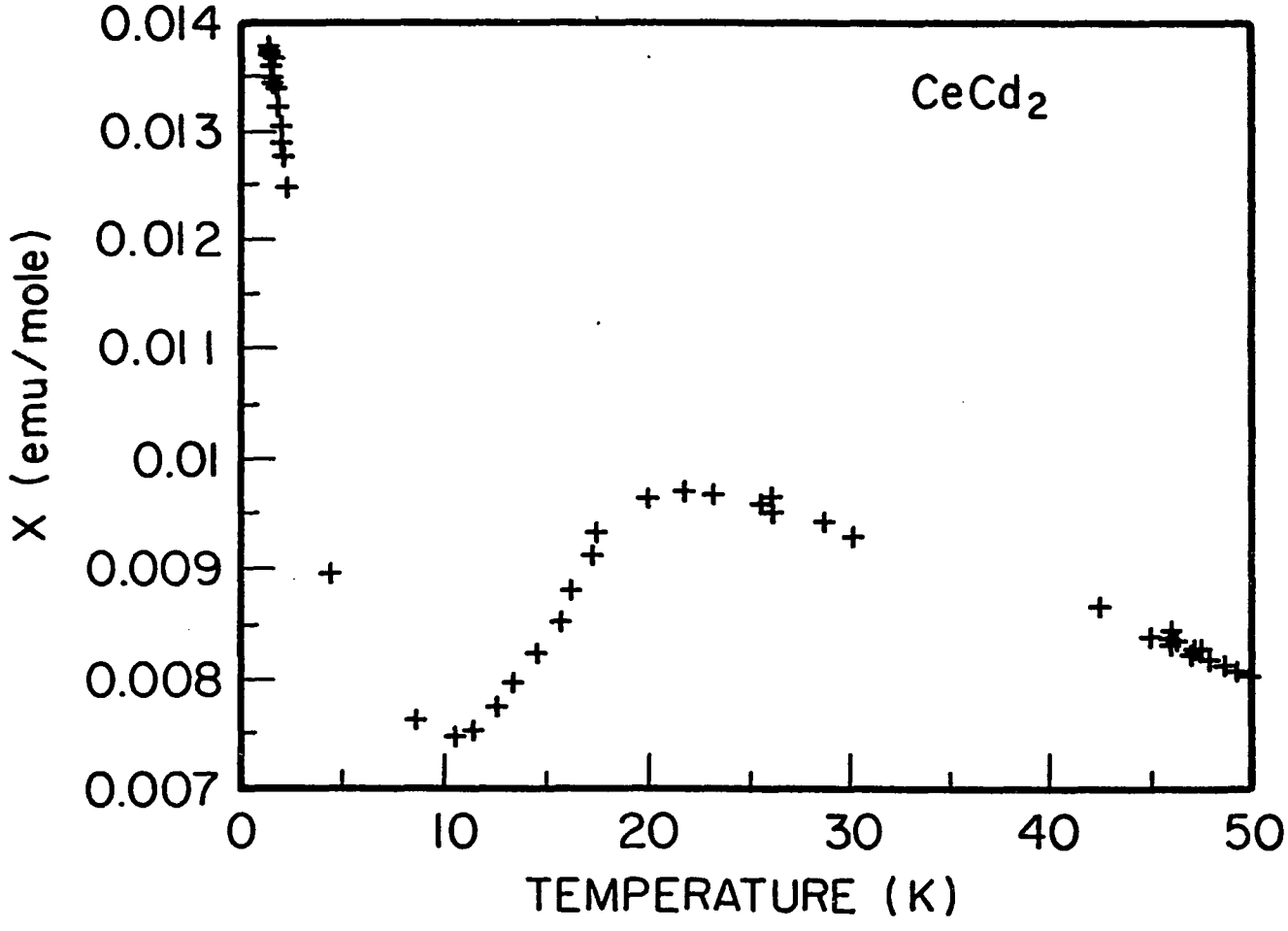

Fig. 41. Magnetic susceptibility versus temperature. (measuring field H = 0.5T)

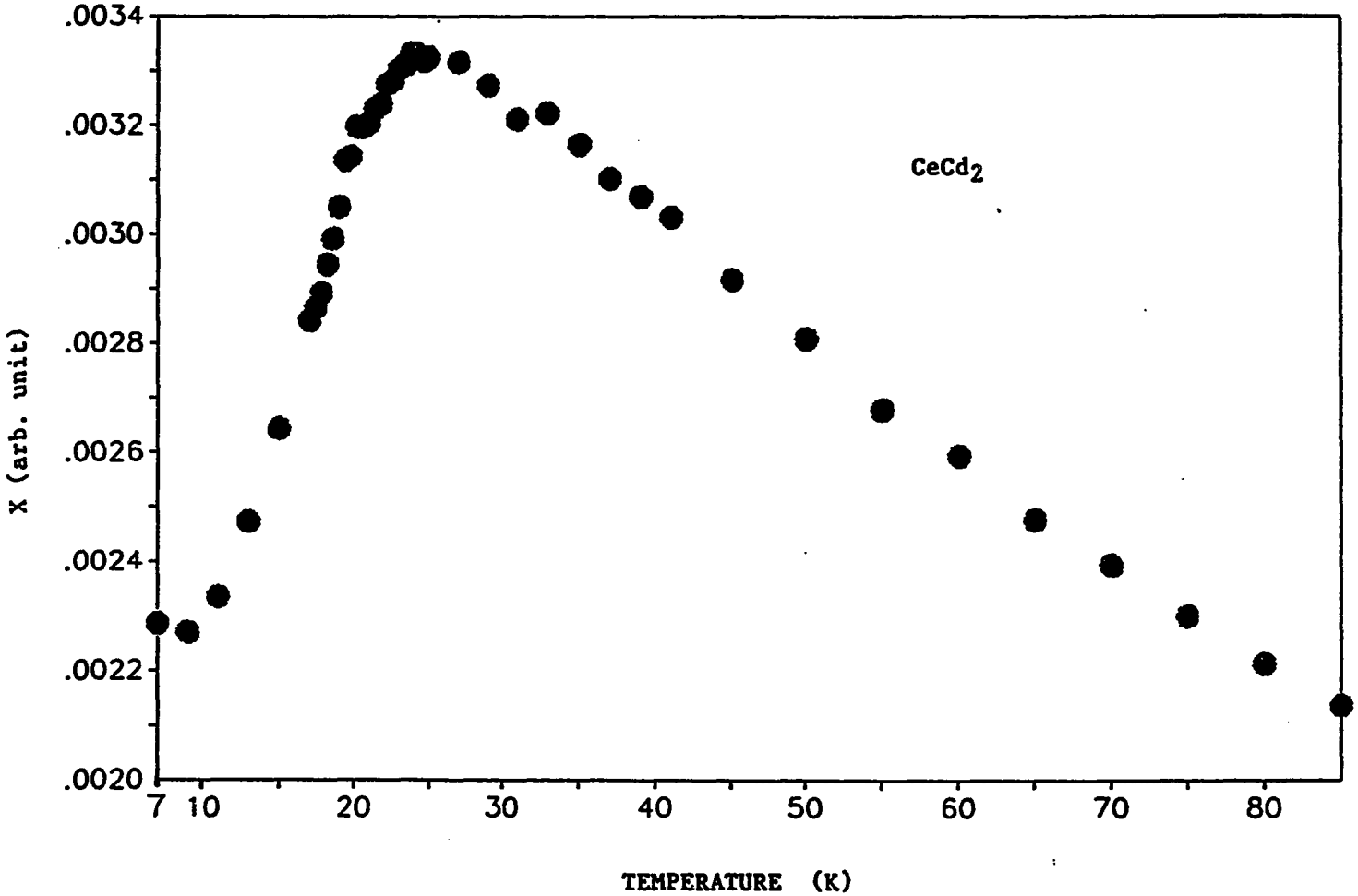

Fig. 42. Magnetic susceptibility versus temperature. (measuring field H = 10 Gauss)

susceptibility measurement on the second sample, which was free of the impurity phase. Shown in Fig. 42 is the dc susceptibility of $CeCd_2$ (clean sample) for an extended temperature scale. The measurement was done using a SQUID magnetometer with a measuring field H = 10 Gauss. Such a small field will assure that the antiferromagnetic phase transition would not be smeared out. As seen, within the experiment error, there is only one peak at ~23K. This indicates that the antiferromagnetic phase transition shows no sign of a "two-step" character. In another words, only one peak in heat capacity is associated with the phase transition, while the other is from the impurity phase.

Also can be seen in Fig. 41, below the maximum χ starts to increase with decreasing temperature at ~8K, which implies that the antiferromagnetic state below ~22K is only a metastable one. The system might go to a stable magnetically ordered ground state at a temperature below 1.3K. A further investigation below 1.3K is needed.

Above ~30K the susceptibility follows Curie-Weiss law (Fig. 43). The Curie temperature and effective moment determined from the linear region in Fig. 43 is listed in the Appendix.

The electronic specific heat coefficient and Debye temperature are difficult to determine in this case. Figure 44

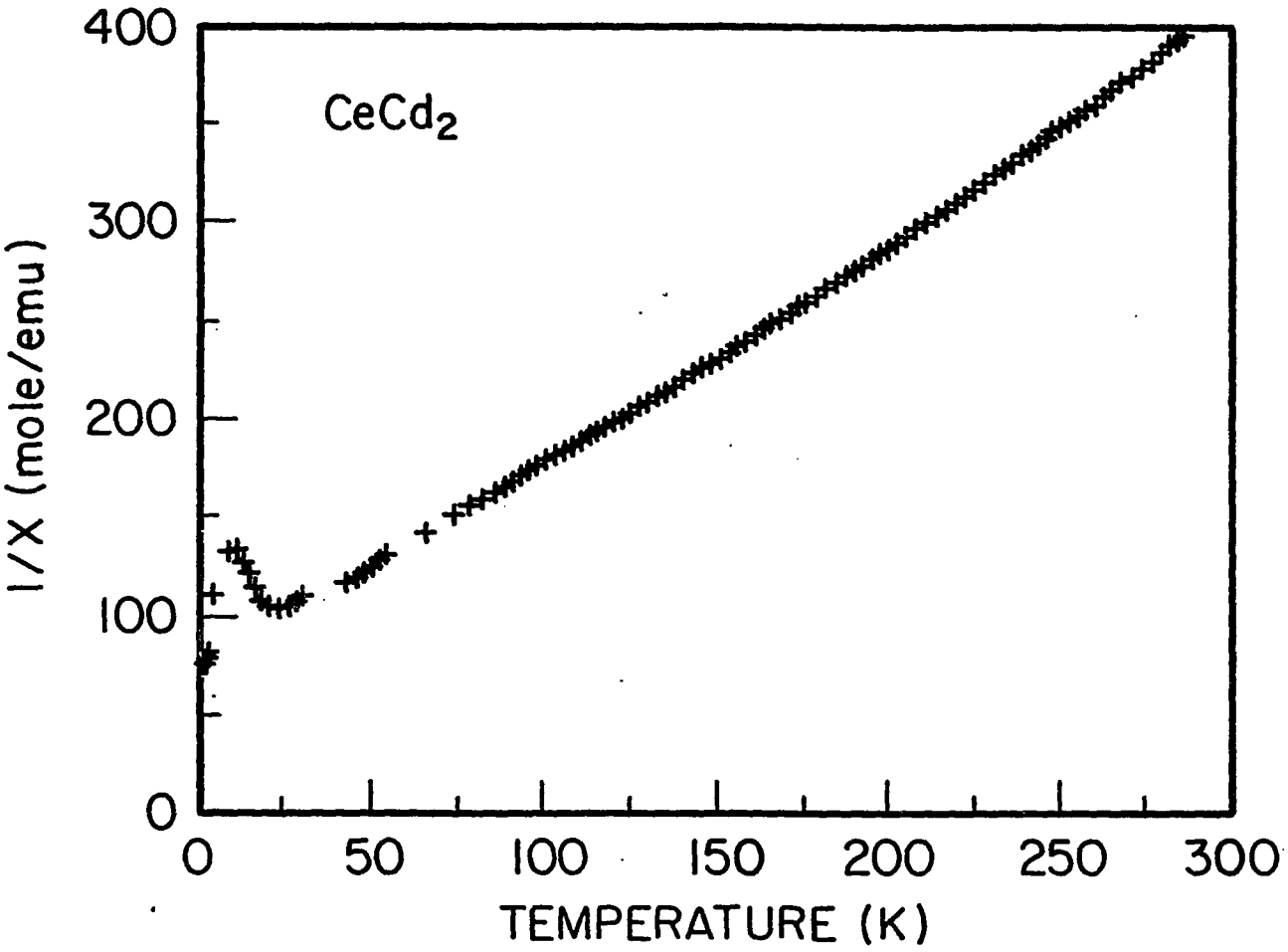

Fig. 43. The inverse susceptibility as a function of temperature

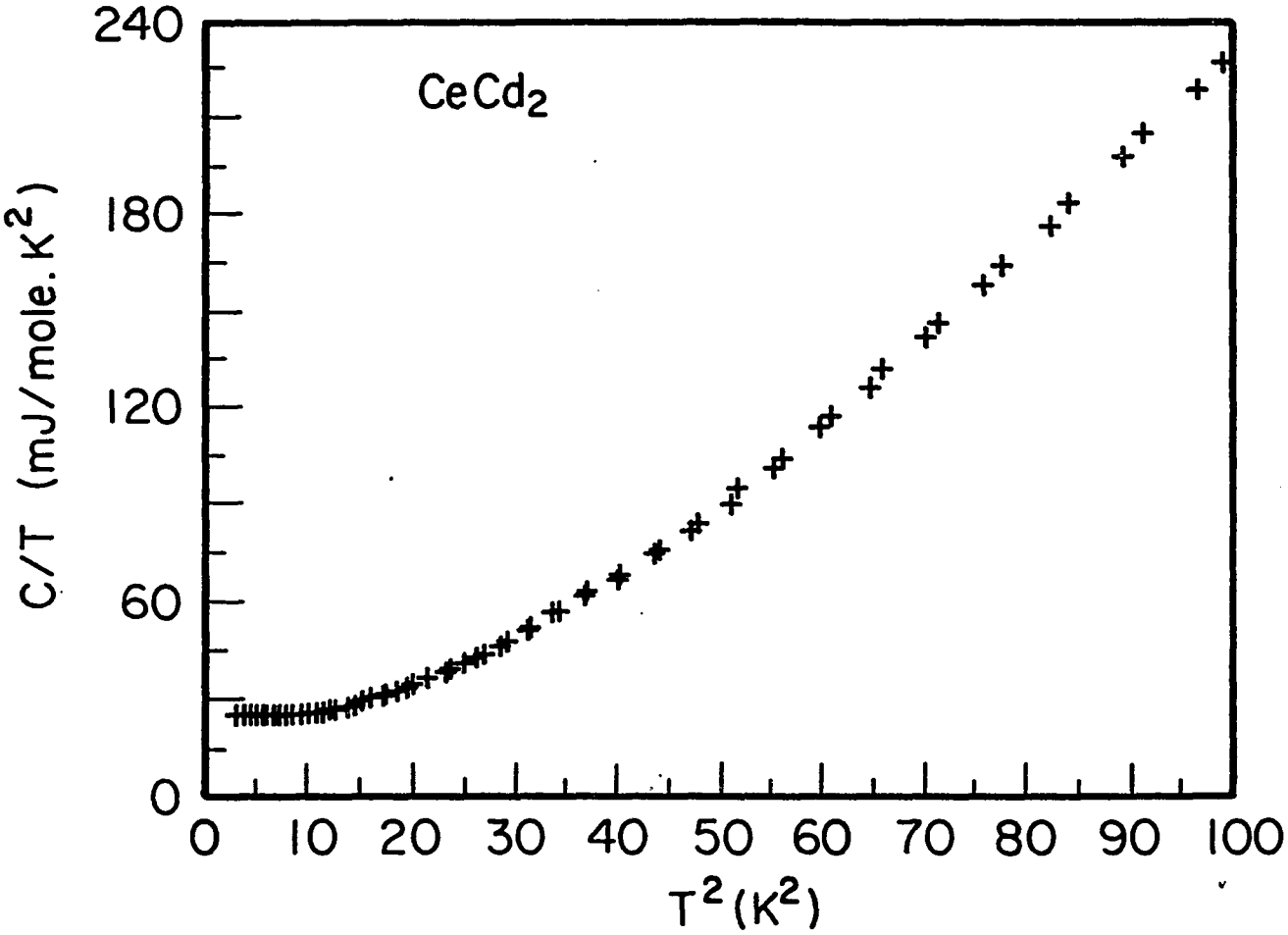

Fig. 44. C/T versus T^2 of $CeCd_2$ for T < 10K (T^2 < $100K^2$)

shows the C/T versus T^2 plot for T < 10K. The non-linear behavior, which is part of the reason that makes it difficult to determine γ and θ_D, is due to the magnetic contribution to the heat capacity. The situation is complicated by the fact that there might be another magnetic phase transition below 1.3K whose contribution to the heat capacity is hard to estimate.

b. $CeCd_3$ The only information available about $CeCd_3$, as we know of, were its crystal structure, effective moment and Curie temperature [72,81]. Therefore, the low temperature heat capacity and magnetic susceptibility of this compound were studied. Shown in Fig. 45 is the susceptibility χ as a function of temperature for temperature range 1.3K < T < 30K. The cusp at 2.0K is a clear indication that the system undergoes a transition into an antiferromagnetic state. The effective moment and Curie temperature determined from the Curie-Weiss type susceptibility (30K < T < 200K) are $\mu_{eff} = 2.60\mu_B$ and $\theta_p = -52K$, respectively. The negative θ_p value, which is twice as large, in amplitude, as the previously reported value ($\theta_p = -29K$) [72], agrees with the fact that $CeCd_3$ is an antiferromagnet at the lowest temperature.

The heat capacity of $CeCd_3$ up to 30K is shown in Fig. 46. The Néel temperature T_N was determined from the location of the peak, which turned out to be 2.0K. The C/T versus T^2 plot (Fig. 47) showed a perfect straight line between ~7K and ~16K

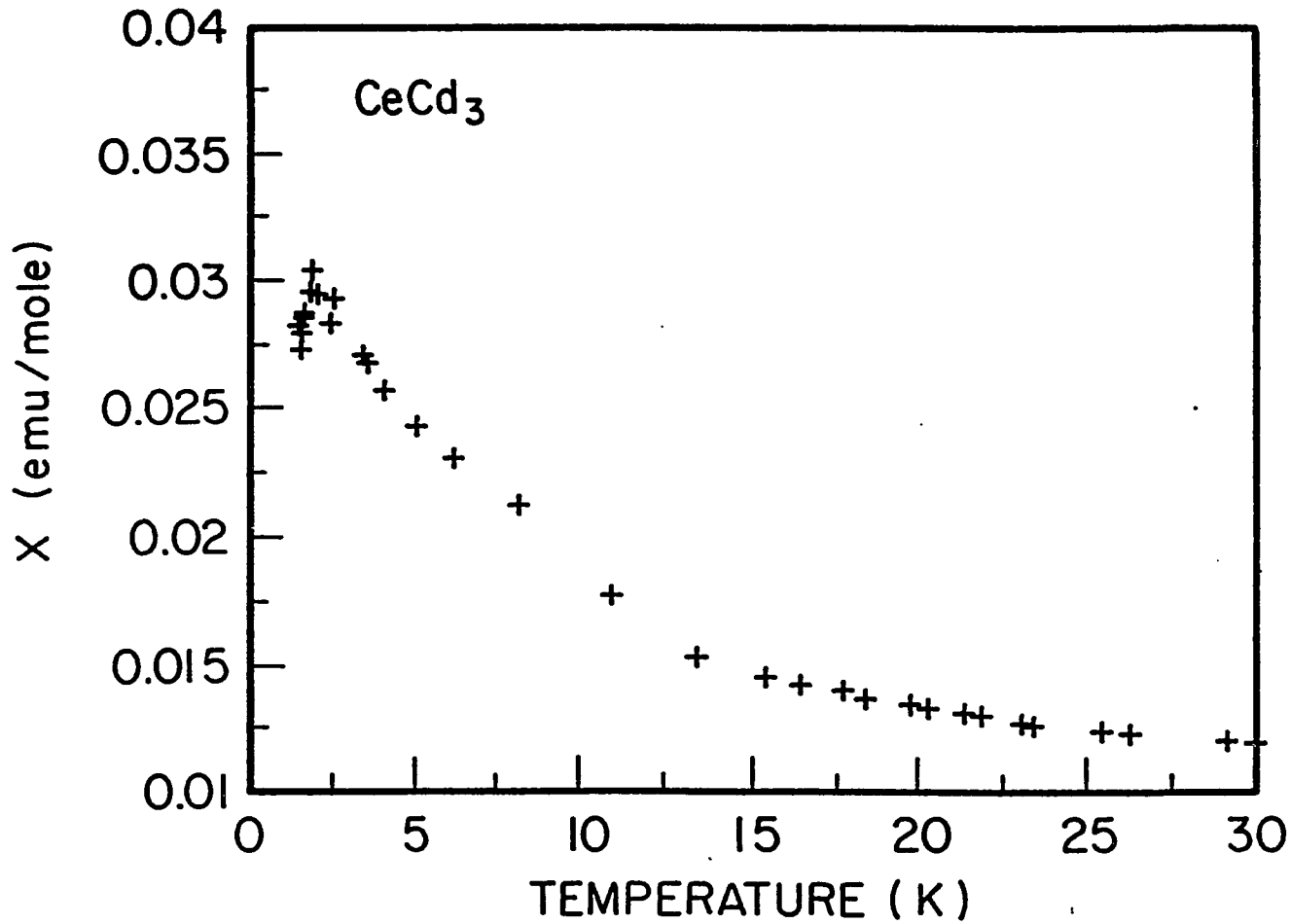

Fig. 45. Magnetic susceptibility χ of $CeCd_3$ for temperature range $1.3K < T < 30K$

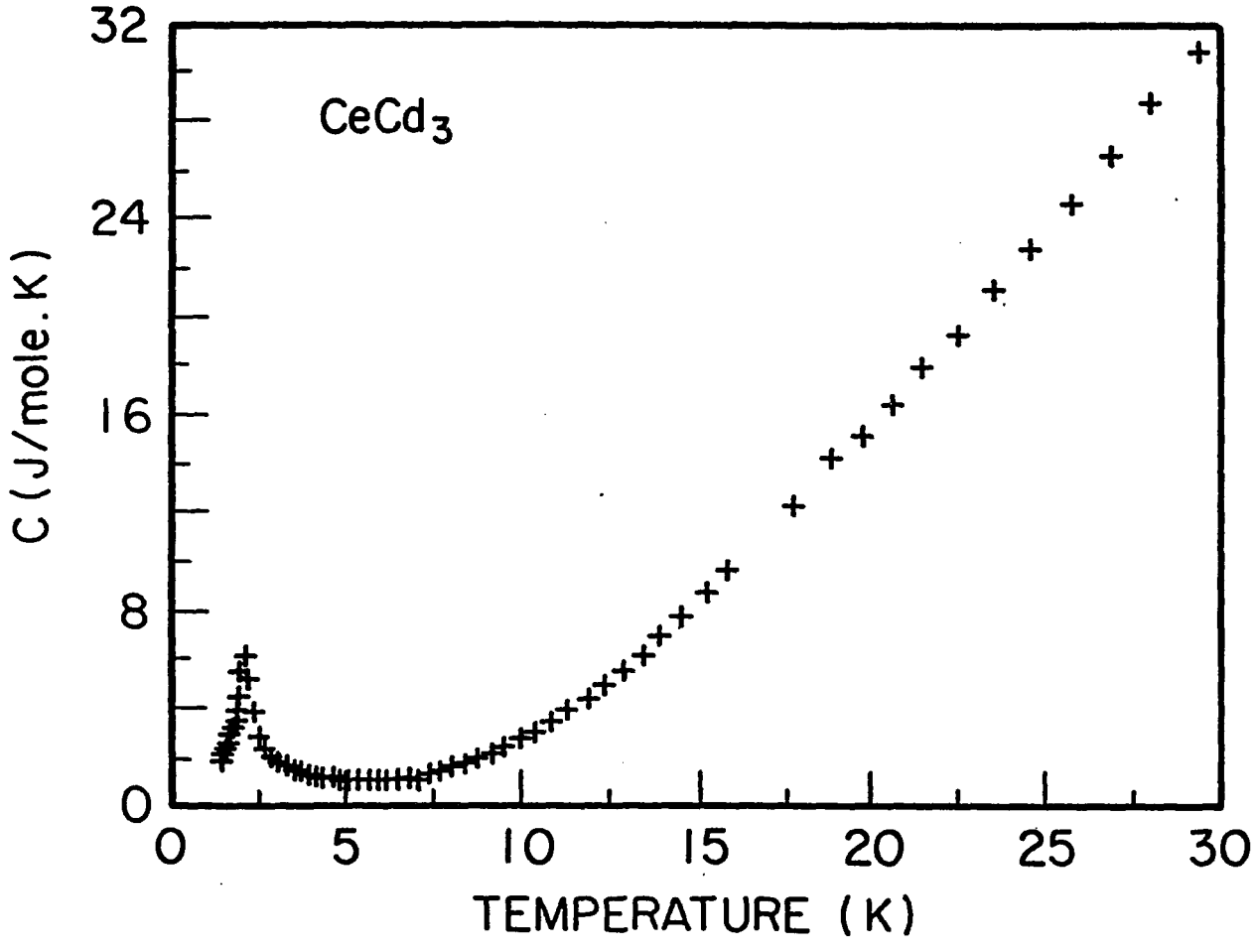

Fig. 46. Heat capacity of $CeCd_3$ for temperature 1.3K < T < 30K

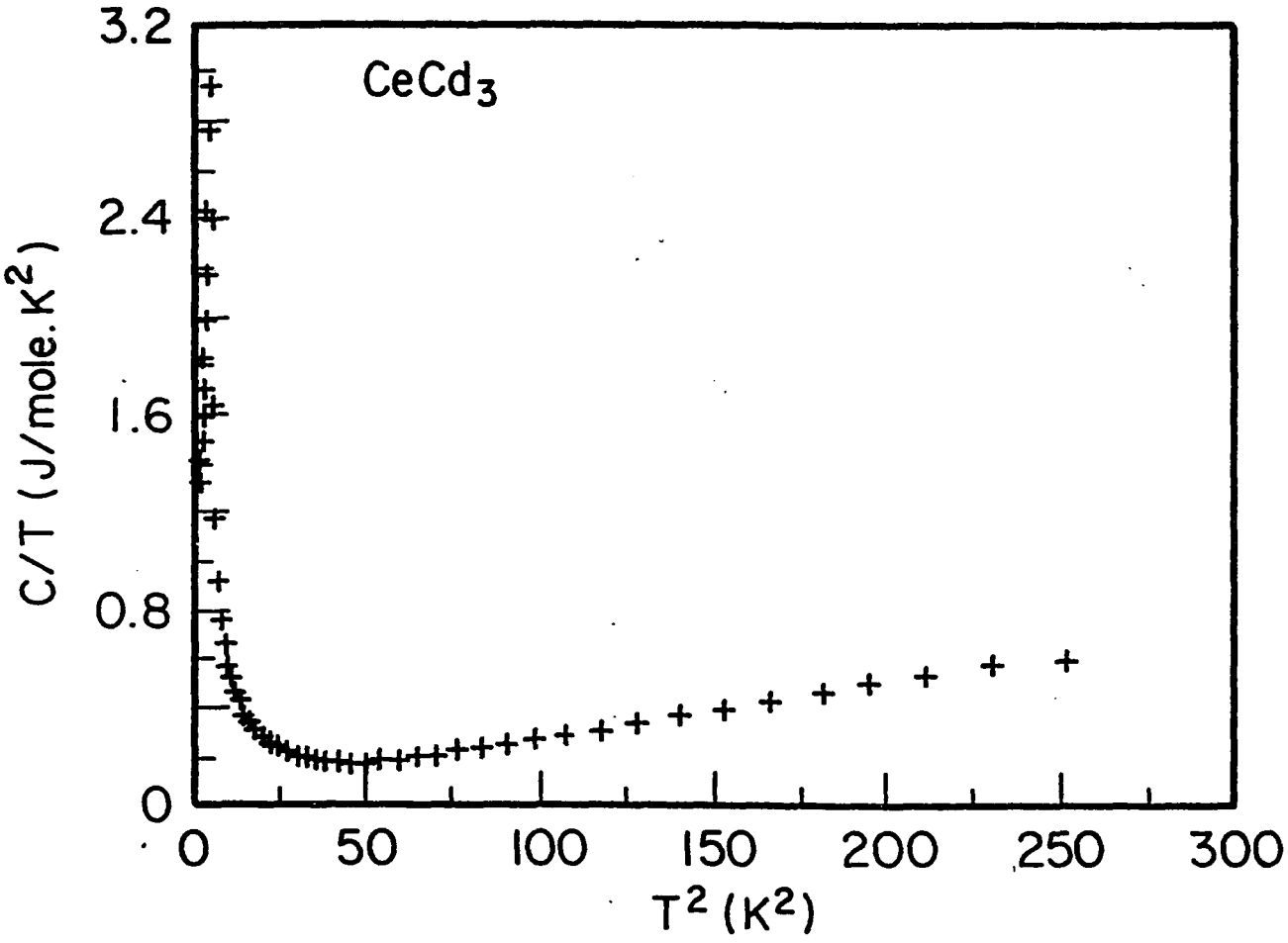

Fig. 47. C/T versus T^2 plot for $CeCd_3$

(~50K^2 and ~260K^2), and the electronic specific heat coefficient and Debye temperature were determined from these data (Appendix).

c. $Ce_{13}Cd_{58}$ $Ce_{13}Cd_{58}$ crystallizes in hexagonal $Pu_{13}Zn_{58}$-type structure [81]. The Ce-Ce spacing determined from the lattice parameters is d_{Ce-Ce} = 4.37Å (Appendix). Since it is larger than the Hill limit, the system is expected to order magnetically [27]. Thus the tendency towards the magnetic ordering at a temperature lower than 1.3K as indicated by the upturn in C/T versus T^2 plot at ~3K (10K^2, Fig. 48) is not surprising.

The inverse of magnetic susceptibility χ^{-1} is plotted as a function of temperature in Fig. 49. The Curie temperature determined from the straight line (a Curie-Weiss behavior) at high temperature is -12K, which implies that the possible magnetic phase transition below 1.3K is of antiferromagnetic type.

d. $CeCd_6$ Similar to $Ce_{13}Cd_{58}$, $CeCd_6$ also showed a tendency towards magnetic ordering at temperature below 1.3K. As shown in Fig. 50, the upturn in C/T versus T^2 plot at ~3K (10K^2) is obvious. The inverse susceptibility of $CeCd_6$ is shown in Fig. 51, and the Curie temperature and effective moment were

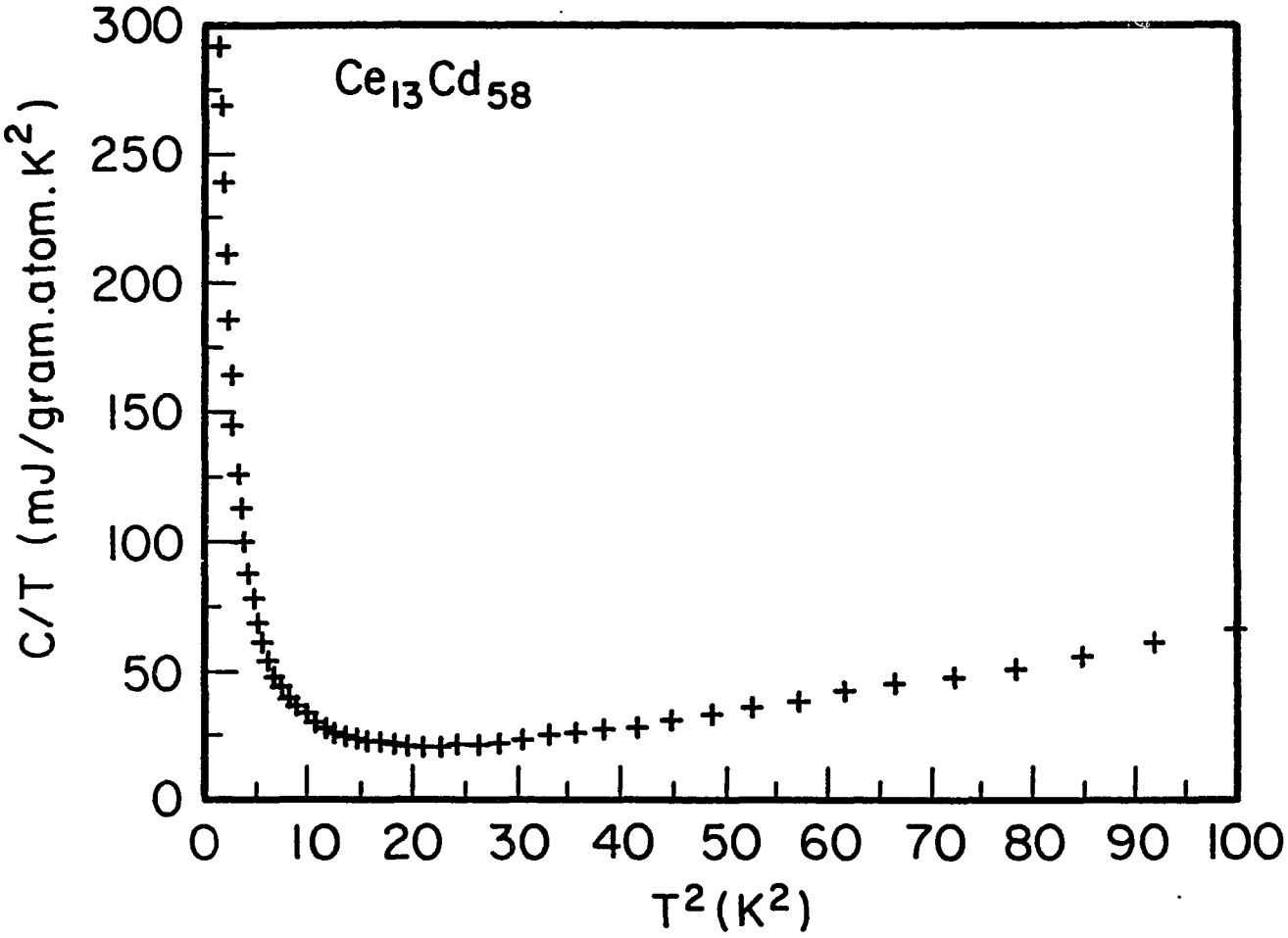

Fig. 48. C/T versus T^2 of $Ce_{13}Cd_{58}$

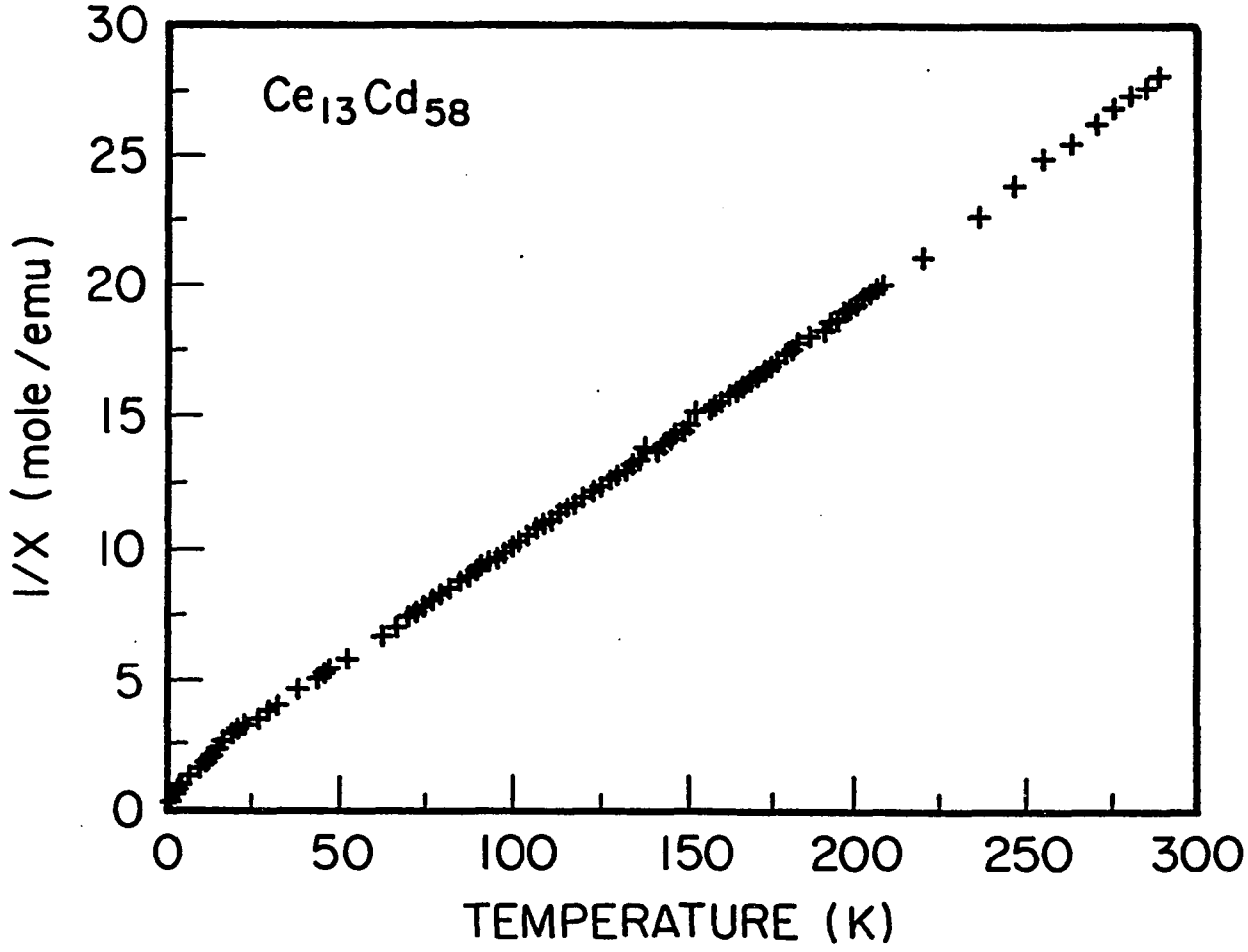

Fig. 49. The inverse susceptibility as a function of temperature

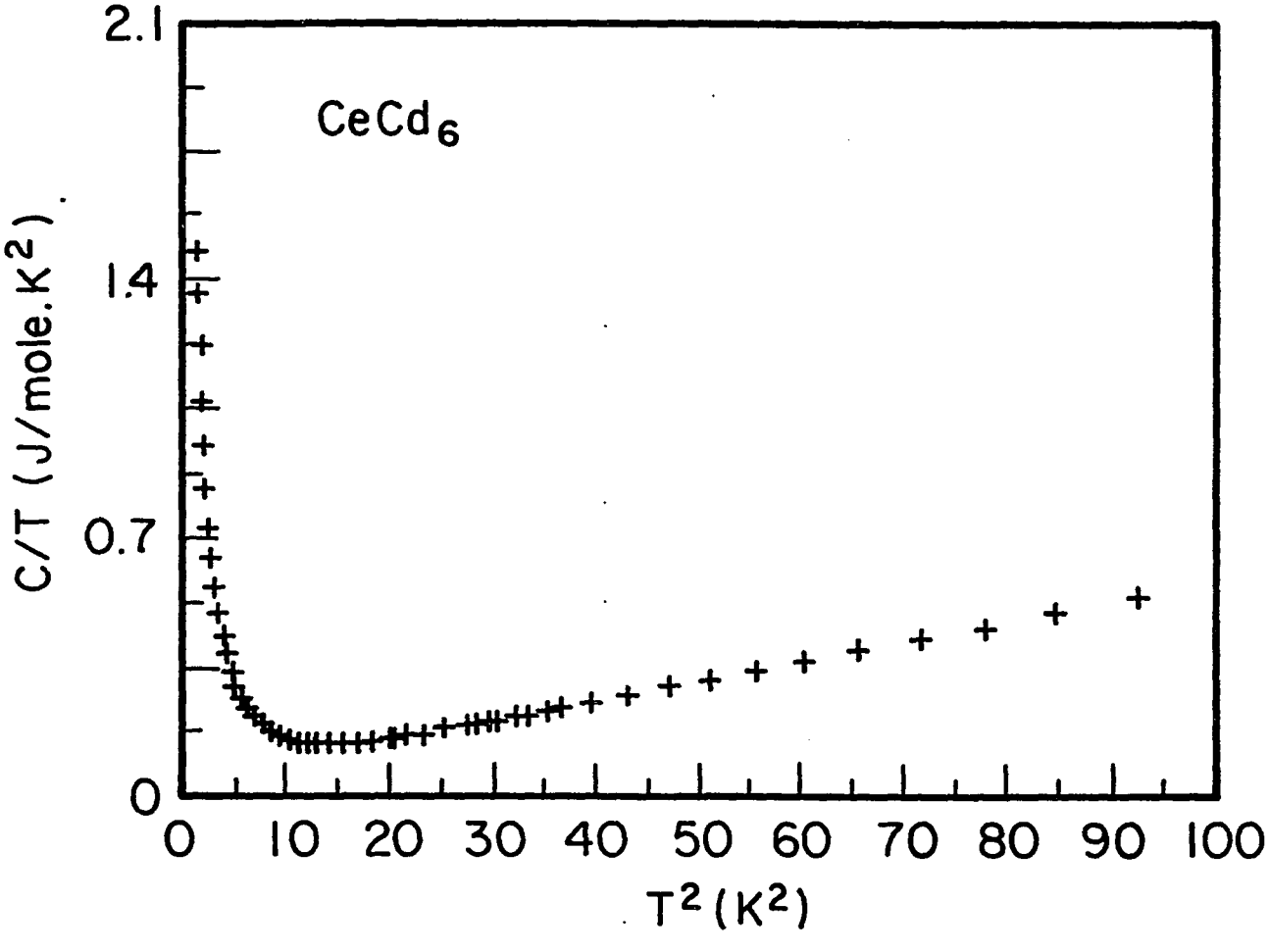

Fig. 50. C/T versus T^2 of $CeCd_6$

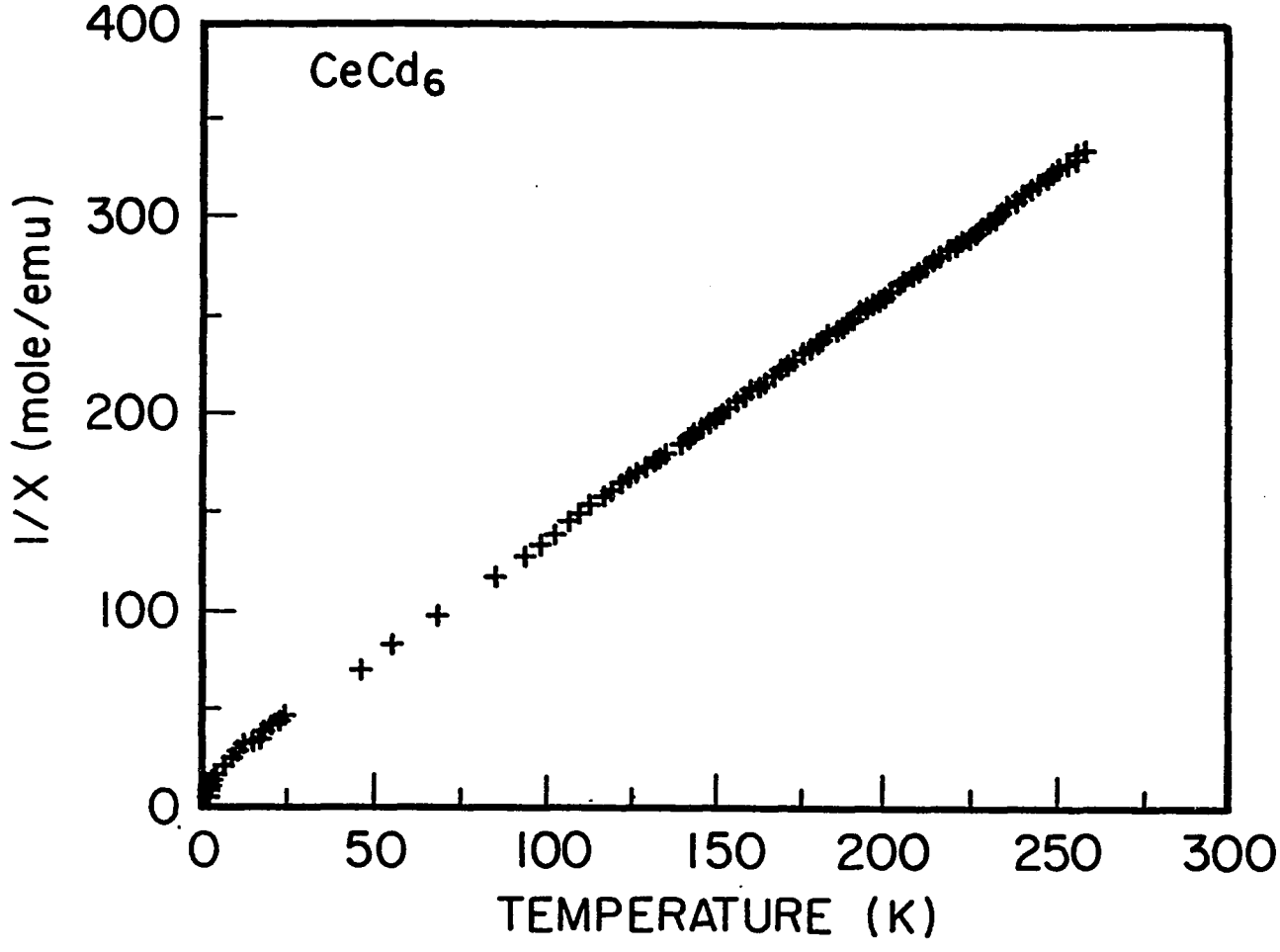

Fig. 51. The inverse susceptibility of $CeCd_6$

determined. Again, a negative Curie temperature was found which infers antiferromagnetic ordering.

Both the electronic specific heat coefficients and Debye temperatures of $CeCd_6$ and $Ce_{13}Cd_{58}$ are listed in the Appendix.

5. Summary

In spite of the fact that the Ce binary system studied satisfy most of the conditions for the formation of heavy fermion state, e.g., the relatively large Ce-Ce spacings and the favorable electronic structures of non-f electron ligand atoms, no heavy fermion behavior was found (the γ values are listed in the Appendix). All compounds, except for superconductor $CeIr_5$, show magnetic ordering or the tendency towards the magnetic ordering. It is demonstrated that a large Ce-Ce spacing is a necessary condition but not a sufficient one for the formation of heavy fermion state.

D. Studies on Some Ce Ternary Compounds

1. CeNiAl and $CeNiAl_{0.5}Ga_{0.5}$

Both CeNiAl and $CeNiAl_{0.5}Ga_{0.5}$ have a hexagonal Fe_2P-type structure [82]. In this structure Ce atoms occupy 3g positions (x,0,1/2), Al (and Ga) atoms occupy 3f positions (x,0,0), and Ni

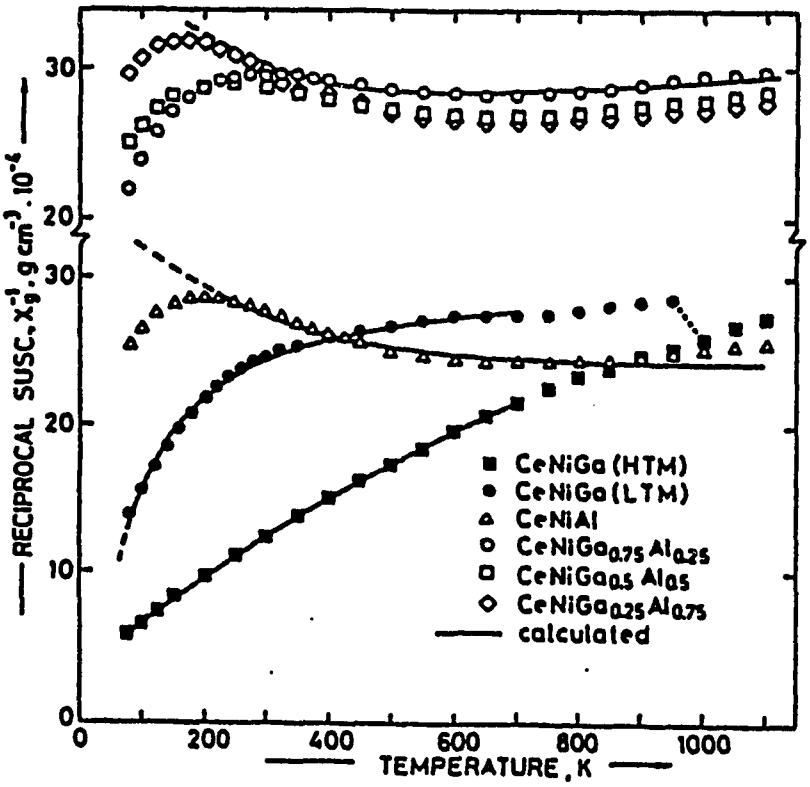

Fig. 52. The inverse susceptibility for $CeNiGa_{1-x}Al_x$ alloys and calculated least squares fit [82]

atoms occupy 1b position (0,0,1/2) and 2c positions (1/3,2/3,0) [83]. The magnetic properties of isostructural $CeNiAl_xGa_{1-x}$ ($0 \leq x \leq 1$) alloys have been studied by Grin et al. [82]. They found a remarkable deviation from the simple Curie-Weiss law in all cases of the $CeNiAl_xGa_{1-x}$ alloys (Fig. 52). With increasing Al content the magnetic properties are characterized by a pronounced minimum in the inverse susceptibility, which is satisfactorily explained with Ce valence fluctuation.

It is certainly of interest to study the calorimetric behavior of this system. Samples CeNiAl, $CeNiAl_{0.5}Ga_{0.5}$ and CeNiGa were prepared by arc-melting. CeNiAl was a single phase compound, while the other two had some second phase in the samples. Therefore, a heat treatment was conducted on these two samples. X-ray diffraction patterns showed that $CeNiAl_{0.5}Ga_{0.5}$ sample after the heat treatment is essentially single phase with the expected crystal structure and that CeNiGa sample still had a significant amount of second phase in it. The heat capacities of the single phase samples CeNiAl and $CeNiAl_{0.5}Ga_{0.5}$ were measured and are shown in Fig. 53 for temperature range $1.3K < T < 20K$. As seen, there is no apparent difference between the two in this temperature range.

The C/T versus T^2 plot is shown in Fig. 54 for a narrower temperature range. Both alloys have a simple straight line

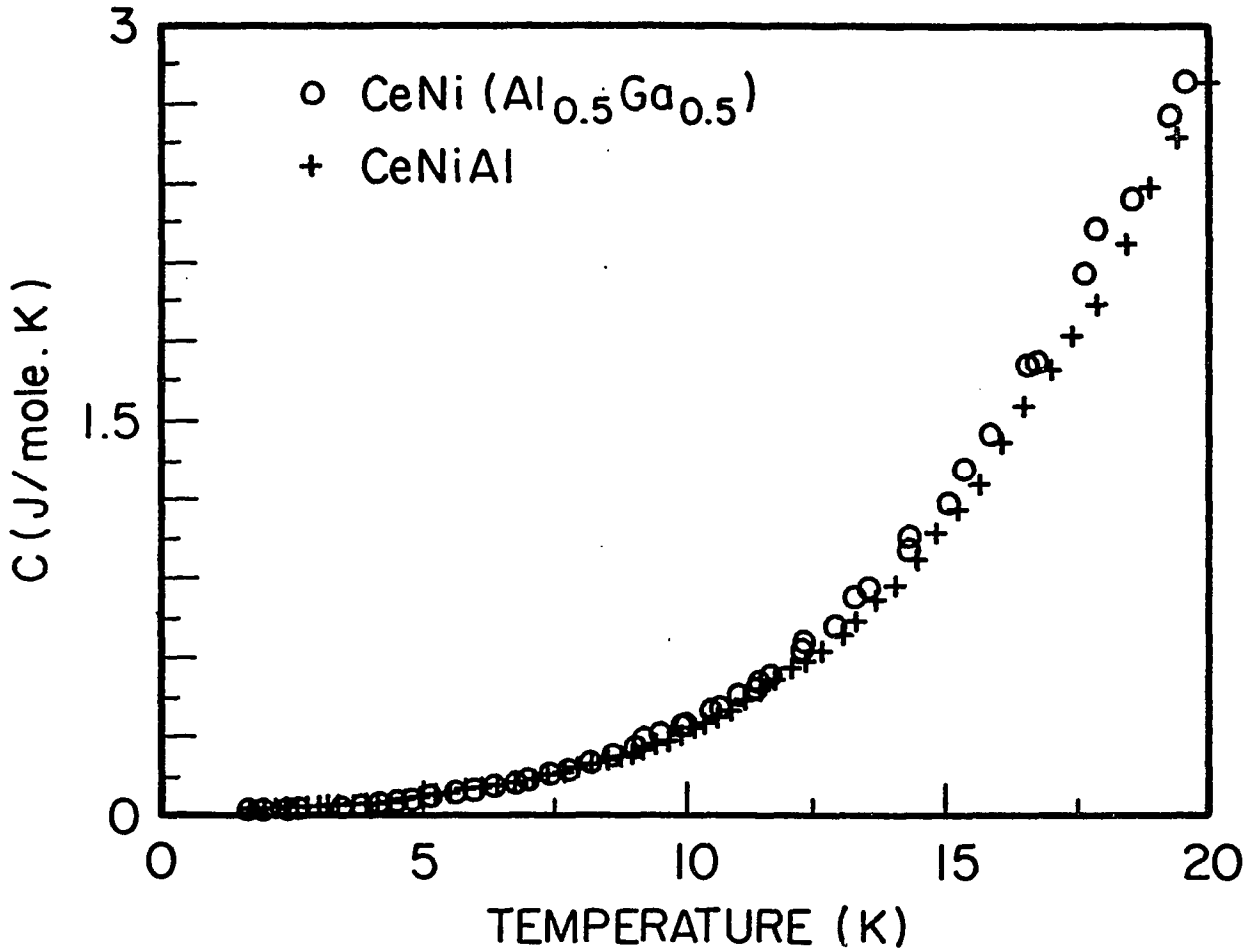

Fig. 53. Heat capacities of CeNiAl and $CeNiAl_{0.5}Ga_{0.5}$

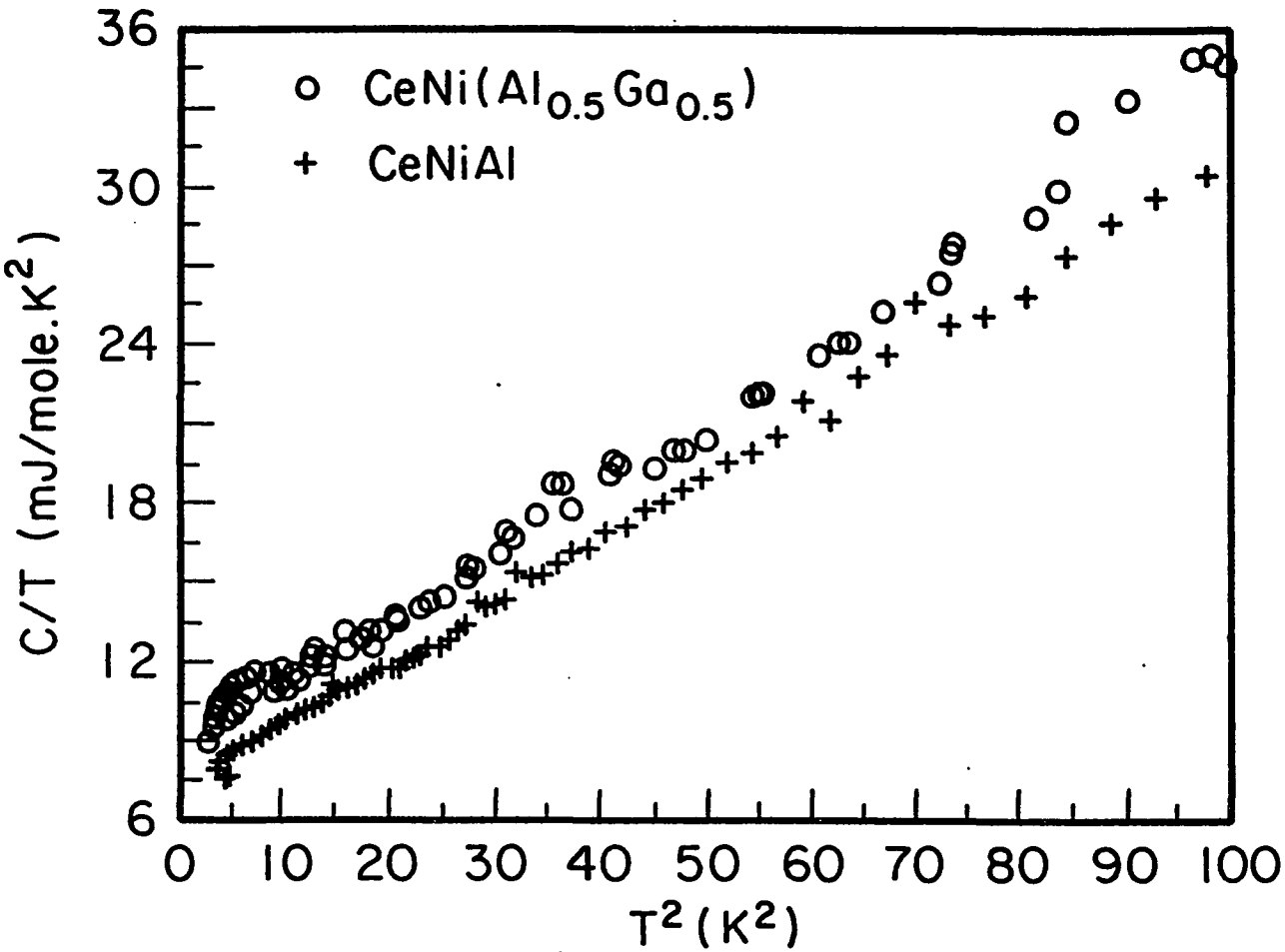

Fig. 54. C/T versus T^2 for CeNiAl and $CeNiAl_{0.5}Ga_{0.5}$

behavior. The Debye temperatures are about the same, θ_D = 290K for CeNiAl and θ_D = 283K for $CeNiAl_{0.5}Ga_{0.5}$. The electronic specific heat coefficient is slightly higher for the latter, but neither one is large (γ = 7.2 mJ/mole K^2 for CeNiAl and γ = 8.7 mJ/mole K^2). As a matter of fact the γ values are smallest of all the Ce samples studied. It is not unusual that a valence fluctuation system has such a γ value, e.g., the valence fluctuator α-Ce has a γ of ~12.8 mJ/mole K^2 [84].

According to Sales and Wohlleben [85], the magnetic susceptibility of a valence fluctuation system involving Ce can be expressed phenomenogically as

$$\chi = N(2.54\mu_B)^2 \upsilon_{(T)} / 3k_B(T+T_{sf}) \quad (28)$$

and

$$\upsilon_{(T)} = 6/\{6+\exp[-E_{ex}/k_B(T+T_{sf})]\} \quad (29)$$

where $E_{ex} = E_1 - E_0$ is the energy difference between the supposed f^1 state and f^0 state, and T_{sf} is the measurement of transition rate between the two states. Grin et al. have used above equations to fit the experimental data, and they obtained an acceptable agreement between the calculation and experiment. The fitting gave E_{ex} = 1400 cm^{-1}, i.e., ~2000K and T_{sf} = -380K [82]. Such a large E_{ex} explains the normal behavior of heat capacity at low temperature (Fig. 54) since the anomalous behavior is expected to occur at ~E_{ex} [86,87]. The difference in γ's

indicates that, by replacing half Al with Ga, the density of state at Fermi level ε_F is increased from CeNiAl to $CeNiAl_{0.5}Ga_{0.5}$ by 20%.

2. $CeNi_{12}B_6$

The crystal structures of $CeNi_{12}B_6$ and $LaNi_{12}B_6$ were reported in ref. [88,89]. The lattice parameters of the orthorhombic unit cell are listed in the Appendix. The closest Ce-Ce spacing in $CeNi_{12}B_6$ is found to be 6.06Å, which is a relatively large separation.

Shown in Fig. 55 is the heat capacity of $CeNi_{12}B_6$ for temperature range 1.3K < T < 55K. The magnetic ordering at 1.7K is clearly indicated by a sharp peak (see Fig. 55 inset for an expanded view). The entropy calculated from the heat capacity data is S = 4.88 J/mole K at ~8K, which is ~85% of the expected value Rln2. In the calculation the contributions to the heat capacity from lattice and conduction electrons have been removed by subtracting the heat capacity of $LaNi_{12}B_6$ from that of $CeNi_{12}B_6$. In another words, the entropy is calculated from the area between the two curves in Fig. 56, inset. As seen, the lattice and conduction electron heat capacities are, in fact, negligible over the temperature range shown.

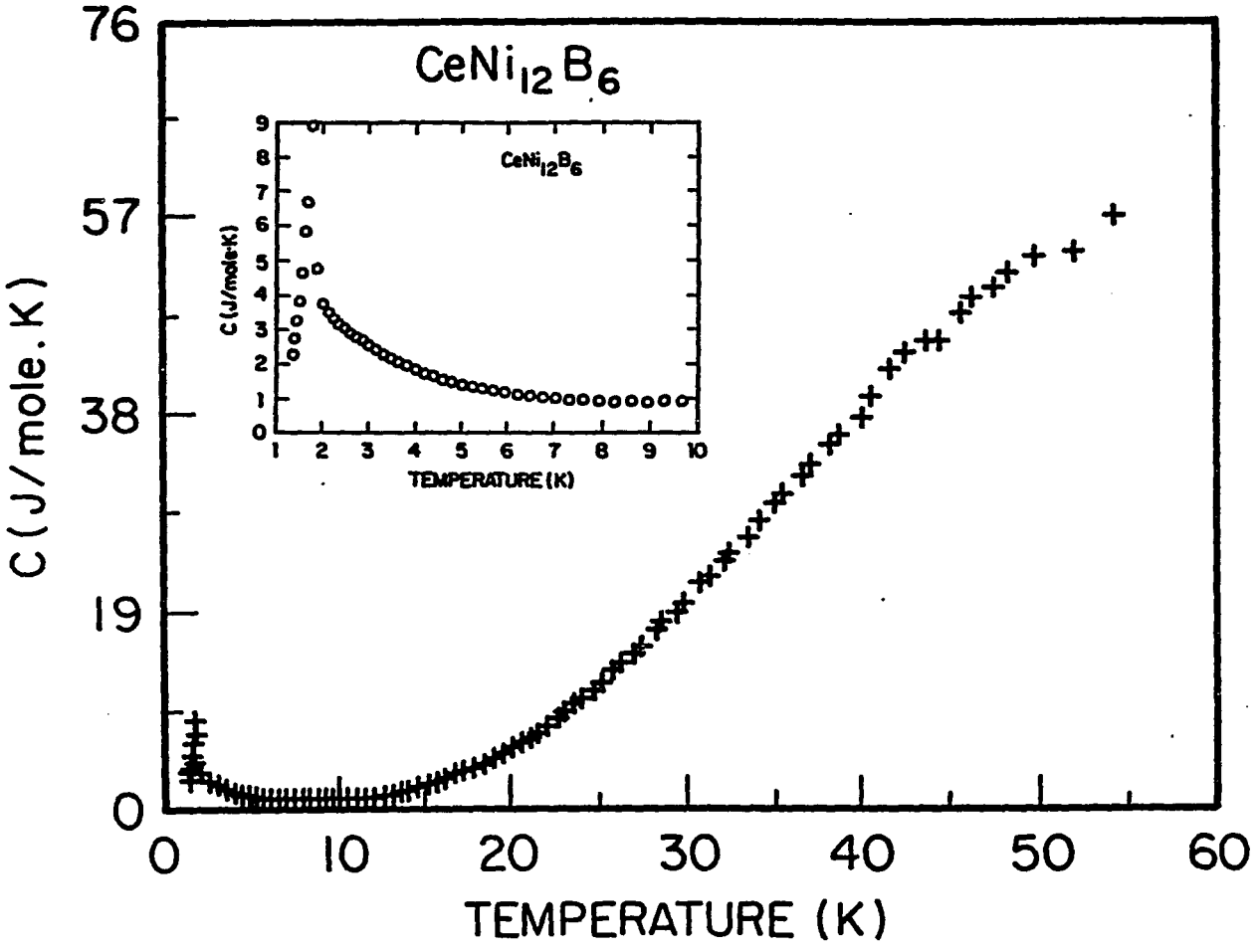

Fig. 55. Heat capacity of $CeNi_{12}B_6$ for temperature 1.3K < T < 55K.

Inset: an expanded plot at low temperatures

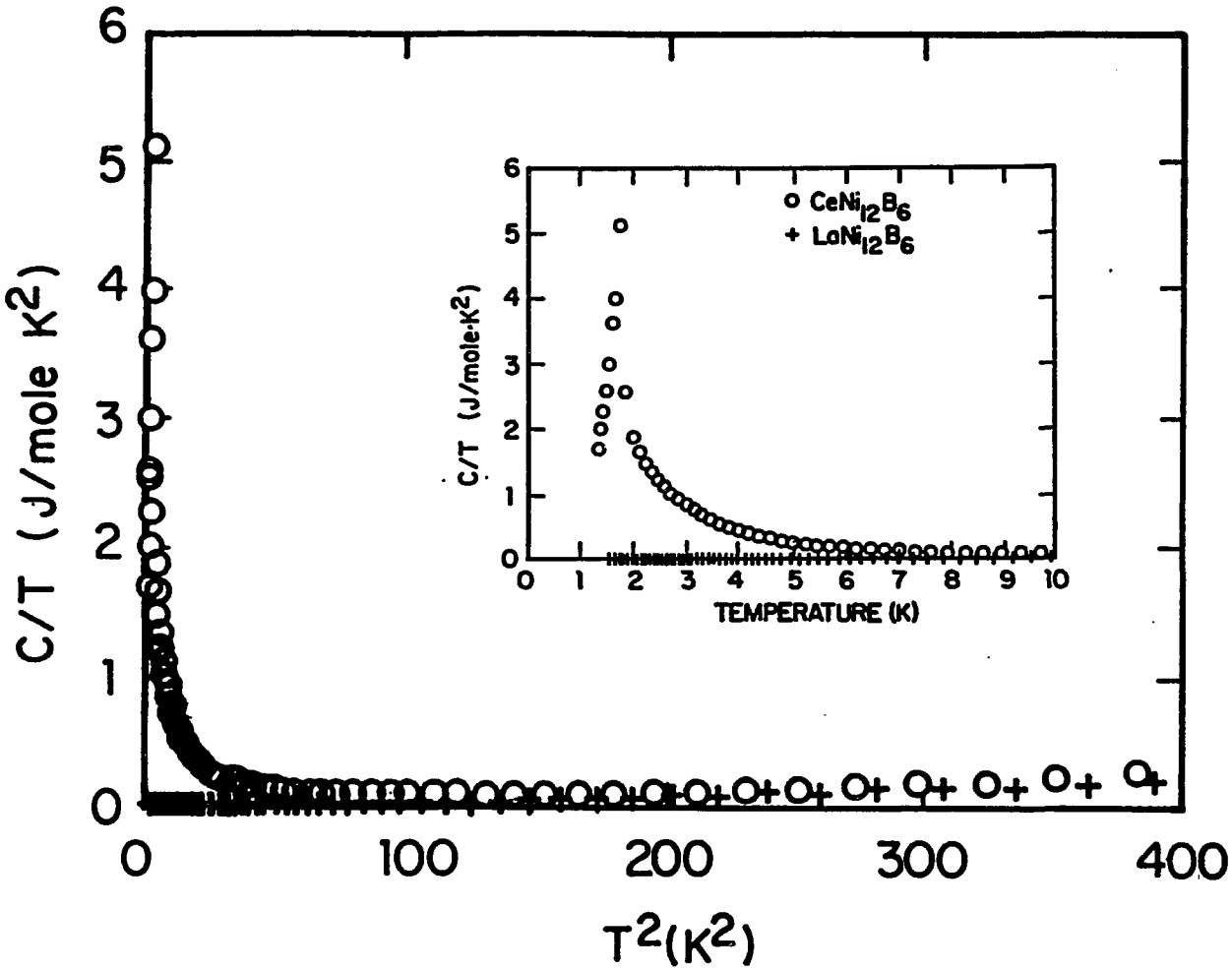

Fig. 56. C/T versus T^2 plot for $CeNi_{12}B_6$. Inset: C/T versus temperature at lower temperatures

The C/T versus T^2 plot (Fig. 56) above the ordering temperature reveals that there is no sign of heavy fermion behavior. The electronic specific heat coefficient γ was determined in the same way as was done in the case of $CePtGa_3$. The difference in C/T between $CeNi_{12}B_6$ and $LaNi_{12}B_6$ in temperature region $10K < T < 20K$ was considered as the γ of the former in excess of that of the latter. The average value of this difference (33 mJ/mole K^2) was added to the γ of $LaNi_{12}B_6$ (32.3 mJ/mole K^2) to give the γ value of $CeNi_{12}B_6$ (~65 mJ/mole K^2). Also shown in Fig. 56 is the same plot for $LaNi_{12}B_6$. Its linear behavior at low temperature ($T < 10K$) allowed us to determine the γ and θ_D for $LaNi_{12}B_6$. At the same time the Debye temperature of $LaNi_{12}B_6$ serves as a good estimation to that of $CeNi_{12}B_6$.

A broad maximum at ~3K in dc magnetic susceptibility (Fig. 57) is associated with the peak in heat capacity at 1.7K, and it indicates that the magnetic ordering is antiferromagnetic. The inverse susceptibility χ^{-1} as a function of temperature is shown in Fig. 58. The positive Curie temperature determined from the data above 80K, $\theta_p = +9.3K$, is contradictory to the antiferromagnetic ordering at 1.7K. A detailed examination of the χ^{-1} versus T curve reveals that it is not a perfect straight line. While the θ_p obtained from low temperature region is

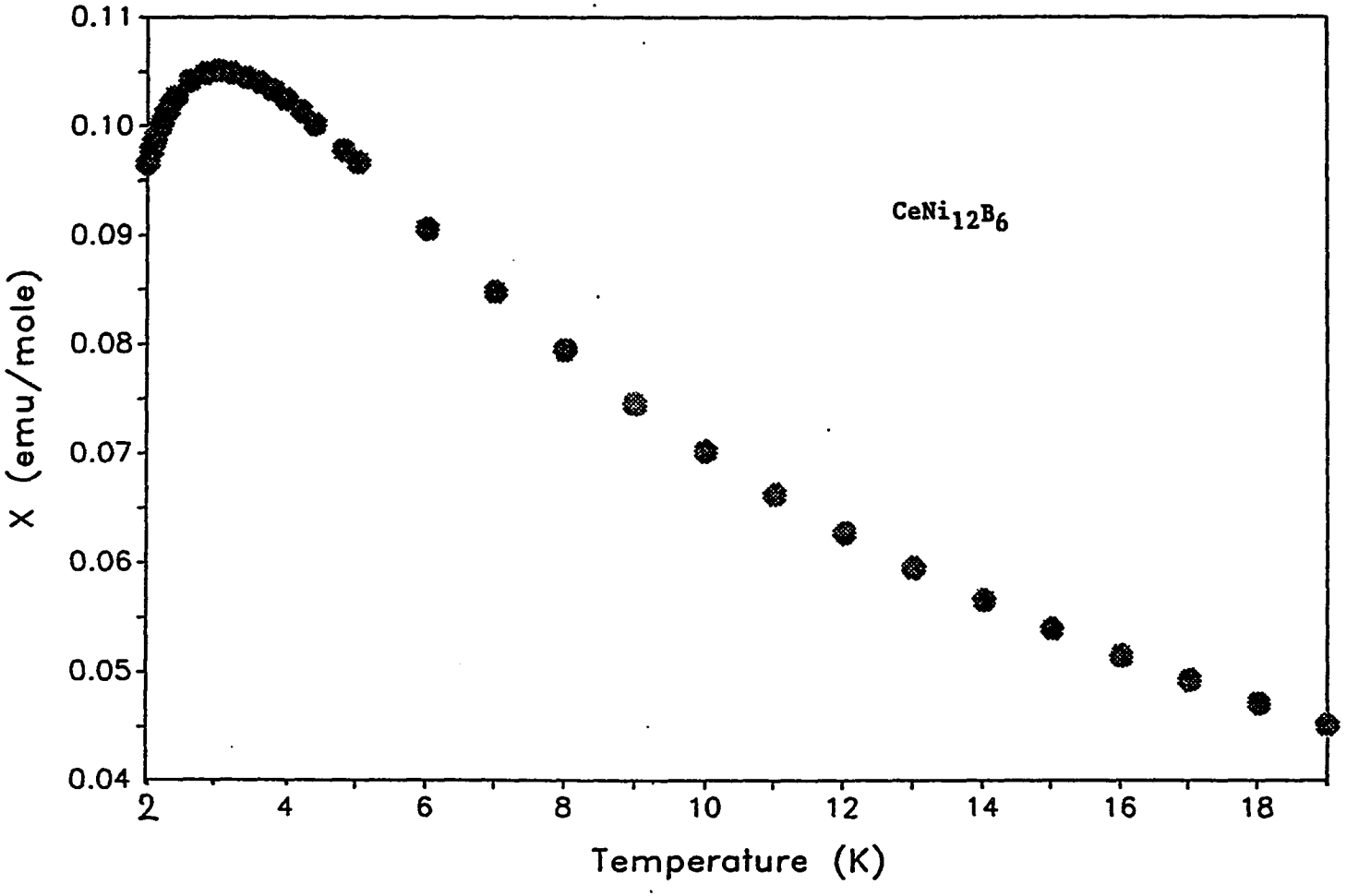

Fig. 57. Magnetic susceptibility of $CeNi_{12}B_6$ for temperature $2K < T < 20K$

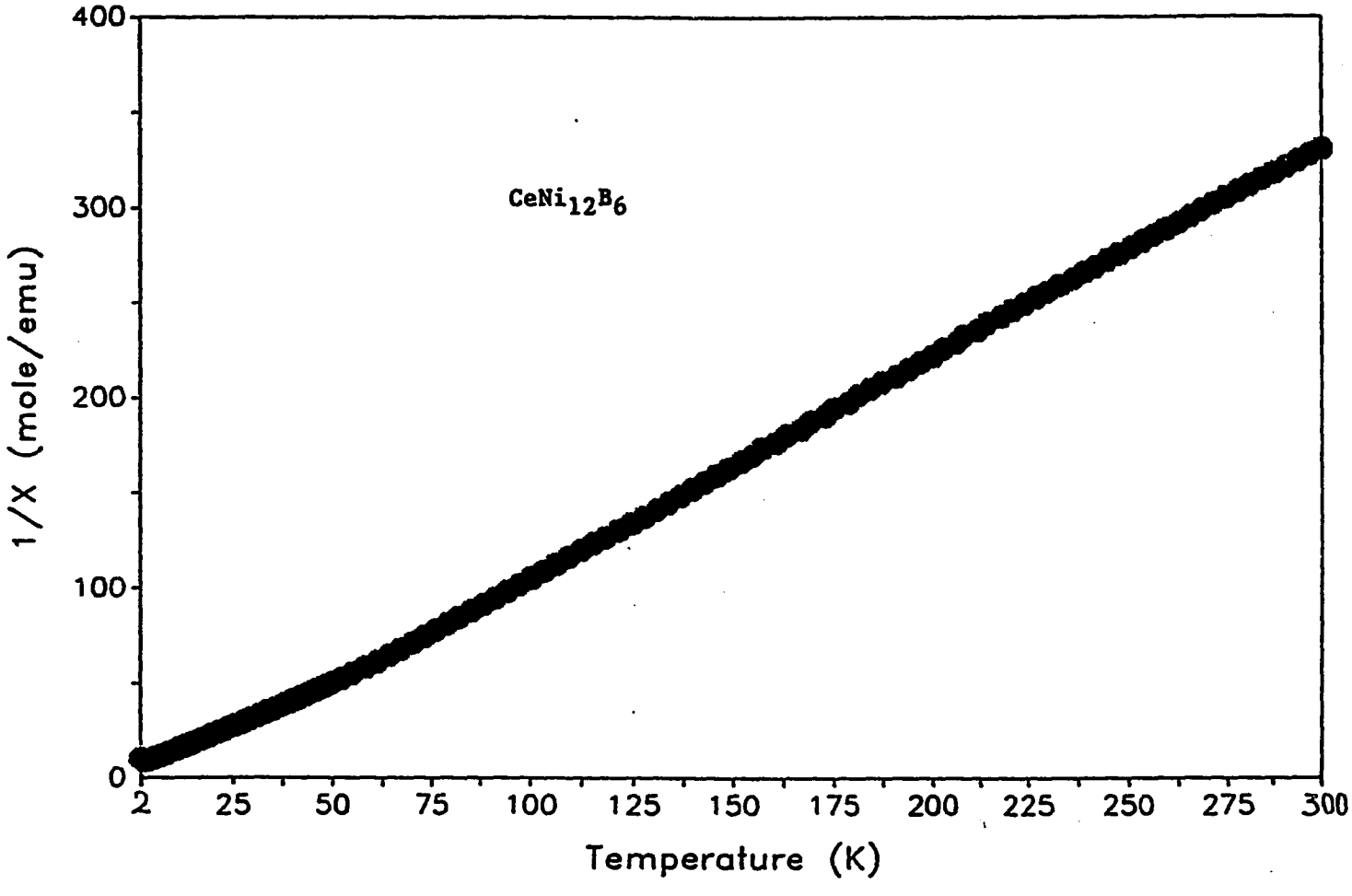

Fig. 58. The inverse susceptibility of $CeNi_{12}B_6$ over a wider temperature range 2K < T < 300K

negative, θ_p obtained from high temperature region is positive. If the temperature is raised near room temperature, the θ_p seems to become negative again. The cause of this deviation from the Curie-Weiss behavior might be the presence of crystalline electric field effect.

3. $Ce_5Ni_6In_{11}$

This sample was prepared by arc-melting. During this process a weight loss of 0.244 gram occurred for the sample of total mass = 22.96 gram. If we assume that only In was lost, which is reasonable because In has a higher vapor pressure than Ce and Ni [90,91], the actual composition should be $Ce_5Ni_6In_{10.8}$.

The crystal structure of this compound was reported by Kalychak et al. [92]. The Ce-Ce spacing in $Ce_5Ni_6In_{11}$ is ~3.99Å.

The heat capacity of $Ce_5Ni_6In_{11}$ measured from 1.5K to 20K is shown in Fig. 59 together with that of $La_5Ni_6In_{11}$. The upturn at ~5K is an indication that $Ce_5Ni_6In_{11}$ will become magnetically ordered below 1.5K. Figure 59 inset is the C/T versus T^2 plot for the same temperature range. Also shown in the inset is the difference $\delta = (C/T_{Ce5Ni6In11} - C/T_{La5Ni6In11})$ as a function of T^2. The electronic specific heat coefficient γ of $Ce_5Ni_6In_{11}$ was determined in the same way as were done in the case of $CePtGa_3$ and $CeNi_{12}B_6$. By adding the average value of the difference δ in

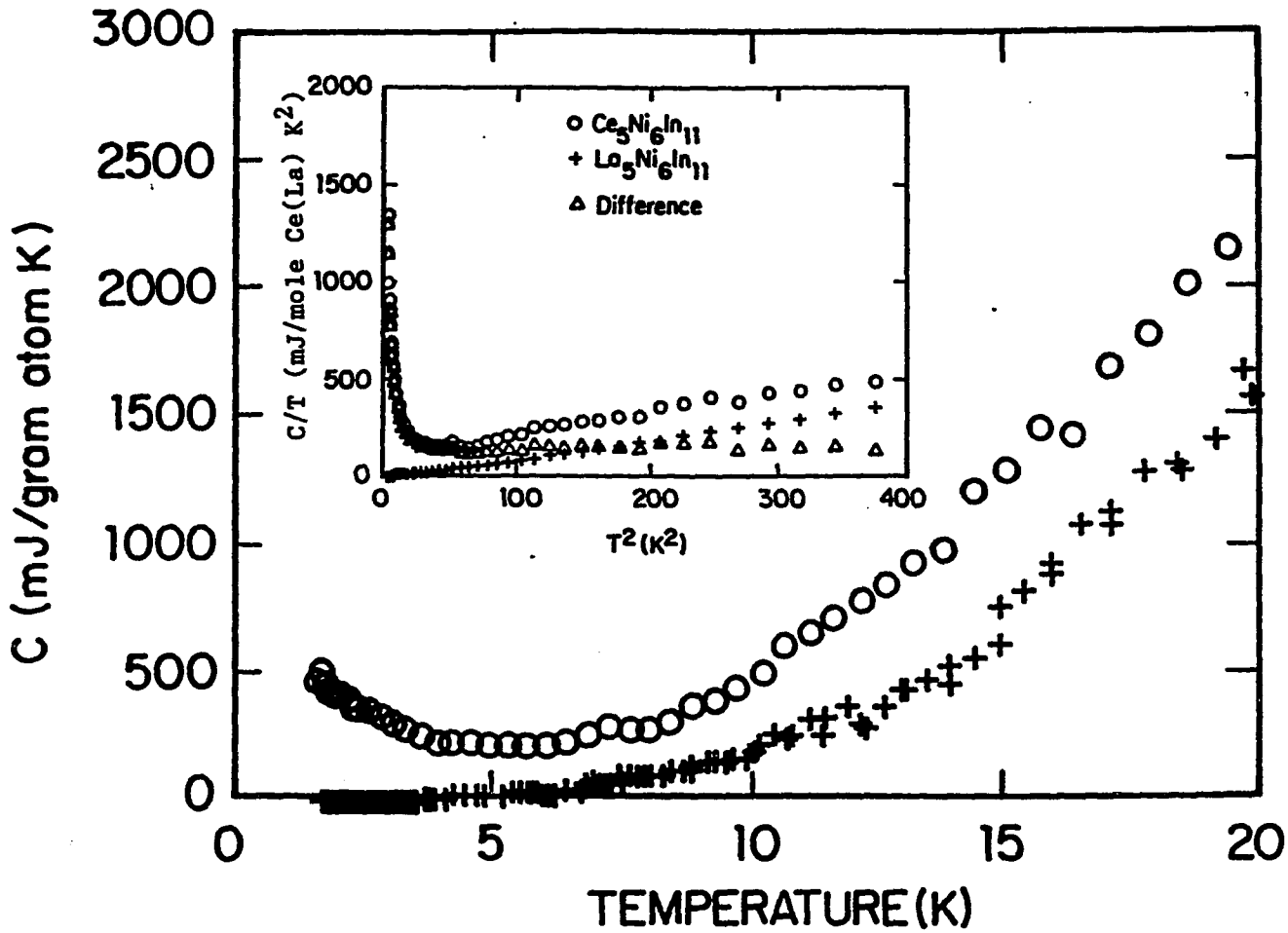

Fig. 59. Heat capacities of $Ce_5Ni_6In_{11}$ and $La_5Ni_6In_{11}$. Inset: C/T versus T^2 plot for both compounds and their difference (see text)

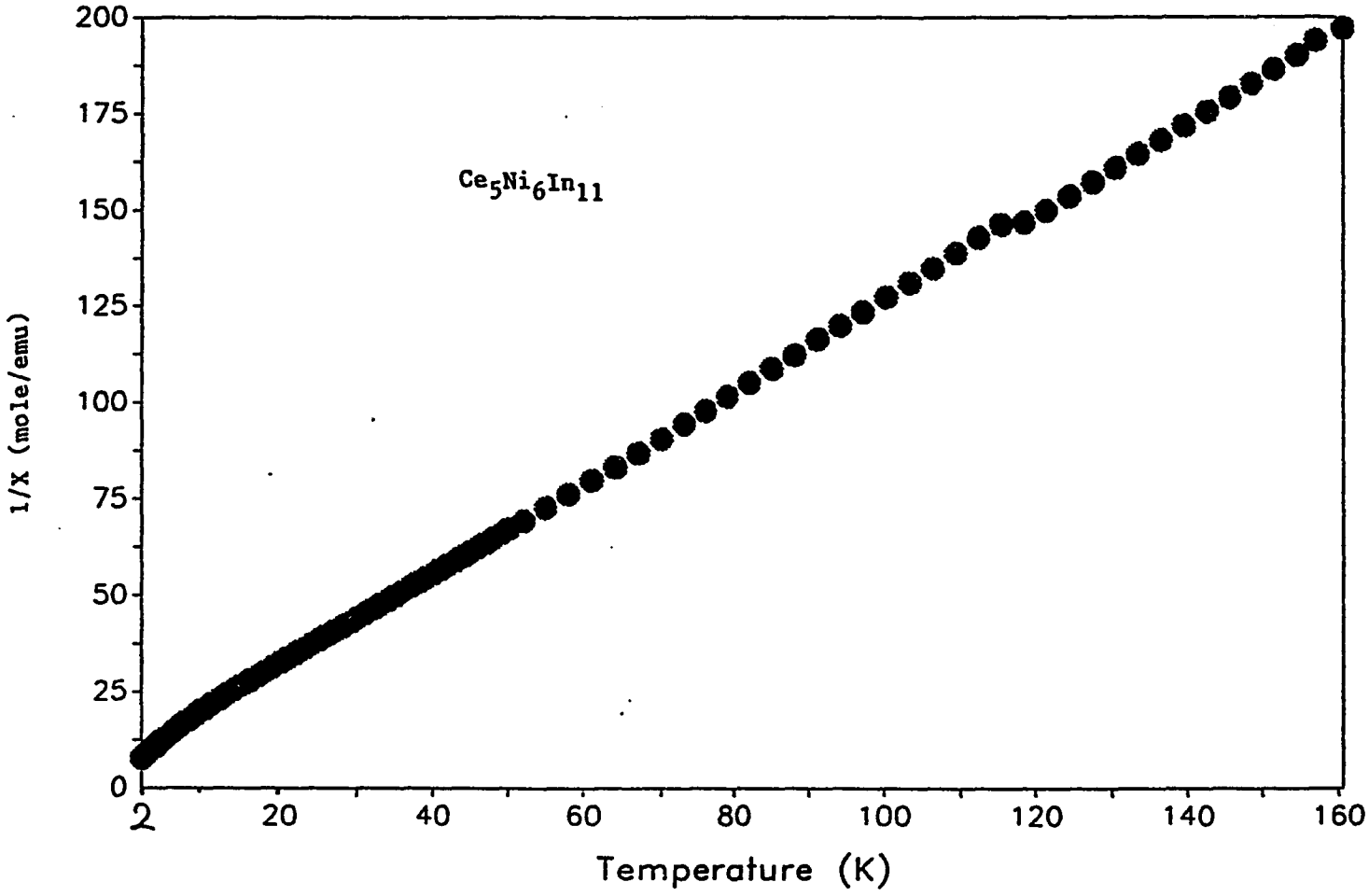

Fig. 60. The inverse susceptibility as a function of temperature.

Temperature range: 2K < T < 160K

temperature region 10K < T < 20K to the γ of $La_5Ni_6In_{11}$, which was determined at lower temperatures (T < 3K), the γ value of $Ce_5Ni_6In_{11}$ was found to be ~160 mJ/mole Ce K^2. This relatively large γ places $Ce_5Ni_6In_{11}$ into an intermediate heavy fermion category.

Figure 60 shows the inverse susceptibility of $Ce_5Ni_6In_{11}$. The effective moment $\mu_{eff} = 2.62\mu_B$ is close to the theoretical value $2.54\mu_B$ for Ce^{3+} ion. The Curie temperature is found to be $\theta_p = -8.0K$, which implies that the ground state of this compound is antiferromagnetic in nature.

IV. CONCLUSION AND SUMMARY

In search of heavy fermion materials, the low temperature properties of a series of cerium intermetallic binary and ternary compounds were studied.

Although the spin-carrying Ce atoms in $CePtGa_3$ form a periodic array, the compound shows a spin glass behavior in its low temperature susceptibility and heat capacity. This spin glass behavior is believed to be due to the random distribution of Pt and Ga atoms around the Ce atoms which induces a random RKKY interaction between the spins. This finding places $CePtGa_3$ as the third known NMAD (non-magnetic atomic disorder) spin glass material after $CeCu_{6.5}Al_{6.5}$ and $CePd_3B_{0.3}$.

Crystalline electric field (CEF) effect plays an important role in both $CeCd_{11}$ and $CeGa_2$. The CEF splittings were determined in the case of $CeCd_{11}$ from the Schottky anomaly in heat capacity. The splitting between the first excited doublet and the ground state E_1 = 17.5K is one of the lowest CEF splittings found in Ce compounds. The Schottky anomaly of this kind of low energy level sometime can show up as a false signal of heavy fermion behavior. An immediate example is found in $CeGa_2$ where the Schottky heat capacity from the relatively small CEF splitting E_1 = ~62K in $CeGa_2$ accounts for ~40% of the large

C/T value (~400mJ/mole Ce K^2) obtained above the ordering temperature.

The antiferromagnetic phase transitions in $CeHg_3$, $CeCd_2$, $CeCd_3$ and $CeNi_{12}B_6$ are reported for the first time, and strong evidence for antiferromagnetic ordering below ~1.4K is presented for $Ce_{13}Cd_{58}$, $CeCd_6$, $CeCd_{11}$ and $Ce_5Ni_6In_{11}$.

It seems that the experimental parameters such as Ce-Ce spacing, crystal structure and the type of non-f ligand atoms which determine the heavy fermion behavior is still unknown. This study shows that a large Ce-Ce spacing might be a necessary condition for heavy fermion but it is surely not a sufficient one.

V. REFERENCES

[1] E. Gopal, Specific Heats at Low Temperatures (Plenum Press, New York, 1966).

[2] Z. Fisk, D. W. Hess, C. J. Pethick, D. Pines, J. L. Smith, J. D. Thompson and J. O. Willis, Science, 239, 31 (1988).

[3] K. Andres, J. E. Graebner and H. R. Ott, Phys. Rev. Lett., 35, 1779 (1975).

[4] G. R. Stewart, Z. Fisk, J. O. Willis and J. L. Smith, Phys. Rev. Lett., 52, 679 (1984).

[5] Z. Fisk, G. R. Stewart, J. O. Willis, H. R. Ott and F. Hulliger, Phys. Rev. B, 30, 6360 (1984).

[6] H. R. Ott, H. Rudigier, E. Felder, Z. Fisk and B. Batlogg, Phys. Rev. Lett., 55, 1595 (1985).

[7] C. Kittel, Introduction to Solid State Physics (John Wiley & Sons, Inc., New York, 1976).

[8] N. W. Ashcroft and N. D. Mermin, Solid State Physics (Holt, Rinehart and Winston, New York, 1976).

[9] P. A. Lee, T. M. Rice, J. W. Serene, L. J. Sham and J. W. Wilkins, Comments on Condensed Matter Physics, 12, No. 3, 99 (1986).

[10] G. R. Stewart, Rev. Mod. Phys., 56, 779 (1984).

[11] H. R. Ott, H. Rudigier, Z. Fisk, J. O. Willis and G. R. Stewart, Solid State Commun., 53, 235 (1985).

[12] H. R. Ott and Z. Fisk, Handbook on Physics and Chemistry of Actinides ed. by A. J. Freeman and G. H. Lander (Elsevier Science Publishers B.V., 1987), vol. 5, p. 89.

[13] D. D. Koelling, Solid State Commun., 43, 247 (1982).

[14] A. Yanase, J. Magn. Magn. Mater., 31-34, 453 (1983).

[15] T. Jarlborg, H. F. Braun and M. Peter, Z. Phys. B, 52, 295 (1983).

[16] A. M. Boring, R. C. Albers, G. R. Stewart and D. D. Koelling, Phys. Rev. B, 31, 3251 (1985).

[17] K. Takegahara, H. Harima and T. Kasuya, J. Magn. Magn. Mater., 47 & 48, 263 (1985).

[18] A. M. Boring, R. C. Albers, F. M. Mueller and D. D. Koelling, Physica 130B, 1711 (1985); R. C. Albers, Phys. Rev. B, 32, 7646 (1985); R. C. Albers, A. M. Boring, P. Weinberger and N. E. Christensen, Phys. Rev. B, 32, 7571 (1985).

[19] P. Strange and B. L. Gyorffy, Physica B, 130, 41 (1985).

[20] T. Oguchi and A. J. Freeman, Proc. 5th Int. Conf. on Crystalline Fields (Sendai, Japan 1985).

[21] J. Sticht and J. Kubler, Solid State Commun., 54, 389 (1985).

[22] G. P. Meisner, A. L. Giorgi, A. C. Lawson, G. R. Stewart, J. O. Willis, M. S. Wire and J. L. Smith, Phys. Rev. Lett., 53, 1829 (1984).

[23] F. Marabelli and P. Wachter, J. Magn. Magn. Mater., 70, 364 (1987).

[24] C. J. Pethick, D. Pines, K. F. Quader, K. S. Bedell and G. E. Brown, Phys. Rev. Lett., 57, 1955 (1986).

[25] D. W. Hess, J. Low Temp. Phys., 68, 311 (1987).

[26] L. D. Landau, Zh. Eksp. & Teor. Fiz., 30, 1058 (1956).

[27] H. H. Hill, in Plutonium 1970, ed. by W.N. Miner, 2 (Metallurgical Society of the AIME, New York 1970).

[28] C. L. Lin, L. W. Zhou, J. E. Crow, T. Michalisin, J. Brooks and R. P. Guertin, J. Less-Common Metals, 127, 273 (1987).

[29] K. Ikeda and K. A. Gschneideer, Jr., Phys. Rev. B, 25, 4623 (1982).

[30] J. R. Cooper, C. Rizzuto and G. Olcese, J. de Phys., 32, C1-1136 (1971).

[31] C. L. Lin, J. Teter, J. E. Crow, T. Michalisin, J. Brooks,

A. I. Abou-Aly and G. R. Stewart, Phys. Rev. Lett., 54, 2541 (1985).

[32] P. H. Frings, Thesis, Univ. of Amsterdam (1984).

[33] H. R. Ott, H. Rudigier, E. Felder, Z. Fisk and J. D. Thompson, Phys. Rev. B, 35, 1452 (1987).

[34] T. H. Geballe, B. T. Matthias, V. B. Compton, E. Corenzwit G. W. Hull, Jr. and L. D. Longinotti, Phys. Rev., 137 No. 1A, A119 (1965).

[35] K. Ikeda, K. A. Gschneidner, Jr., B. J. Beaudry and U. Atzmony, Phys. Rev. B, 25, 4604 (1982).

[36] R. J. Stierman, K. A. Gschneidner, Jr., T.-W. E. Tsang, F. A. Schmidt, P. Klavins, R. N. Shelton, J. Queen and S. Legvold, J. Magn. Magn. Mater., 36, 249 (1983).

[37] V. Cannella, J. A. Mydosh and J. I. Budnick, J. Appl. Phys., 42, 1689 (1971).

[38] C. A. M. Mulder, A. J. vanDuyneveldt and J. A. Mydosh, Phys. Rev. B, 23, 1384 (1981).

[39] K. Binder, Festkorperprobleme, 17, 55 (1977).

[40] K. Moorjani and J. M. D. Coey, Magnetic Glasses (Elsevier, Amsterdam - Oxford - New York - Tokyo, 1984).

[41] R. D. Shull, H. Okamoto and P. A. Beck, Solid State Commun., 20, 863 (1976).

[42] H. Maletta, J. Appl. Phys., 53, 2185 (1982).

[43] J. Durand, Amorphous Magnetism II, ed. by R. A. Levy and R. Hasegawa, (Plenum Press, New York, 1977), p. 305.

[44] A. Amamou, Amorphous Magnetism II, ed. by R. A. Levy and R. Hasegawa, (Plenum Press, New York, 1977), p. 265.

[45] U. Rauchschwalbe, U. Gottwick, U. Ahlheim, H. M. Mayer and F. Steglich, J. Less-Common Metals, 111, 265 (1985).

[46] S. K. Dhar, K. A. Gschneidner, Jr., C. D. Bredl and F. Steglich, Phys. Rev. B, 39, 2439 (1989).

[47] V. Cannella and J. A. Mydosh, Phys. Rev. B, 6, 4220 (1972).

[48] F. Holtzberg, J. L. Tholence and R. Tournier, Amorphous Magnetism II, ed. by R. A. Levy and R. Hasegawa, (Plenum Press, New York, 1977), p. 155.

[49] K. Binder and A. P. Young, Rev. Mod. Phys., 58, 801 (1986).

[50] L. E. Wenger and P. H. Keesom, Phys. Rev. B, 13, 4053 (1976).

[51] J. G. Sereni, T. E. Huber and C. A. Luengo, Solid State Commun., 29, 671 (1979).

[52] Yu. N. Grin, P. Rogl and K. Hiebl, J. Less-Common Metals, 136, 329 (1988).

[53] J. Tang and K. A. Gschneidner, Jr., to be published in J. Less-Common Metals.

[54] I. Johnson and R. M. Yonco, Metall. Trans., 1, 905 (1970).

[55] S. Horn, E. Holland-Moritz, M. Loewenhaupt, F. Steglich, H. Scheuer, A. Benoit and J. Flouquet, Phys. Rev. B, 23, 3171 (1981).

[56] N. Hutchings, Solid State Phys., 16, 227 (1964).

[57] H. Meyer and P. L. Smith, J. Phys. Chem. Solid 9, 285 (1959).

[58] E. Gopal, Specific Heat at Low Temperatures (Plenum Press, New York, 1966), p. 105.

[59] V. Rao, and W. Wallace, Phys. Rev. B, 2, 4613 (1970).

[60] N. Mott and H. Jones, The Theory of Properties of Metals and Alloys (Dover, New York, 1958), p. 274.

[61] C. Kittel, Introduction to Solid State Physics 6th ed., (John Wiley, New York, 1986), p. 405.

[62] R. Weast, CRC Handbook of Chemistry and Physics 68th ed., (CRC Press, Cleveland, 1987), p. E-119.

[63] H. Fischer, E. Swartz, R. Pohl, B. Jones, J. Wilkins and Z. Fisk, Phys. Rev. B, 36 5330 (1987).

[64] L. Colombo and G. L. Olcese, Atti Lincei Rend. Sci. Fis. Mat. Nat. 35, 12 (1963).

[65] T. H. Tsai, J. A. Gerber, J. W. Weymouth and D. J. Sellmeyer, J. Appl. Phys., 49, 1507 (1978).

[66] T. H. Tsai and D. J. Sellmeyer, Phys. Rev. B, 20, 4577 (1979).

[67] W. H. Dijkman, Thesis, University of Amsterdam (1982).

[68] P. Burlet, M. A. Fremy, D. Jignoux, G. Lapertot, S. Quezel, L. P. Regnault, J. Rossat-Mignod and E. Roudant, J. Magn. Magn. Mater., 63 & 64, 151 (1987).

[69] M. Takahashi, H. Tanaka, T. Satoh, M. Kohgi, Y. Ishikawa, T. Miura and H. Takei, J. Phys. Soci. of Japan, 57, 1377 (1988).

[70] N. W. Ashcroft and N. D. Mermin, Solid State Physics (Holt, Rinehart and Winston, New York, 1976), p. 711.

[71] W. E Wallace, Rare Earth Intermetallics (Academic Press, Inc., New York, 1973), p. 18.

[72] G. Olcese, Atti Accad. Naz. Lincei, Cl. Sci. Fis., Mat. Nat., Rent., 35, 7 (1963).

[73] N. W. Ashcroft and N. D. Mermin, Solid State Physics (Holt, Rinehart and Winston, New York, 1976), p. 747.

[74] Dmitr, Metallofizika, 49, 109 (1973).

[75] J. G. Huber, to be presented at APS meeting in St. Louis March 20-24, (1989).

[76] H. J. van Daal, K. H. J. Buschow, P. B. van Aken and M. H. van Maaren, Phys. Rev. Lett., 34, 1457 (1975).

[77] A. Schroder, R. van den Berg and H. V. Lohneysen, Solid State Commun., 65, 99 (1988).

[78] M. Olivier, T. Siegrist and S. P. McAlister, J. Magn. Magn. Mater., 66, 281 (1987).

[79] N. Sato, M. Kontani, H. Abe and K. Adachi, J. Phys. Soc. of

Japan, 57, 1069 (1988).

[80] A. Iandelli and R. Ferro, Gazz. Chim. Ital., 84, 463 (1954).

[81] G. Bruzzone, M. L. Fornasini and F. Merlo, J. Less-Common Metals, 30, 361 (1973).

[82] Yu. N. Grin, K. Hiebl and P. Rogl, J. Less-Common Metals, 110, 299 (1985).

[83] H. Oesterreicher, J. Less-Common Metals, 30, 225 (1973).

[84] D. C. Koskimaki and K. A. Gschneidner, Jr., Phys. Rev. B, 11, 4463 (1975).

[85] B. C. Sales and D. K. Wohlleben, Phys. Rev. Lett., 35, 1240 (1975).

[86] T. Kasuya, Theory of Heavy Fermions and Valence Fluctuations ed. by T. Kasuya and T. Saso (Springer-Verlag, New York, 1985), p. 2.

[87] G. Gruner and N. F. Mott, J. Phys. F : Metal Phys., 4, L16 (1974).

[88] L. G. Aksel'rud, Yu. B. Kuz'ma and V. A. Bruskov, Dopovidi Akad. Nauk Ukr. RSR, Ser.B, 3, 31 (1985).

[89] O. M. Dub and Yu. B. Kuz'ma, Inorg. Mater., 23, 42 (1987).

[90] R. Loebel, CRC Handbook of Chemistry and Physics 68th ed., ed. by R. Weast (CRC Press, Cleveland, 1987), p. D-215.

[91] K. A. Gschneidner, Jr., CRC Handbook of Chemistry and Physics 69th ed., ed. by R. Weast (CRC Press, Boca Raton, FL, 1988), p. B-208.

[92] Ya. M. Kalychak, P. Yu. Zavalii, V. M. Baranyak, O. V. Dmytrakh and O. I. Bodak, Sov. Phys. Crystallogr., 34 No.4, 600 (1987).

[93] K. H. J. Buschow, Rep. Prog. Phys., 42, 1461 (1979).

VI. APPENDIX

Table A.1. Crystal structures and lattice parameters of the Ce compounds studied

compound	structure	a (Å)	b (Å)	c (Å)	d_{Ce-Ce} (Å)
$CePtGa_3$	tI10	4.307		10.513	4.307
$CePt_{1.1}Ga_{2.9}$	tI10	4.306		10.495	4.306
$CePt_{0.9}Ga_{3.1}$	oF20	6.100	6.113	10.512	4.318
$LaPtGa_3$	tI10	4.344		10.522	
$CeCd_{11}$	cP36	9.319			6.59
$LaCd_{11}$	cP36	9.334			
$CeGa_2$	hP3	4.321		4.320	4.32
$LaGa_2$	hP3	4.329		4.405	
$CeHg_3$	hP8	6.760		4.941	4.62
$CeIr_5$	cF24	7.510			5.31
$CePt_5$	hP6	5.368		4.383	4.38
Ce_2Zn_{17}	hR19	9.071		13.28	4.43
$CeCd_2$	hP3	5.075		3.448	3.44
$CeCd_3$	cF16	7.223			5.11
$Ce_{13}Cd_{58}$	hP142	15.77		15.57	4.37
$CeCd_6$	cI168	15.782			5.83
CeNiAl	hP9	6.973		4.019	3.62

Table A.1. (Continued)

compound	structure	a (Å)	b (Å)	c (Å)	d_{Ce-Ce} (Å)
$CeNiAl_{0.5}Ga_{0.5}$	hP9	6.955		4.014	3.61
$CeNi_{12}B_6$	oC76	9.586	7.409	11.071	6.06
$LaNi_{12}B_6$	oC76	9.587	7.428	11.063	
$Ce_5Ni_6In_{11}$	oC44	14.600	14.601	4.413	3.99
$La_5Ni_6In_{11}$	oC44	14.640	14.674	4.439	

Table A.2. Selected properties of the Ce compounds studied

compound	γ[a]	θ_D (K)	p_{eff} (μ_B)	θ_p (K)	T_s, T_C, T_N, T_{SG} (K)
$CePtGa_3$	71(120)[b]	282[c]	2.89	-14	~1.7 (SG)[d]
$CePt_{1.1}Ga_{2.9}$	76	282[c]			<1.5 (SG)[d]
$CePt_{0.9}Ga_{3.1}$	56	282[c]			~2.0 (SG)[d]
$LaPtGa_3$	5.9	282			
$CeCd_{11}$	26.2	280[c]	2.57	-7.8	<1.3 (N)
$LaCd_{11}$	17.2	280			
$CeGa_2$	32.6	326[c]	2.85	1.8	8.4 (C)
$LaGa_2$	5.6	326			
$CeHg_3$	52	117	2.32	-10	1.6 (N)
$CeIr_5$	19	188			1.8 (s)
$CePt_5$	15.0	200	2.45[e]	-34[e]	1.0 (N)
Ce_2Zn_{17}	15.0	253	2.91	-1.7	1.7 (N)
$CeCd_2$	12.0[f]	173[f]	2.65	-56	22 (N)
$CeCd_3$	49.4	150	2.60	-52	2.0 (N)
$Ce_{13}Cd_{58}$	23.1	146	2.60	-12	<1.3 (N)
$CeCd_6$	51.6	138	2.53	-9.5	<1.3 (N)
CeNiAl	7.2	290	VF[g]		

$CeNiAl_{0.5}Ga_{0.5}$	8.7	283	VF[g]		
$CeNi_{12}B_6$	65	553[c]	2.62	9.3[f]	1.7 (N)
$LaNi_{12}B_6$	32.3	553			
$Ce_5Ni_6In_{11}$	160	266[c]	2.62	-8.0	<1.5 (N)
$La_5Ni_6In_{11}$	4.5	266			

[a] In units of mJ/mole Ce(La) K^2.

[b] 71, obtained above the spin glass transition; 120, below the transition.

[c] Data estimated from $LaPtGa_3$, $LaCd_{11}$, $LaGa_2$, $LaNi_{12}B_6$ and $La_5Ni_6In_{11}$.

[d] T_{SG} refers to the peak temperature in heat capacity.

[e] After [93].

[f] Data not reliable.

[g] VF = valence fluctuation.

VII. ACKNOWLEDGEMENTS

This is a great opportunity to express my sincere thanks to Karl Gschneidner, my major professor, who directed me through this study. His enormously rich knowledge and great sense of understanding has made the last three years rewarding and pleasant.

I would also like to thank my co-major professor Douglas Finnemore for his help in both scientific and administrative aspects.

I thank Bernie Beaudry, Nile Beymer, Kelly Funke and Randy Doran for their assistances in preparing the samples studied.

I specially thank Jack Moorman who taught me how to use and maintain the apparatus and provided a trouble free environment.

I also thank Bruce Cook and Joel Harringa for their help in operating the X-ray diffractometer.

A special thanks is directed to Mike Damento, James Herchenroeder and Sudesh Dhar for the fruitful and enjoyable discussions with them.

I would also like to thank Francis Laabs for his assistance in analyzing the sample using SEM and TEM.

I sincerely thank Wonchoon Lee, Kevin Dennis and Krishna Athreya who made the low field susceptibility measurements with their SQUID magnetometers for me.

Thanks also go to Jennings "Cap" Capellen for his help in search for publications in RIC's library.

Finally, I sincerely thank other members of my thesis committee: Kai Ming Ho, David Johnston and John Hauptman.

This work was performed at Ames Laboratory under contract No. W-7405-eng-82 with the U. S. Department of Energy. The United States government has assigned the DOE Report number IS-T 1387 to this thesis.

THIS THESIS IS DEDICATED TO MY PARENTS

WHO HAVE DEVOTED MOST OF THEIR LIVES TO THE SCIENCE.